Title
Elucidating the role of p73a1, a p73 C-terminal isoform, in oncogenesis and lipid metabolism

Author
Laubach, Kyra Nicole

Publication Date
2022

Peer reviewed|Thesis/dissertation

Elucidating the role of p73α1, a p73 C-terminal isoform, in oncogenesis and lipid metabolism

By

KYRA LAUBACH
DISSERTATION

Submitted in partial satisfaction of the requirements for the degree of

DOCTOR OF PHILOSOPHY

in

Integrative Pathobiology

in the

OFFICE OF GRADUATE STUDIES

of the

UNIVERSITY OF CALIFORNIA

DAVIS

Approved:

Xinbin Chen, Chair

Robert Rebhun

Hongwu Chen

Committee in Charge

2022

Acknowledgements

The completion of this dissertation would not be possible without the support of my PhD advisor and committee chair, Dr. Xinbin Chen. Additionally, I would like to extend my gratitude to the other members of my dissertation committee for their valuable feedback and guidance during my Qualifying Exam and dissertation.

I would like to thank the UC Davis Lung Center Pre-doctoral T32 Training Program that has graciously supported me financially over the past year and a half.

I would not have been able to successfully complete my PhD without the support, advice, and encouragement from the members of the Chen lab. Specifically, the moral and technical support from Drs. Chris Lucchesi and Shakur Mohibi.

Infinite thanks to my friends who supported me throughout this entire process. Jenn and Zach, thanks for keeping me mildly sane and for all of the experimental and life advice.

Finally, I want to thank my family for their unlimited support and always wanting the best for me.

Abstract

The p53 protein is an indispensable tumor suppressor that is involved in numerous cellular processes, such as regulation of the cell cycle and metabolism. About two decades ago, two proteins with significant homology to p53 were discovered, and termed p63 and p73. To date, these three proteins make up the p53 family of transcription factors. Each gene has the capacity to form multiple protein isoforms through the use of various promoters and alternative splicing, with p73 forming the most isoforms. At the 5` end of the p73 gene, transcription initiation from promoters 1 and 2 form the TAp73 and ΔNp73 N-terminal isoforms, respectively. At the 3` end, alternative splicing in p73 exons 11 through 13 give rise to seven known C-terminal isoforms (α, β, γ, δ, ε, ζ, η). The function of a majority of the C-terminal isoforms is not well-studied. As such, the work in this dissertation focuses on characterizing the function of the p73 C-terminal isoforms.

Chapter one serves as an introduction to the p53 family of proteins, while comprehensively compiling the literature that describes how these three proteins are involved in regulating lipid and iron metabolism. This chapter highlights the numerous ways in which p53 regulates lipid and iron metabolism, while revealing the limited literature on the role of p63 and p73 in these processes.

Chapter two lays the foundation for the rest of the dissertation, which focuses on characterizing the function of a novel p73 C-terminal isoform that we discovered. This novel isoform, termed p73α1, results from the exclusion of p73 exon 12 (*E12*). By using CRIPSR to remove *E12* from multiple cancer cell lines, the role of p73α1 in oncogenesis was studied. To study the physiological function of p73α1, *E12* heterozygous ($E12^{+/-}$) mice were generated and life-span, tumor burden, and histopathology were analyzed. It was found that p73α1 functions as a tumor suppressor, both *in vitro* and *in vivo*. Moreover, $E12^{+/-}$ mice exhibited widespread systemic inflammation. As a result, the findings from this study identified Notch1 as a direct target of p73α1-mediated tumor suppression and inflammation.

Chapter three integrates the previous two chapters to investigate the role of p73α1 in regulating lipid metabolism. A multi-omic approach was taken and integrated with molecular biology techniques to identify lipid classes and lipid metabolism-associated genes that were altered by p73α1. Specifically, p73α1 was found to directly inhibit expression of Stearoyl-CoA Desaturase 1 (SCD1), leading to altered lipid profiles. Furthermore, the tumor suppressive function of p73α1 was found to be mediated in part through SCD1. Through these findings, a previously unidentified p73 target, SCD1, was established and a role for p73α1 in lipid metabolism was determined.

Table of Contents

The p53 Family: A Role in Lipid and Iron Metabolism

*Kyra Laubach, Jin Zhang and Xinbin Chen**

Comparative Oncology Laboratory, Schools of Veterinary Medicine and Medicine, University of California, Davis, Davis, CA, United States

The p53 family of tumor suppressors, which includes p53, p63, and p73, has a critical role in many biological processes, such as cell cycle arrest, apoptosis, and differentiation. In addition to tumor suppression, the p53 family proteins also participate in development, multiciliogenesis, and fertility, indicating these proteins have diverse roles. In this review, we strive to cover the relevant studies that demonstrate the roles of p53, p63, and p73 in lipid and iron metabolism.

Keywords: p53, p63, p73, metabolism, lipid, iron

INTRODUCTION

For over 40 years, p53 has been characterized as a master transcriptional regulator that mediates the expression of various genes to prevent aberrant cell growth (Ko and Prives, 1996). Just before the turn of the century, the *TP63* and *TP73* genes were discovered due to their significant homology to *TP53*, particularly in the DNA-binding domain (Kaghad et al., 1997; Schmale and Bamberger, 1997; Trink et al., 1998; Borremans et al., 2001). These three genes constitute the p53 family.

The *TP53, TP63,* and *TP73* genes are expressed as multiple N- and C-terminal isoforms through two promoters and alternative splicing (**Figure 1**). In *TP53*, promoter 1 (P1) gives rise to two translation initiation start sites, termed ATG1 and ATG40, which produce full-length p53 (FLp53) and Δ40p53, respectively (Courtois et al., 2002; Yin et al., 2002). Both isoforms possess transactivation function even though Δ40p53 contains a truncated form of the conventional transactivation domain (Zhu et al., 1998; 2000; Harms and Chen, 2005). Similarly driven by P1, *TP63/73* express TAp63/73 isoforms, which have a transactivation domain that is comparable to the one found in FLp53 (Arrowsmith, 1999). By using promoter 2 (P2), all family members produce the N-terminally truncated isoforms, termed Δ133p53 and Δ160p53 in *TP53*, which arise from translation initiation start sites ATG133 and ATG160 (Bourdon et al., 2005), and ΔNp63/73 in *TP63/73* (Yang et al., 1998; 2000). Interestingly, despite lacking the conventional transactivation domain, ΔNp63 and ΔNp73 are transcriptionally active and can induce some p53 targets (Liu et al., 2004; Helton et al., 2006). Alternative splicing at the C-terminus of each gene generates additional isoforms. *TP53* produces three (α, β, γ) C-terminal isoforms (Bourdon et al., 2005), *TP63* produces four (α, β, γ, δ) C-terminal isoforms (Yang et al., 1998; Mangiulli et al., 2009), and *TP73* produces at least seven C-terminal isoforms (α, β, γ, δ, ε, ζ, η) (De Laurenzi et al., 1998; 1999). While the N-terminal isoforms of p53, p63, and p73 are well studied, the C-terminal isoforms remain largely uncharacterized.

The biological function of the p53 family proteins has been demonstrated through various mouse models. The very first p53-knockout model showed that mice deficient in p53 were prone to spontaneous tumors, but otherwise developed normally (Donehower et al., 1991). Later, it was discovered that p53 dysregulation, predominantly overexpression, can lead to impaired embryogenesis and other developmental defects (Luna et al., 1995; Sah et al., 1995; Parant et al., 2001; Zhang et al., 2012; Nostrand et al., 2014). Unlike p53, total p63-knockout mice exhibit severe epidermal and craniofacial abnormalities and die shortly after birth (Celli et al., 1999; Mills et al., 1999; Yang et al., 1999). Further studies revealed that ΔNp63 is responsible for the

observed phenotype (Candi et al., 2006; Koster et al., 2007). In contrast, TAp63-knockout mice did not exhibit birth defects, but were prone to spontaneous tumors, indicating that TAp63 functions as a tumor suppressor to maintain genome stability (Suh et al., 2006; Guo et al., 2009; Su et al., 2009). Similarly, total p73-knockout mice were runty and had severe neurological defects, chronic inflammation, fertility issues (Yang et al., 2000), and impaired multiciliogenesis (Marshall et al., 2016; Nemajerova et al., 2016). It was later found that ΔNp73-knockout mice exhibited neurodegeneration (Wilhelm et al., 2010), whereas TAp73-knockout mice were prone to spontaneous tumors (Tomasini et al., 2008).

Continued research efforts into the more nuanced cancer-associated roles of the p53 family proteins is undeniably valuable. However, emerging evidence suggests that these proteins possess additional important functions that can affect various human diseases, such as diabetes mellitus and liver steatosis. This review will focus specifically on the roles of the p53 family in lipid and iron metabolism.

LIPID METABOLISM

Lipids play an important role in various biological processes and serve as an essential building block for many cellular structures. Tight regulation of lipid metabolism is crucial for proper organismal function, and dysregulation has been implicated in numerous diseases, such as Alzheimer's disease and fatty liver disease (Hooijmans and Kiliaan, 2008; Hasson et al., 2016). There are three main sources of lipids: dietary lipids, fatty acids produced by hepatocytes and adipocytes, and lipoproteins produced by hepatocytes (Giammanco et al., 2015). In the lumen of the gastrointestinal tract, dietary lipids become emulsified by combining with bile salts, which allows for lipid hydrolysis and subsequent import to enterocytes (Hussain, 2014). In enterocytes, lipids are processed by the endoplasmic reticulum and packaged into lipoprotein bundles, called chylomicrons (Hussain, 2014; Giammanco et al., 2015), to allow for transport through the circulation (Alekos et al., 2020). Once chylomicrons arrive at a target cell, lipases break them down to permit cellular import of lipids (Alekos et al., 2020). Hepatocytes are then responsible for recycling chylomicron components to allow for later use (Alekos et al., 2020).

At the cellular level, lipids are categorized into three groups: structural lipids, lipid droplets, and bioactive lipids. Structural lipids are comprised of phospholipids and form cell and organelle membranes (Bohdanowicz and Grinstein, 2013), which are important for cellular compartmentalization. Lipids are also a main source of energy and are stored as modified sterols and fatty acids in specialized organelles called lipid droplets, which are predominantly found in adipocytes (Röhrig and Schulze, 2016; Olzmann and Carvalho, 2019). This modification gives sterols and fatty acids a neutral charge to form sterol esters (Korber et al., 2017) and triglycerides (Alves-Bezerra and Cohen, 2018), respectively. Bioactive lipids are unique in that they are involved in signal transduction and are categorized into multiple classes, including sphingolipids (Hannun and Obeid, 2008), diacylglycerols (Peter-Riesch et al., 1988), and eicosanoids (Levy et al., 2001). Sphingolipids are further categorized into several sub-classes, such as sphingomyelin, galactosylceramide, glucosylceramide, and sphingosine (Hannun and Obeid, 2018). Studies have shown that sphingolipids can modulate cell death and survival pathways, including apoptosis, cell growth/inhibition, and migration (Hannun and Obeid, 2018). Diacylglycerols serve as a secondary messenger in many critical cellular processes, such as neurotransmitter release (Ma et al., 2013) and insulin signaling in islet cells (Peter-Riesch et al., 1988). Eicosanoids have been implicated in mediating the inflammatory response (Levy et al., 2001). Lipids are exceedingly important for many cellular processes, from structure to signaling. In this review, we focus on the role of the p53 family proteins in cholesterol and fatty acid metabolism. **Table 1** provides a summary of the p53 family targets that are involved in lipid metabolism, and **Figure 2** briefly outlines cholesterol and fatty acid metabolism pathways.

p53

Cholesterol

Multiple studies have shown that p53 is implicated in regulating the levels of intracellular free cholesterol. Sterol Regulatory Element-Binding Protein 2 (SREBP-2) is a master transcriptional regulator of the mevalonate pathway and responds to sterol depletion by promoting cholesterol synthesis (Brown and Goldstein, 1997). It was found that p53 inhibits SREBP-2 maturation through the upregulation of *ABCA1* (Moon et al., 2019), an ATP-binding cassette transporter that inhibits cholesterol synthesis and drives cholesterol export when cholesterol stores are high (Yamauchi et al., 2015). Additionally, p53 can promote cholesterol export through the upregulation of *CAV1* (Bist et al., 2000), a scaffold protein that binds intracellular free cholesterol and facilitates its efflux (Fielding and Fielding, 1995). To enhance cellular cholesterol storage, p53 transactivates dehydrogenase/reductase member 3 (DHSR3) (Kirschner et al., 2010; Deisenroth et al., 2011), which decreases intracellular free cholesterol by increasing lipid droplet formation (Martin and Parton, 2006). Conversely, p53 has been shown to inhibit cholesterol storage by negatively regulating *SOAT1* (Oni et al., 2020). SOAT1 decreases intracellular free cholesterol by increasing cholesterol storage, thus disrupting the negative feedback loop that prevents cholesterol synthesis when free intracellular cholesterol levels are high (Oelkers et al., 1998). Furthermore, *Cyp19*, an aromatase essential for estrogen synthesis (Thompson and Siiteri, 1974), was found to be upregulated by p53, which prevents intracellular free cholesterol overload and adipocyte formation (Wang et al., 2013). One study revealed a potential link between p53 and *LIMA1*, also called *SREBP3*, in mediating cholesterol absorption in the gastrointestinal tract. p53 was shown to upregulate *LIMA1* through p53-response elements in its promoter (Ohashi et al., 2017), and LIMA1 promotes cholesterol absorption in the intestine (Zhang et al., 2018). Interestingly, there are some conflicting findings regarding p53 regulation of other mevalonate pathway genes. For example, one group showed that p53

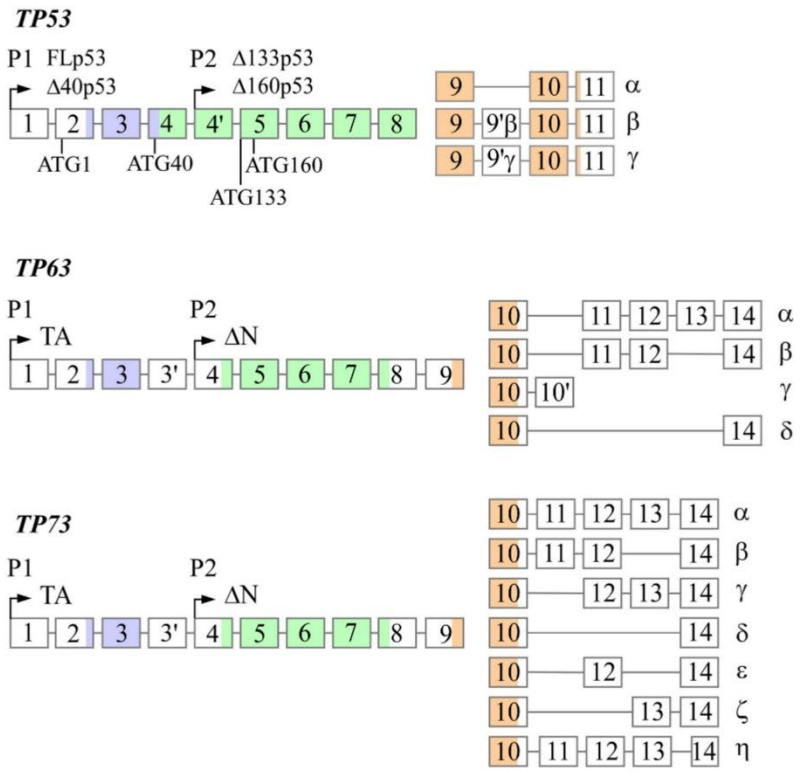

FIGURE 1 | The genomic loci of *TP53*, *TP63*, and *TP73*. All three genes contain two promoters (P1 and P2) through which transcription initiation may occur, resulting in the formation of the N-terminal isoforms. *TP53* contains four alternative translation start sites termed ATG1, ATG40, AG133, and ATG160 that give rise to FLp53, Δ40p53, Δ133p53, and Δ160p53, respectively. Alternative splicing at the 3′ end produces the C-terminal isoforms in each gene with the exception of p63γ, which results from transcriptional termination in intron 10. There exists significantly homology between each gene in the transactivation domains (purple), DNA-binding domains (green), and oligomerization domains (orange).

inhibited expression of mevalonate pathway genes *HMGCR*, *MVK*, *FDPS*, and *FDFT1* (Moon et al., 2019), but another group showed that p53 enhanced expression of these genes (Laezza et al., 2015), suggesting that p53 may regulate some mevalonate pathway genes in a context-dependent manner. Collectively, these findings suggest that multiple targets are regulated by p53 to prevent intracellular free cholesterol accumulation and to maintain the integrity of the negative feedback loop that regulates cholesterol storage and synthesis.

Fatty Acids

Fatty acid oxidation, also known as β-oxidation and hereafter referred to as FAO, is the process of breaking down long-chain fatty acids (LCFAs), primarily in the mitochondria; FAO can be initiated in peroxisomes, but the byproducts undergo complete oxidation in the mitochondria (Qu et al., 2016). LCFAs are metabolized by long-chain acyl-CoA synthetase to form acyl-CoA (Mashek et al., 2007), which is then transported into the mitochondrial matrix by a series of reactions catalyzed by the carnitine palmitoyltransferase system (Rufer et al., 2009). Acyl-CoA is then used as a substrate to initiate FAO (Qu et al., 2016). Each cycle of FAO in the matrix removes two carbons from the fatty acid, until four carbons remain; these are then used to synthesize acetyl-CoA (Qu et al., 2016).

De novo fatty acid synthesis (FAS) is the process by which cells generate fatty acids that are used in various cellular processes (Röhrig and Schulze, 2016). FAS starts with citrate produced by the tricarboxylic acid (TCA) cycle or glutamine metabolism (Akram, 2014; Röhrig and Schulze, 2016). Citrate is then cleaved by ATP-citrate lyase to form acetyl-CoA, which is the starting substrate for FAS (Zaidi et al., 2012). Acetyl-CoA carboxylases convert acetyl-CoA to malonyl-CoA (Abu-Elheiga et al., 2000), at which point fatty acid synthase (encoded by *FASN*) catalyzes the reaction between seven malonyl-CoA molecules and one acetyl-CoA molecule to form palmitate, a long-chain fatty acid (Smith et al., 2003). Palmitate is then modified in length (Jakobsson et al., 2006) and degree of saturation (Igal, 2010) to form additional fatty acids.

p53 has been shown to predominantly promote FAO (Parrales and Iwakuma, 2016). RNA-seq analysis revealed that p53 upregulates *CrOT* (peroxisomal carnitine O-octanoyltransferase) (Goldstein et al., 2012), which is responsible for transporting byproducts of peroxisomal FAO to mitochondria to allow for complete oxidation (Longo et al., 2016). Similarly, another group

showed that p53 pathway activation following γ-irradiation led to increased *CrOT* expression (Hage-Sleiman et al., 2017). In regards to mitochondrial FAO, p53 was found to upregulate *Acad11* (Jiang et al., 2015), which encodes acyl-CoA dehydrogenase and catalyzes the first step of FAO in the mitochondrial matrix (He et al., 2011). p53 can additionally promote FAO through upregulation of *MLYCD* (Liu et al., 2014), which encodes malonyl-CoA decarboxylase and converts the FAO inhibitor malonyl-CoA to acetyl-CoA (Foster, 2004). As evidenced by the name of many FAO intermediates, CoA is a critical molecule in many FAO reactions (Leonardi et al., 2005), and p53 was found to upregulate *PANK1*, which promotes CoA production (Wang et al., 2013). By complexing with FOXO3a, p53 transactivates *SIRT1* (Nemoto et al., 2004), a deacetylase that acts on histones and transcription factors to promote FAO (Rahman and Islam, 2011; Derdak et al., 2013). Activation of p53 in response to DNA damage and glucose starvation results in increased expression of *LPIN1*, a transcriptional co-activator, to promote FAO (Assaily et al., 2011). Lipin-1 also aids in diacylglycerol formation (Donkor et al., 2007), suggesting a role for p53 in diacylglycerol metabolism. There is evidence that p53 directly upregulates *CPT1C,* a neuron-specific carnitine palmitoyltransferase that transfers the acyl group from long chain fatty acyl to carnitine to initiate FAO (Lee and Wolfgang, 2012; Sanchez-Macedo et al., 2013). In addition to CPT1C, there are other tissue-specific carnitine palmitoyltransferase family members, such as CPT1a in the liver and CPT1b in muscle (Greenberg et al., 2009). Thus, it is possible that p53 might regulate FAO through CPT1a and CPT1b. p53 was shown to transactivate *ADRB3* (Kang et al., 2020), which promotes lipolysis, or the breakdown of triglycerides into fatty acids to allow for FAO (Arner and Langin, 2014). Interestingly, a p53 mutant could induce *ADRB3* to a higher degree (Kang et al., 2020). Likewise, studies showed that p53 can prevent lipogenesis through upregulation of *OPN*, which encodes osteopontin (Gómez-Santos et al., 2020). *In vivo* analyses in mouse livers showed that *OPN* levels were increased in response to an increase in p53 (Gómez-Santos et al., 2020). Conversely, a recent report showed that p53 inhibits FAO through *PGC1A* and *APLNR* in response to doxorubicin treatment in cardiomyocytes (Saleme et al., 2020). These data lead us to hypothesize that p53 could have tissue/cell-specific effects on FAO.

p53 has been shown to inhibit FAS (Parrales and Iwakuma, 2016). For example, p53 can negatively regulate transcription of SREBP-1c to inhibit FAS (Yahagi et al., 2003). SREBP-1c, a SREBP family member, is involved in triglyceride and fatty acid synthesis predominantly in the liver, which leads to fat accumulation (Shimano et al., 1997; Shimomura et al., 1998). Additionally, p53 has been implicated in inhibiting FAS through repression of NADPH production, a critical energy source utilized during FAS (Brose et al., 2016). p53 can inhibit NADPH production through negative transcriptional regulation of malic enzyme 1 and 2 (ME1 and 2) (Jiang et al., 2013). ME1/2 catalyze the formation of pyruvate from malate, which produces NADPH (Wise and Ball, 1964). Additionally, p53 prevents NADPH production through inhibition of glucose-6-phosphate dehydrogenase (G6PD) via protein-protein interaction, which requires p53's C-terminus,

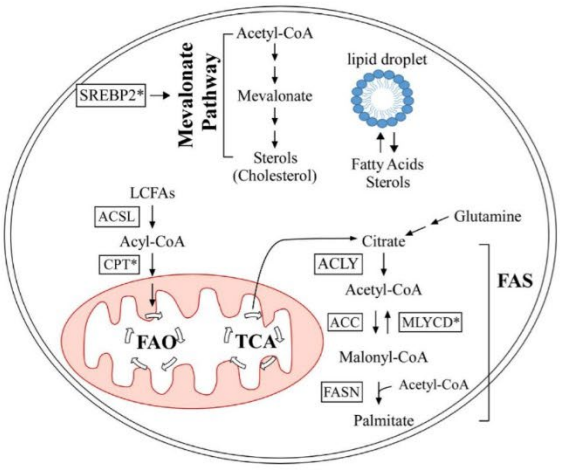

FIGURE 2 | Summary of lipid metabolism, as it pertains to the p53 family. The mevalonate pathway is out lined in the upper half. Fatty acid oxidation and synthesis are portrayed in the lower half. Proteins marked with an asterisk are regulated by the p53 family. FAO, fatty acid oxidation; TCA, tricarboxylic acid cycle; FAS, fatty acid synthesis; ACSL, long-chain acyl-CoA synthetase; CPT, carnitine palmitoyltransferase; ACLY, ATP citrate lyase; MLYCD, malonyl-CoA decarboxylase; ACC, acetyl-CoA carboxylase; FASN, fatty acid synthase; SREBP2, sterol regulatory element-binding protein 2.

DNA-binding domain, and tetramerization domain (Jiang et al., 2011). G6PD is an enzyme that catalyzes the first step of the pentose phosphate pathway (PPP), a major source of NADPH production (Ge et al., 2020). While reports show that p53 predominately inhibits NADPH production, some p53 targets have been identified as promoters of NADPH production. For example, TIGAR, a well-defined p53 target, activates PPP to drive NADPH production, which has been shown to prevent ROS formation (Bensaad et al., 2006). Additionally, it was found that p53 promotes NADPH production through suppression of PFKFB3 expression, which favors glycolysis over PPP (Franklin et al., 2016).

p63 and p73

Several studies have unveiled an important role for p63 in lipid metabolism, although the mechanisms are not fully understood. It was shown that TAp63 deficiency in mice increases the incidence of obesity and liver steatosis and impairs FAO function (Su et al., 2012; Liao et al., 2017). It was found that TAp63 promotes FAO through upregulation of *SIRT1* (a previously described p53 target) and the LKBI/AMPK pathway, the latter of which prevents the conversion of acetyl-CoA to the FAO inhibitor malonyl-CoA (Li et al., 2020). As previously mentioned, p53 promotes the production of acetyl-CoA from malonyl-CoA (Liu et al., 2014), suggesting that the p53 family can transactivate multiple targets to prevent malonyl-CoA formation. Additionally, TAp63 was shown to inhibit FAS by upregulating *CCDC3* (Liao et al., 2017), which encodes a soluble protein that binds to hepatocyte receptors (Kobayashi et al., 2010). While there is limited research on p63 and cholesterol regulation, it

has been shown that p63, like p53, inhibits cellular cholesterol accumulation through *DHSR3* (Kirschner et al., 2010) and promotes intestinal cholesterol absorption through *LIM1A* (Zhang et al., 2018).

Phenotypic similarities between p63- and p73-deficient mice suggest that p73 has an analogous role in regulating lipid metabolism. In response to nutrient deprivation, loss of p73 leads to lipid accumulation in mouse livers (He et al., 2013). Mechanistically, TAp73α/β were shown to modulate lipid metabolism through *ATG5*, a gene that is necessary for autophagy (He et al., 2013). Autophagy is an intracellular process that, among other things, can break down lipid droplets to allow for FAO (Ye et al., 2018; Saito et al., 2019). As such, gene transfer of *ATG5* to p73-knockout mice mitigated the accumulation of lipid droplets in the mouse livers (He et al., 2013). As with p53 and p63, p73β can upregulate *LIM1A* to increase cholesterol absorption (Y. Y. Zhang et al., 2018). These data suggest that p73 prevents lipid accumulation through a mechanism that is quite different from how p53 and p63 regulate this process.

IRON METABOLISM

Iron is an essential element for all living entities and plays an important role in many cellular processes, such as oxygen transport and cell proliferation (Kim and Nemeth, 2015; Wallace, 2019). Additionally, iron is a critical cofactor that is required for various metabolic activities, such as DNA synthesis (Puig et al., 2017). An organism's main source of iron is through dietary intake (Waldvogel-Abramowski et al., 2014). In the gastrointestinal tract, iron exists as non-heme- or heme-iron (Waldvogel-Abramowski et al., 2014); heme is a porphyrin that contains iron (Fiorito et al., 2020). At physiological pH, non-heme iron is present in the ferric (Fe^{3+}) state, but cells can only absorb it in the ferrous (Fe^{2+}) state (Wallace, 2019). Duodenal cytochrome B (Dcytb) reduces Fe^{3+} to Fe^{2+} in the lumen and ferrous iron is absorbed by enterocytes through divalent metal cation transporter 1 (DMCT1) (Wallace, 2019). On the other hand, heme-iron is directly imported by haem carrier protein 1 (HCP1). Once in enterocytes, iron is exported by ferroportin 1 (FPN1), whose function is inhibited by hepcidin (Waldvogel-Abramowski et al., 2014). In the plasma, Fe^{2+} is converted back to Fe^{3+} by ceruloplasmin and binds to transferrin for transport through the circulation (Attieh et al., 1999). A summary schematic of this process is shown in **Figure 3**. Once iron has entered the target cell, it binds ferritin until it is needed (Waldvogel-Abramowski et al., 2014). Regulation of iron metabolism is exceedingly important because iron overload, like in hemochromatosis (Bacon et al., 2011), can lead to heart disease and liver cirrhosis, while deficiency can result in anemia

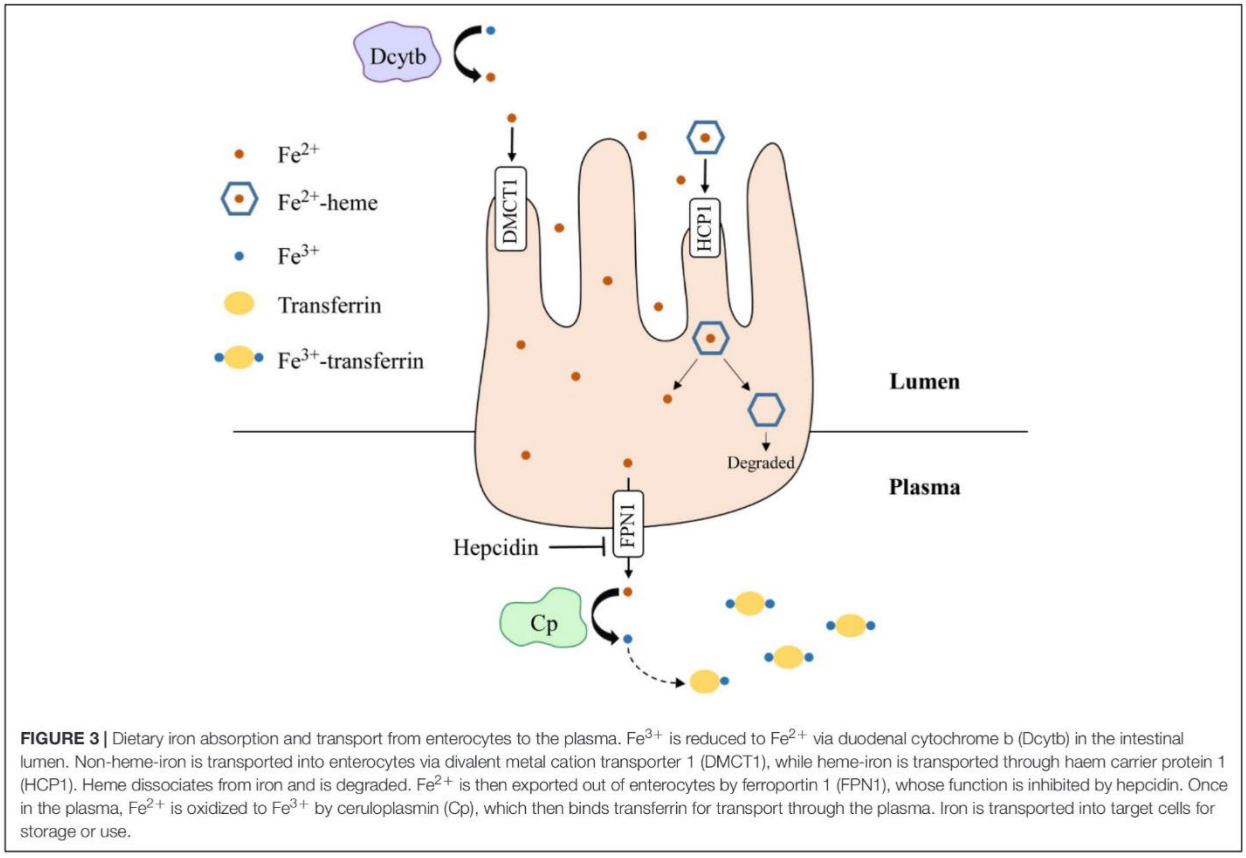

FIGURE 3 | Dietary iron absorption and transport from enterocytes to the plasma. Fe^{3+} is reduced to Fe^{2+} via duodenal cytochrome b (Dcytb) in the intestinal lumen. Non-heme-iron is transported into enterocytes via divalent metal cation transporter 1 (DMCT1), while heme-iron is transported through haem carrier protein 1 (HCP1). Heme dissociates from iron and is degraded. Fe^{2+} is then exported out of enterocytes by ferroportin 1 (FPN1), whose function is inhibited by hepcidin. Once in the plasma, Fe^{2+} is oxidized to Fe^{3+} by ceruloplasmin (Cp), which then binds transferrin for transport through the plasma. Iron is transported into target cells for storage or use.

and developmental impairments (Abbaspour et al., 2014). The p53 family has been implicated in mediating iron metabolism to prevent iron dysregulation.

p53

Iron metabolism exerts regulatory functions over p53 and in turn, p53 can regulate iron metabolism. Excess iron leads to decreased p53 expression (Shen et al., 2014), whereas iron depletion leads to p53 accumulation (Liang and Richardson, 2003; Kim et al., 2007). Additionally, direct binding of heme to p53 protein inhibits p53 transcriptional activity and possibly promotes p53 degradation (Shen et al., 2014). As such, a feedback loop between iron and p53 exists wherein iron overload inhibits p53 activity and p53 inhibits iron accumulation. At the systemic level, p53 upregulates *HAMP* (encoding hepcidin) to inhibit iron efflux from enterocytes (Weizer-Stern et al., 2007) and thus, prevents iron from entering the circulation when it is not needed. To prevent iron overload at the cellular level, p53 directly transactivates several targets, including *FXN* (frataxin) (Shimizu et al., 2014), *FDXR* (ferredoxin reductase) (Hwang et al., 2001; Liu and Chen, 2002), and *ISCU* (iron-sulfur cluster assembly enzyme) (Funauchi et al., 2015). Frataxin is an iron binding protein that regulates mitochondrial iron homeostasis to prevent iron overload (Cavadini et al., 2000) and thus, p53 upregulates frataxin to inhibit mitochondrial iron overload. Additionally, frataxin is necessary for iron-sulfur cluster (ISC) biogenesis (Shimizu et al., 2014) and ISCs are critical for mitochondrial function (Shimizu et al., 2014). In addition to aiding in electron transport during redox reactions (Johnson et al., 2005), ISCs serve as a co-factor for many essential enzymes (Baranovskiy et al., 2012). We also showed that p53 regulates mitochondrial iron metabolism through a FDXR-p53 loop (Liu and Chen, 2002; Zhang et al., 2017). FDXR plays a critical role in ISC biogenesis and steroid hormone synthesis by transferring electrons from NADPH to ferredoxin 1 and 2 (FDX1 and 2) (Brandt and Vickery, 1992; Sheftel et al., 2010). p53 drives the FDXR-p53 loop to upregulate FDXR, which then transfers electrons to FDX2, ultimately preventing iron overload at the cellular level (Zhang et al., 2017). Furthermore, p53 upregulates ISCU, which increases translation of ferritin heavy chain mRNA (*FTH1*) and destabilizes transferrin receptor mRNA (*TFRC*) (Funauchi et al., 2015), therefore increasing cellular iron storage and decreasing cellular iron import. p53 can also regulate iron metabolism through post-transcriptional modifications of Iron Regulatory Protein 1 and 2 (IRP1 and IRP2) (Zhang et al., 2008). IRP1/2 alter the expression of proteins associated with iron transport and storage by binding to conserved iron-regulatory elements (IRE) in target mRNAs (Volz, 2008). Interestingly, the binding of IRP1/2 to a target mRNA has context-dependent outcomes, wherein binding can promote both mRNA degradation and mRNA translation (Volz, 2008). Studies showed that overexpression of p53 led to reduced IRP1 and 2 activity, resulting in increased translation of ferritin mRNA and decreased stability of transferrin receptor mRNA (Zhang et al., 2008). This regulation ultimately leads to an increase in cellular iron stores and a decrease in cellular iron import.

Ferroptosis is a specific form of iron-mediated cell death in which oxidative stress from reactive oxygen species (ROS) leads to the formation of lipid peroxides and accumulation of lipid peroxides triggers the ferroptotic response (Dixon et al., 2012; Lu et al., 2018). Iron has a critical role in promoting ROS formation through several mechanisms. First, iron functions as a co-factor for enzymes that catalyze the formation of ROS (Dixon and Stockwell, 2014). In addition, Fe^{2+} reacts with hydrogen peroxide through the Fenton reaction, resulting in the production of free radicals, a potent form of ROS (Wardman and Candeias, 1996). ROS can then promote lipid peroxidation of cellular membranes, which leads to compromised membrane integrity and cellular damage (Yin et al., 2011). However, several intracellular reducing pathways have been found to block ROS and subsequent accumulation of lipid peroxides (Lu et al., 2018). Import of

TABLE 1 | Targets of the p53 family that are associated with lipid metabolism.

Gene/protein target	Function	Regulation by p53 family member
SREBP-2	Upregulates mevalonate pathway genes	Down by p53 via ABCA1
CAV1	Promotes cellular cholesterol efflux	Up by p53
DHRS3	Promotes lipid droplet formation	Up by p53 and p63
SOAT1	Promotes cholesterol storage	Down by p53
Cyp19	Prevents cholesterol accumulation	Up by p53
LIMA1	Promotes cholesterol absorption in GI tract	Up by p53/p63/p73
HMGCR, MVK, FDPS, FDFT1	Promote mevalonate pathway	Up and Down by p53
CrOT	Transports byproducts of peroxisomal FAO to mitochondria	Up by p53
Acad11	Catalyzes first step of FAO	Up by p53
MLYCD	Converts malonyl-CoA to acetyl-CoA	Up by p53
PANK1	Catalyzes rate-limiting step of CoA production	Up by p53
SIRT1	Modulates histones and transcription factors to promote FAO	Up by p53 and p63
LPIN1	Upregulates FAO-associated genes	Up by p53
CPT1C	Transfers acyl group from long-chain fatty acyl to carnitine	Up by p53
ADRB3	Promotes lipolysis	Up by p53
OPN	Inhibits lipogenesis	Up by p53
PGC1A/APLNR	Inhibits FAO in cardiomyocytes	Up by p53
SREBP-1c	Promotes triglyceride synthesis and FAS	Down by p53
ME1/ME2	Converts malate to pyruvate, which produces NADPH	Down by p53
G6PD	Catalyzes first step of PPP, which produces NADPH	Down by p53 via protein-protein interaction
TIGAR	Promotes PPP activation	Up by p53
PFKFB3	Inhibits PPP activation	Down by p53
LKB1/AMPK	Pathway represses conversion of acetyl-CoA to malonyl-CoA	Pathway activated by p63
CCDC3	Inhibits FAS by binding hepatocyte receptors	Up by p63
ATG5	Promotes lipid droplet degradation	Up by p73

cystine into the cell via system x_c^- (encoded by *SCL7A11*) ultimately results in the synthesis of glutathione, a strong antioxidant (Lu et al., 2018; Sato et al., 2018). GPX4, a member of the glutathione peroxidase family, uses glutathione as a co-activator to reduce lipid peroxides, thus preventing ferroptosis (Lu et al., 2018). Ferroptosis has been implicated in a variety of diseases, such as cell death during ischemia (Gao et al., 2015) and neurodegeneration in Alzheimer's disease (Masaldan et al., 2019). Interestingly, p53 can promote and inhibit ferroptosis in a context-dependent manner (Liu et al., 2020). For example, p53 is able to inhibit ferroptosis through p21, a primary p53 target that inhibits glutathione degradation (Tarangelo and Dixon, 2018). As such, upregulation of p21 by p53 inhibits glutathione degradation and promotes GPX4 activity (Tarangelo and Dixon, 2018). p53 was also shown to prevent ferroptosis by promoting the nuclear, but inhibiting the plasma membrane, accumulation of dipeptidyl-peptidase 4 (DPP4) (Xie et al., 2017). DPP4 in the nucleus upregulates *SLC7A11*, leading to increased GPX4 function and subsequent inhibition of ferroptosis (Xie et al., 2017). Interestingly, p53 can promote ferroptosis by directly inhibiting *SLC7A11* expression (Jiang et al., 2015). Additionally, p53 promotes ferroptosis through upregulation of *SAT1*, which facilitates the production of lipid peroxides (Ou et al., 2016). A recent study showed that Mdm2 and Mdm4 can induce ferroptosis (Venkatesh et al., 2020). Since Mdm2 is a target of p53, it is possible that p53 can act through Mdm2/4 to modulate the induction of ferroptosis. The role of both wild-type and mutant p53 in ferroptosis was discussed comprehensively in a recent review (Liu et al., 2020).

p63 and p73

Recent evidence suggests an important role for p63 and p73 in iron metabolism. Like p53, p63, and p73 can be destabilized by an excess of heme (Shen et al., 2014). Conversely, iron depletion was found to stabilize p73, and possibly p63, to promote apoptosis and cell cycle arrest in a p53-independent manner (Calabrese et al., 2020). These data suggest that iron overload inhibits, whereas iron depletion promotes, p63 and p73 activity, which is similar to the effect of iron overload and depletion on p53. Recent studies in our lab revealed a potential mechanism through which iron overload can influence p63/p73 mRNA stability and protein expression. We showed that TAp63 expression can be repressed by IRP2 and likewise, IRP2 deficiency lead to increased expression of TAp63 (Zhang et al., 2020). Additionally, we showed that IRP2 binds to the IRE in p63 mRNA to regulates its stability (Zhang et al., 2020). Similarly, we found that FDXR regulates p73 mRNA stability through IRP2 (Zhang et al., 2020). These observations represent an important step in understanding how iron metabolism regulates p63 and p73.

Several lines of evidence suggest a role for p63 and p73 in mediating ferroptosis. For example, ferroptosis has been shown to promote liver steatosis and inflammation (Tsurusaki et al., 2019). We and others found that p63-deficient mice were prone to liver steatosis (Jiang et al., 2018). Additionally, both p63- and p73-deficient mice exhibited a high degree of liver inflammation (Jiang et al., 2018; Zhang et al., 2020). Moreover, before the term ferroptosis was coined, we found that p63 inhibited cell death caused by oxidative stress through GPX2 (Yan and Chen, 2006), a member of the same phospholipid peroxidase family as GPX4 (Chu, 1994). Aforementioned, ferroptosis ensues when the cell is unable to overcome oxidative stress. Another study revealed that ΔNp63 promoted glutathione metabolism, thus permitting GPX4 function and inhibiting the ferroptotic pathway (G. X. Wang et al., 2017). These findings suggest that p63 regulates ferroptosis through multiple glutathione peroxidase family members. As previously mentioned, p63 activates the LKB1/AMPK pathway and a group recently showed that this pathway inhibits ferroptosis (Li et al., 2020). While the role of p73 in ferroptosis is less studied, one report showed that TAp73-knockout mouse embryonic fibroblasts were particularly prone to oxidative stress (Agostini et al., 2016). Another study showed that TAp73 is able to mitigate the effect of oxidative stress on mitochondrial integrity (Marini et al., 2018). These data suggest a role for TAp73 in suppressing ferroptosis.

FUTURE DIRECTIONS

There is growing evidence that, in addition to mediating tumor suppression, the p53 family plays an important role in lipid and iron metabolism. However, there is a need for more research on these critical topics. It would be of interest to further explore how p53 is involved in regulating bioactive lipids. Additionally, it would be worthwhile to delve into the mechanisms by which p63/p73 regulate lipid and iron metabolism. While there is evidence that aberrant iron metabolism affects lipid metabolism and ferroptosis, how p53 engages lipid and iron metabolism in ferroptosis needs to be further explored. Moreover, several fundamental questions remain unanswered: Can p63 and p73 function independently of p53 in both lipid and iron metabolism? How does regulation of lipid and iron metabolism differ between the N- and C-terminal isoforms of each protein? Does regulation of lipid and iron metabolism by the p53 family contribute to common diseases associated with these processes, such as diabetes or anemia? Finally, can the p53 family proteins themselves, or the pathways regulated by the p53 family, be manipulated to ameliorate the effect of lipid or iron dysregulation on pathogenesis of diabetes and other diseases? A comprehensive understanding of how the p53 family mediates lipid and iron metabolism will likely provide an insight into the pathways that drive various human diseases.

AUTHOR CONTRIBUTIONS

KL, JZ, and XC wrote the article. All authors contributed to the article and approved the submitted version.

FUNDING

This work was supported in part by the NIH Grants R01 CA081237, CA224433, CA250338, and CA195828 (to XC), T32 HL007013 (to KL), and T31IP1727 (to JZ).

REFERENCES

Abbaspour, N., Hurrell, R., and Kelishadi, R. (2014). Review on iron and its importance for human health. *J. Res. Med. Sci.* 19:2.

Abu-Elheiga, L., Brinkley, W. R., Zhong, L., Chirala, S. S., Woldegiorgis, G., and Wakil, S. J. (2000). The subcellular localization of acetyl-CoA carboxylase 2. *Proc. Natl. Acad. Sci. U. S. A.* 97:4. doi: 10.1073/pnas.97.4.1444

Agostini, M., Annicchiarico-Petruzzelli, M., Melino, G., and Rufini, A. (2016). Metabolic pathways regulated by TAp73 in response to oxidative stress. *Oncotarget*. 7:21. doi: 10.18632/oncotarget.8935

Akram, M. (2014). Citric Acid Cycle and Role of its Intermediates in Metabolism. *Cell Biochem. Biophys.* 68:3. doi: 10.1007/s12013-013-9750-1

Alekos, N. S., Moorer, M. C., and Riddle, R. C. (2020). Dual Effects of Lipid Metabolism on Osteoblast Function. *Front. Endocrinol. (Lausanne).* 11:578194. doi: 10.3389/fendo.2020.578194

Alves-Bezerra, M., and Cohen, D. E. (2018). Triglyceride metabolism in the liver. *Compr. Physiol.* 8:1. doi: 10.1002/cphy.c170012

Arner, P., and Langin, D. (2014). Lipolysis in lipid turnover, cancer cachexia, and obesity-induced insulin resistance. *Trends Endocrinol. Metab.* 25:5. doi: 10.1016/j.tem.2014.03.002

Arrowsmith, C. H. (1999). Structure and function in the p53 family. *Cell Death Differ.* 6:12. doi: 10.1038/sj.cdd.4400619

Assaily, W., Rubinger, D. A., Wheaton, K., Lin, Y., Ma, W., Xuan, W., et al. (2011). ROS-mediated p53 induction of Lpin1 regulates fatty acid oxidation in response to nutritional stress. *Mol. Cell.* 44:3. doi: 10.1016/j.molcel.2011.08.038

Attieh, Z. K., Mukhopadhyay, C. K., Seshadrit, V., Tripoulas, N. A., and Fox, P. L. (1999). Ceruloplasmin ferroxidase activity stimulates cellular iron uptake by a trivalent cation-specific transport mechanism. *J. Biol. Chem.* 274:2. doi: 10.1074/jbc.274.2.1116

Bacon, B. R., Adams, P. C., Kowdley, K. V., Powell, L. W., and Tavill, A. S. (2011). Diagnosis and management of hemochromatosis: 2011 Practice Guideline by the American Association for the Study of Liver Diseases. *Hepatology.* 54:1. doi: 10.1002/hep.24330

Baranovskiy, A. G., Lada, A. G., Siebler, H. M., Zhang, Y., Pavlov, Y. I., and Tahirov, T. H. (2012). DNA polymerase δ and ζ switch by sharing accessory subunits of DNA polymerase δ. *J. Biol. Chem.* 287:21. doi: 10.1074/jbc.M112.351122

Bensaad, K., Tsuruta, A., Selak, M. A., Vidal, M. N. C., Nakano, K., Bartrons, R., et al. (2006). TIGAR, a p53-Inducible Regulator of Glycolysis and Apoptosis. *Cell*. 126:1. doi: 10.1016/j.cell.2006.05.036

Bist, A., Fielding, C. J., and Fielding, P. E. (2000). P53 Regulates Caveolin Gene Transcription, Cell Cholesterol, and Growth By a Novel Mechanism. *Biochemistry*. 39:8. doi: 10.1021/bi991721h

Bohdanowicz, M., and Grinstein, S. (2013). Role of phospholipids in endocytosis, phagocytosis, and macropinocytosis. *Physiol. Rev.* 93:1. doi: 10.1152/physrev.00002.2012

Borremans, B., Hobman, J. L., Provoost, A., and Brown, N. L. (2001). Cloning and functional analysis of human p51, which structurally and functionally resembles p53. *Nat. Med.* 4:7.

Bourdon, J.-C., Fernandes, K., Murray-Zmijewski, F., Liu, G., Diot, A., Xirodimas, D. P., et al. (2005). P53 isoforms can regulate p53 transcriptional activity. *Genes Dev.* 19:18. doi: 10.1101/gad.1339905

Brandt, M. E., and Vickery, L. E. (1992). Expression and characterization of human mitochondrial ferredoxin reductase in *Escherichia coli*. *Arch. Biochem. Biophys.* 294:2. doi: 10.1016/0003-9861(92)90749-M

Brose, S. A., Golovko, S. A., and Golovko, M. Y. (2016). Fatty acid biosynthesis inhibition increases reduction potential in neuronal cells under hypoxia. *Front. Neurosci.* 2016:10. doi: 10.3389/fnins.2016.00546

Brown, M. S., and Goldstein, J. L. (1997). The SREBP pathway: Regulation of cholesterol metabolism by proteolysis of a membrane-bound transcription factor. *Cell*. 89:3. doi: 10.1016/S0092-8674(00)80213-5

Calabrese, C., Panuzzo, C., Stanga, S., Andreani, G., Ravera, S., Maglione, A., et al. (2020). Deferasirox-dependent iron chelation enhances mitochondrial dysfunction and restores p53 signaling by stabilization of p53 family members in leukemic cells. *Int. J. Mol. Sci.* 21:20. doi: 10.3390/ijms21207674

Candi, E., Rufini, A., Terrinoni, A., Dinsdale, D., Ranalli, M., Paradisi, A., et al. (2006). Differential roles of p63 isoforms in epidermal development: Selective genetic complementation in p63 null mice. *Cell Death Differ.* 13:6. doi: 10.1038/sj.cdd.4401926

Cavadini, P., Gellera, C., Patel, P. I., and Isaya, G. (2000). Human frataxin maintains mitochondrial iron homeostasis in Saccharomyces cerevisiae. *Hum. Mol. Genet.* 9:17. doi: 10.1093/hmg/9.17.2523

Celli, J., Duijf, P., Hamel, B. C. J., Bamshad, M., Kramer, B., Smits, A. P. T., et al. (1999). Heterozygous Germline Mutations in the p53 Homolog p63 Are the Cause of EEC Syndrome. *Cell* 1999:99.

Chu, F. F. (1994). The human glutathione peroxidase genes GPX2, GPX3, and GPX4 map to chromosomes 14, 5, and 19, respectively. *Cytogenet. Genome Res.* 66:2. doi: 10.1159/000133675

Courtois, S., Verhaegh, G., North, S., Luciani, M. G., Lassus, P., Hibner, U., et al. (2002). ΔN-p53, a natural isoform of p53 lacking the first transactivation domain, counteracts growth suppression by wild-type p53. *Oncogene.* 21:44. doi: 10.1038/sj.onc.1205874

Deisenroth, C., Itahana, Y., Tollini, L., Jin, A., and Zhang, Y. (2011). P53-inducible DHRS3 is an endoplasmic reticulum protein associated with lipid droplet accumulation. *J. Biol. Chem.* 286:32. doi: 10.1074/jbc.M111.254227

Derdak, Z., Villegas, K. A., Harb, R., Wu, A. M., Sousa, A., and Wands, J. R. (2013). Inhibition of p53 attenuates steatosis and liver injury in a mouse model of non-alcoholic fatty liver disease. *J. Hepatol.* 58:4. doi: 10.1016/j.jhep.2012.11.042

Dixon, S. J., and Stockwell, B. R. (2014). The role of iron and reactive oxygen species in cell death. *Nat. Chem. Biol.* 10:1. doi: 10.1038/nchembio.1416

Dixon, S. J., Lemberg, K. M., Lamprecht, M. R., Skouta, R., Zaitsev, E. M., Gleason, C. E., et al. (2012). Ferroptosis: An iron-dependent form of nonapoptotic cell death. *Cell*. 149:5. doi: 10.1016/j.cell.2012.03.042

Donehower, L. A., Harvey, M., Slagle, B. L., Mcarthurt, M. J., Jrt, C. A. M., Butel, J. S., et al. (1991). Mice deficient for p53 are developmentally normal but susceptible to sponatenous tumors. *Nature* 1991:365.

Donkor, J., Sariahmetoglu, M., Dewald, J., Brindley, D. N., and Reue, K. (2007). Three mammalian lipins act as phosphatidate phosphatases with distinct tissue expression patterns. *J. Biol. Chem.* 282:6. doi: 10.1074/jbc.M610745200

Fielding, P. E., and Fielding, C. J. (1995). Plasma Membrane Caveolae Mediate the Efflux of Cellular Free Cholesterol. *Biochemistry* 34:44. doi: 10.1021/bi00044a004

Fiorito, V., Chiabrando, D., Petrillo, S., Bertino, F., and Tolosano, E. (2020). The Multifaceted Role of Heme in Cancer. *Front. Oncol.* 9:1540. doi: 10.3389/fonc.2019.01540

Foster, D. W. (2004). The role of the carnitine system in human metabolism. *Ann. N. Y. Acad. Sci.* 1033:1. doi: 10.1196/annals.1320.001

Franklin, D. A., He, Y., Leslie, P. L., Tikunov, A. P., Fenger, N., MacDonald, J. M., et al. (2016). P53 coordinates DNA repair with nucleotide synthesis by suppressing PFKFB3 expression and promoting the pentose phosphate pathway. *Sci. Rep.* 6:38067. doi: 10.1038/srep38067

Funauchi, Y., Tanikawa, C., Yi, Lo, P. H., Mori, J., Daigo, Y., et al. (2015). Regulation of iron homeostasis by the p53-ISCU pathway. *Sci. Rep.* 5:16497. doi: 10.1038/srep16497

Gao, M., Monian, P., Quadri, N., Ramasamy, R., and Jiang, X. (2015). Glutaminolysis and Transferrin Regulate Ferroptosis. *Mol. Cell.* 59:2. doi: 10.1016/j.molcel.2015.06.011

Ge, T., Yang, J., Zhou, S., Wang, Y., Li, Y., and Tong, X. (2020). The Role of the Pentose Phosphate Pathway in Diabetes and Cancer. *Front. Endocrinol.* 11:365. doi: 10.3389/fendo.2020.00365

Giammanco, A., Cefalù, A. B., Noto, D., and Averna, M. R. (2015). The pathophysiology of intestinal lipoprotein production. *Front. Physiol.* 6:61. doi: 10.3389/fphys.2015.00061

Goldstein, I., Ezra, O., Rivlin, N., Molchadsky, A., Madar, S., Goldfinger, N., et al. (2012). P53, a novel regulator of lipid metabolism pathways. *J. Hepatol.* 56:3. doi: 10.1016/j.jhep.2011.08.022

Gómez-Santos, B., Saenz, de Urturi, D., Nuñez-García, M., Gonzalez-Romero, F., Buque, X., et al. (2020). Liver osteopontin is required to prevent the progression of age-related nonalcoholic fatty liver disease. *Aging Cell.* 19:8. doi: 10.1111/acel.13183

Greenberg, C. R., Dilling, L. A., Thompson, G. R., Seargeant, L. E., Haworth, J. C., Phillips, S., et al. (2009). The paradox of the carnitine palmitoyltransferase type Ia P479L variant in Canadian Aboriginal populations. *Mol. Genet. Metab.* 96:4. doi: 10.1016/j.ymgme.2008.12.018

Guo, X., Keyes, W. M., Papazoglu, C., Zuber, J., Li, W., Lowe, S. W., et al. (2009). TAp63 induces senescence and suppresses tumorigenesis in vivo. *Nat. Cell Biol.* 11:12. doi: 10.1038/ncb1988

Hage-Sleiman, R., Bahmad, H., Kobeissy, H., Dakdouk, Z., Kobeissy, F., and Dbaibo, G. (2017). Genomic alterations during p53-dependent apoptosis induced by γ-irradiation of Molt-4 leukemia cells. *PLoS One* 12:e0190221. doi: 10.1371/journal.pone.0190221

Hannun, Y. A., and Obeid, L. M. (2008). Principles of bioactive lipid signalling: Lessons from sphingolipids. *Nat. Rev. Mol. Cell Biol.* 9:2. doi: 10.1038/nrm2329

Hannun, Y. A., and Obeid, L. M. (2018). Sphingolipids and their metabolism in physiology and disease. *Nat. Rev. Mol. Cell Biol.* 2018:107. doi: 10.1038/nrm.2017.107

Harms, K. L., and Chen, X. (2005). The C Terminus of p53 Family Proteins Is a Cell Fate Determinant. *Mol. Cell. Biol.* 25:5. doi: 10.1128/mcb.25.5.2014-2030.2005

Hasson, D., Feliú, F., and Gormaz, J. G. (2016). Non-alcoholic fatty liver disease and the metabolic syndrome. *Nonalcoholic Fat. Liver Dis.* 2016, 79–106. doi: 10.2174/138161207781039652

He, M., Pei, Z., Mohsen, A. W., Watkins, P., Murdoch, G., Veldhoven, P. P., et al. (2011). Identification and characterization of new long chain Acyl-CoA dehydrogenases. *Mol. Genet. Metab.* 102:4. doi: 10.1016/j.ymgme.2010.12.005

He, Z., Liu, H., Agostini, M., Yousefi, S., Perren, A., Tschan, M. P., et al. (2013). P73 regulates autophagy and hepatocellular lipid metabolism through a transcriptional activation of the ATG5 gene. *Cell Death Differ.* 20:10. doi: 10.1038/cdd.2013.104

Helton, E. S., Zhu, J., and Chen, X. (2006). The unique NH2-terminally deleted (ΔN) residues, the PXXP motif, and the PPXY motif are required for the transcriptional activity of the ΔN variant of p63. *J. Biol. Chem.* 281:5. doi: 10.1074/jbc.M507964200

Hooijmans, C. R., and Kiliaan, A. J. (2008). Fatty acids, lipid metabolism and Alzheimer pathology. *Eur. J. Pharmacol.* 585:1. doi: 10.1016/j.ejphar.2007.11.081

Hussain, M. M. (2014). Intestinal lipid absorption and lipoprotein formation. *Curr. Opin. Lipidol.* 25:3. doi: 10.1097/MOL.0000000000000084

Hwang, P. M., Bunz, F., Yu, J., Rago, C., Chan, T. A., Murphy, M. P., et al. (2001). Ferredoxin reductase affects p53-dependent, 5-fluorouracil-induced apoptosis in colorectal cancer cells. *Nat. Med.* 7:10. doi: 10.1038/nm1001-1111

Igal, R. A. (2010). Stearoyl-coa desaturase-1: A novel key player in the mechanisms of cell proliferation, programmed cell death and transformation to cancer. *Carcinogenesis.* 31:9. doi: 10.1093/carcin/bgq131

Jakobsson, A., Westerberg, R., and Jacobsson, A. (2006). Fatty acid elongases in mammals: Their regulation and roles in metabolism. *Prog. Lipid Res.* 45:3. doi: 10.1016/j.plipres.2006.01.004

Jiang, D., LaGory, E. L., KenzelmannBrož, D., Bieging, K. T., Brady, C. A., Link, N., et al. (2015). Analysis of p53 Transactivation Domain Mutants Reveals Acad11 as a Metabolic Target Important for p53 Pro-Survival Function. *Cell Rep.* 10:7. doi: 10.1016/j.celrep.2015.01.043

Jiang, L., Kon, N., Li, T., Wang, S. J., Su, T., Hibshoosh, H., et al. (2015). Ferroptosis as a p53-mediated activity during tumour suppression. *Nature.* 520:7545. doi: 10.1038/nature14344

Jiang, P., Du, W., Mancuso, A., Wellen, K. E., and Yang, X. (2013). Reciprocal regulation of p53 and malic enzymes modulates metabolism and senescence. *Nature.* 493:7434. doi: 10.1038/nature11776

Jiang, P., Du, W., Wang, X., Mancuso, A., Gao, X., Wu, M., et al. (2011). P53 regulates biosynthesis through direct inactivation of glucose-6-phosphate dehydrogenase. *Nat. Cell Biol.* 13:3. doi: 10.1038/ncb2172

Jiang, Y., Xu, E., Zhang, J., Chen, M., Flores, E., and Chen, X. (2018). The Rbm38-p63 feedback loop is critical for tumor suppression and longevity. *Oncogene.* 37:21. doi: 10.1038/s41388-018-0176-5

Johnson, D. C., Dean, D. R., Smith, A. D., and Johnson, M. K. (2005). Structure, function, and formation of biological iron-sulfur clusters. *Annu. Rev. Biochem.* 74:1. doi: 10.1146/annurev.biochem.74.082803.133518

Kaghad, M., Bonnet, H., Yang, A., Creancier, L., Biscan, J. C., Valent, A., et al. (1997). Monoallelically expressed gene related to p53 at 1p36, a region frequently deleted in neuroblastoma and other human cancers. *Cell.* 90:4. doi: 10.1016/S0092-8674(00)80540-1

Kang, J. G., Lago, C. U., Lee, J. E., Park, J. H., Donnelly, M. P., Starost, M. F., et al. (2020). A Mouse Homolog of a Human TP53 Germline Mutation Reveals a Lipolytic Activity of p53. *Cell Rep.* 30:3. doi: 10.1016/j.celrep.2019.12.074

Kim, A., and Nemeth, E. (2015). New insights into iron regulation and erythropoiesis. *Curr. Opin. Hematol.* 22:3. doi: 10.1097/MOH.0000000000000132

Kim, B. M., Choi, J. Y., Kim, Y. J., Woo, H. D., and Chung, H. W. (2007). Desferrioxamine (DFX) has genotoxic effects on cultured human lymphocytes and induces the p53-mediated damage response. *Toxicology.* 229:3. doi: 10.1016/j.tox.2006.10.022

Kirschner, R. D., Rother, K., Müller, G. A., and Engeland, K. (2010). The retinal dehydrogenase/reductase retSDR1/DHRS3 gene is activated by p53 and p63 but not by mutants derived from tumors or EEC/ADULT malformation syndromes. *Cell Cycle.* 9:11. doi: 10.4161/cc.9.11.11844

Ko, L. J., and Prives, C. (1996). P53: Puzzle and paradigm. *Genes Dev.* 10:9. doi: 10.1101/gad.10.9.1054

Kobayashi, S., Fukuhara, A., Taguchi, T., Matsuda, M., Tochino, Y., Otsuki, M., et al. (2010). Identification of a new secretory factor, CCDC3/Favine, in adipocytes and endothelial cells. *Biochem. Biophys. Res. Commun.* 392:1. doi: 10.1016/j.bbrc.2009.12.142

Korber, M., Klein, I., and Daum, G. (2017). Steryl ester synthesis, storage and hydrolysis: A contribution to sterol homeostasis. *Biochim. Biophys. Acta - Mol. Cell Biol. Lipids.* 1862:12. doi: 10.1016/j.bbalip.2017.09.002

Koster, M. I., Dai, D., Marinari, B., Sano, Y., Costanzo, A., Karin, M., et al. (2007). P63 Induces Key Target Genes Required for Epidermal Morphogenesis. *Proc. Natl. Acad. Sci. U. S. A.* 104:9. doi: 10.1073/pnas.0611376104

Laezza, C., D'Alessandro, A., Croce, L., Di, Picardi, P., Ciaglia, E., et al. (2015). P53 regulates the mevalonate pathway in human glioblastoma multiforme. *Cell Death Dis.* 6:10. doi: 10.1038/cddis.2015.279

Laurenzi, V., De Catani, M. V., Terrinoni, A., Corazzari, M., Melino, G., Constanzo, A., et al. (1999). Additional complexity in p73: Induction by mitogens in lymphoid cells and identification of two new splicing variants ε and ζ. *Cell Death Differ.* 6:5. doi: 10.1038/sj.cdd.4400521

Laurenzi, V., De Costanzo, A., Barcaroli, D., Terrinoni, A., Falco, M., Annicchiarico-Petruzzelli, M., et al. (1998). Two new p73 splice variants, γ and δ, with different transcriptional activity. *J. Exp. Med.* 188:9. doi: 10.1084/jem.188.9.1763

Lee, J., and Wolfgang, M. J. (2012). Metabolomic profiling reveals a role for CPT1c in neuronal oxidative metabolism. *BMC Biochem.* 13:23. doi: 10.1186/1471-2091-13-23

Leonardi, R., Zhang, Y. M., Rock, C. O., and Jackowski, S. (2005). Coenzyme A: Back in action. *Prog. Lipid Res.* 44, 2–3. doi: 10.1016/j.plipres.2005.04.001

Levy, B. D., Clish, C. B., Schmidt, B., Gronert, K., and Serhan, C. N. (2001). Lipid mediator class switching during acute inflammation: Signals in resolution. *Nat. Immunol.* 2:7. doi: 10.1038/89759

Li, C., Dong, X., Du, W., Shi, X., Chen, K., Zhang, W., et al. (2020). LKB1-AMPK axis negatively regulates ferroptosis by inhibiting fatty acid synthesis. *Signal Transduct. Target. Ther.* 5:187. doi: 10.1038/s41392-020-00297-2

Liang, S. X., and Richardson, D. R. (2003). The effect of potent iron chelators on the regulation of p53: Examination of the expression, localization and DNA-binding activity of p53 and the transactivation of WAF1. *Carcinogenesis.* 24:10. doi: 10.1093/carcin/bgg116

Liao, W., Liu, H., Zhang, Y., Jung, J. H., Chen, J., Su, X., et al. (2017). Ccdc3: A new P63 target involved in regulation of liver lipid metabolism. *Sci. Rep.* 7:1. doi: 10.1038/s41598-017-09228-8

Liu, G., and Chen, X. (2002). The ferredoxin reductase gene is regulated by the p53 family and sensitizes cells to oxidative stress-induced apoptosis. *Oncogene.* 21:47. doi: 10.1038/sj.onc.1205862

Liu, G., Nozell, S., Xiao, H., and Chen, X. (2004). ΔNp73β Is Active in Transactivation and Growth Suppression. *Mol. Cell. Biol.* 24:2. doi: 10.1128/mcb.24.2.487-501.2004

Liu, J., Zhang, C., Wang, J., Hu, W., and Feng, Z. (2020). The regulation of ferroptosis by tumor suppressor p53 and its pathway. *Int. J. Mol. Sci.* 21:21. doi: 10.3390/ijms21218387

Liu, Y., He, Y., Jin, A., Tikunov, A. P., Zhou, L., Tollini, L. A., et al. (2014). Ribosomal protein-Mdm2-p53 pathway coordinates nutrient stress with lipid metabolism by regulating MCD and promoting fatty acid oxidation. *Proc. Natl. Acad. Sci. U. S. A.* 111:23. doi: 10.1073/pnas.1315605111

Longo, N., Frigeni, M., and Pasquali, M. (2016). Carnitine transport and fatty acid oxidation. *Biochim. Biophys. Acta - Mol. Cell Res.* 1863:10. doi: 10.1016/j.bbamcr.2016.01.023

Lu, B., Chen, X. B., Ying, M. D., He, Q. J., Cao, J., and Yang, B. (2018). The role of ferroptosis in cancer development and treatment response. *Front. Pharmacol.* 8:992. doi: 10.3389/fphar.2017.00992

Luna, R. M. D. O., Wagner, D. S., and Lozano, G. (1995). Rescue of early embryonic lethality in mdm2-deficient mice by deletion of p53. *Nature* 378:6553. doi: 10.1038/378203a0

Ma, C., Liging, S., Seven, A. B., Xu, Y., and Rizo, J. (2013). Reconstitution of the Vital Functions of Munc18 and Munc13 in Neurotransmitter Release. *Science* 2013:339.

Mangiulli, M., Valletti, A., Caratozzolo, M. F., Tullo, A., Sbisà, E., Pesole, G., et al. (2009). Identification and functional characterization of two new transcriptional variants of the human p63 gene. *Nucleic Acids Res.* 37:18. doi: 10.1093/nar/gkp674

Marini, A., Rotblat, B., Sbarrato, T., Niklison-Chirou, M. V., Knight, J. R. P., Dudek, K., et al. (2018). TAp73 contributes to the oxidative stress response by regulating protein synthesis. *Proc. Natl. Acad. Sci. U. S. A.* 115:24. doi: 10.1073/pnas.1718531115

Marshall, C. B., Mays, D. J., Beeler, J. S., Rosenbluth, J. M., Boyd, K. L., Santos Guasch, G. L., et al. (2016). P73 Is Required for Multiciliogenesis and Regulates the Foxj1-Associated Gene Network. *Cell Rep.* 14:10. doi: 10.1016/j.celrep.2016.02.035

Martin, S., and Parton, R. G. (2006). Lipid droplets: a unified view of a dynamic organelle. *Mol. Cell* 7:912.

Masaldan, S., Belaidi, A. A., Ayton, S., and Bush, A. I. (2019). Cellular senescence and iron dyshomeostasis in alzheimer's disease. *Pharmaceuticals*. 12:2. doi: 10.3390/ph12020093

Mashek, D. G., Li, L. O., and Coleman, R. A. (2007). Long-chain acyl-CoA synthetases and fatty acid channeling. *Future Lipidol.* 2:4. doi: 10.2217/17460875.2.4.465

Mills, A. A., Zheng, B., Wang, X. J., Vogel, H., Roop, D. R., and Bradley, A. (1999). P63 Is a P53 Homologue Required for Limsb and Epidermal Morphogenesis. *Nature*. 398:6729. doi: 10.1038/19531

Moon, S. H., Huang, C. H., Houlihan, S. L., Regunath, K., Freed-Pastor, W. A., Morris, J. P., et al. (2019). P53 Represses the Mevalonate Pathway to Mediate Tumor Suppression. *Cell*. 176:3. doi: 10.1016/j.cell.2018.11.011

Nemajerova, A., Kramer, D., Siller, S. S., Herr, C., Shomroni, O., Pena, T., et al. (2016). TAp73 is a central transcriptional regulator of airway multiciliogenesis. *Genes Dev.* 30:11. doi: 10.1101/gad.279836.116

Nemoto, S., Fergusson, M. M., and Finkel, T. (2004). Nutrient availability regulates SIRT1 through a forkhead-dependent pathway. *Science* 306:5704. doi: 10.1126/science.1101731

Nostrand, J. L., Van, Brady, C. A., Jung, H., Fuentes, D. R., Kozak, M. M., et al. (2014). Inappropriate p53 activation during development induces features of CHARGE syndrome. *Nature*. 514:7521. doi: 10.1038/nature13585

Oelkers, P., Behari, A., Cromley, D., Billheimer, J. T., and Sturleyt, S. L. (1998). Characterization of two human genes encoding acyl coenzyme A: Cholesterol acyltransferase-related enzymes. *J. Biol. Chem.* 273:41. doi: 10.1074/jbc.273.41.26765

Ohashi, T., Idogawa, M., Sasaki, Y., and Tokino, T. (2017). P53 mediates the suppression of cancer cell invasion by inducing LIMA1/EPLIN. *Cancer Lett.* 390:34. doi: 10.1016/j.canlet.2016.12.034

Olzmann, J. A., and Carvalho, P. (2019). Dynamics and functions of lipid droplets. *Nat. Rev. Mol. Cell Biol.* 20:3. doi: 10.1038/s41580-018-0085-z

Oni, T. E., Biffi, G., Baker, L. A., Hao, Y., Tonelli, C., Somerville, T. D. D., et al. (2020). SOAT1 promotes mevalonate pathway dependency in pancreatic cancer. *J. Exp. Med.* 217:9. doi: 10.1084/jem.20192389

Ou, Y., Wang, S. J., Li, D., Chu, B., and Gu, W. (2016). Activation of SAT1 engages polyamine metabolism with p53-mediated ferroptotic responses. *Proc. Natl. Acad. Sci. U. S. A.* 113:44. doi: 10.1073/pnas.1607152113

Parant, J., Chavez-Reyes, A., Little, N. A., Yan, W., Reinke, V., Jochemsen, A. G., et al. (2001). Rescue of embryonic lethality in Mdm4-null mice by loss of Trp53 suggests a nonoverlapping pathway with MDM2 to regulate p53. *Nat. Genet.* 29:1. doi: 10.1038/ng714

Parrales, A., and Iwakuma, T. (2016). P53 As a Regulator of Lipid Metabolism in Cancer. *Int. J. Mol. Sci.* 17:2074. doi: 10.3390/ijms17122074

Peter-Riesch, B., Fathi, M., Schlegel, W., and Wolheim, C. B. (1988). Glucose and carbachol generate 1,2-diacylglycerols by different mechanisms in pancreatic islets. *J. Clin. Invest.* 81:4. doi: 10.1172/JCI113430

Puig, S., Ramos-Alonso, L., Romero, A. M., and Martínez-Pastor, M. T. (2017). The elemental role of iron in DNA synthesis and repair. *Metallomics*. 9:1483. doi: 10.1039/c7mt00116a

Qu, Q., Zeng, F., Liu, X., Wang, Q. J., and Deng, F. (2016). Fatty acid oxidation and carnitine palmitoyltransferase I: Emerging therapeutic targets in cancer. *Cell Death Dis.* 7:5. doi: 10.1038/cddis.2016.132

Rahman, S., and Islam, R. (2011). Mammalian Sirt1: Insights on its biological functions. *Cell Commun. Signal.* 9:11. doi: 10.1186/1478-811X-9-11

Röhrig, F., and Schulze, A. (2016). The multifaceted roles of fatty acid synthesis in cancer. *Nat. Rev. Cancer*. 16:11. doi: 10.1038/nrc.2016.89

Rufer, A. C., Thoma, R., and Hennig, M. (2009). Structural insight into function and regulation of carnitine palmitoyltransferase. *Cell. Mol. Life Sci.* 66:15. doi: 10.1007/s00018-009-0035-1

Sah, V. P., Attardi, L. D., Mulligan, G. J., Williams, B., Bronson, R. T., and Jacks, T. (1995). A subset of p53-deficient embryos exhibit exencephaly. *Nat Genet.* 10, 175–180. doi: 10.1038/ng0695-175

Saito, T., Kuma, A., Sugiura, Y., Ichimura, Y., Obata, M., Kitamura, H., et al. (2019). Autophagy regulates lipid metabolism through selective turnover of NCoR1. *Nat. Commun.* 10:1. doi: 10.1038/s41467-019-08829-3

Saleme, B., Das, S. K., Zhang, Y., Boukouris, A. E., Lorenzana Carrillo, M. A., Jovel, J., et al. (2020). P53-Mediated Repression of the PGC1A (PPARG Coactivator 1α) and APLNR (Apelin Receptor) Signaling Pathways Limits Fatty Acid Oxidation Energetics: Implications for Cardio-oncology. *J. Am. Heart Assoc.* 9:15. doi: 10.1161/JAHA.120.017247

Sanchez-Macedo, N., Feng, J., Faubert, B., Chang, N., Elia, A., Rushing, E. J., et al. (2013). Depletion of the novel p53-target gene carnitine palmitoyltransferase 1C delays tumor growth in the neurofibromatosis type i tumor model. *Cell Death Differ.* 20:4. doi: 10.1038/cdd.2012.168

Sato, M., Kusumi, R., Hamashima, S., Kobayashi, S., Sasaki, S., Komiyama, Y., et al. (2018). The ferroptosis inducer erastin irreversibly inhibits system xc- and synergizes with cisplatin to increase cisplatin's cytotoxicity in cancer cells. *Sci. Rep.* 8:968. doi: 10.1038/s41598-018-19213-4

Schmale, H., and Bamberger, C. (1997). A novel protein with strong homology to the tumor suppressor p53. *Oncogene*. 15:11. doi: 10.1038/sj.onc.1201500

Sheftel, A. D., Stehling, O., Pierik, A. J., Elsässer, H. P., Mühlenhoff, U., Webert, H., et al. (2010). Humans possess two mitochondrial ferredoxins, Fdx1 and Fdx2, with distinct roles in steroidogenesis, heme, and Fe/S cluster biosynthesis. *Proc. Natl. Acad. Sci. U. S. A.* 107:26. doi: 10.1073/pnas.1004250107

Shen, J., Sheng, X., Chang, Z. N., Wu, Q., Wang, S., Xuan, Z., et al. (2014). Iron metabolism regulates p53 signaling through direct Heme-p53 interaction and modulation of p53 localization, stability, and function. *Cell Rep.* 7:1. doi: 10.1016/j.celrep.2014.02.042

Shimano, H., Horton, J. D., Shimomura, I., Hammer, R. E., Brown, M. S., and Goldstein, J. L. (1997). Isoform 1c of sterol regulatory element binding protein is less active than isoform 1a in livers of transgenic mice and in cultured cells. *J. Clin. Invest.* 99:5. doi: 10.1172/JCI119248

Shimizu, R., Lan, N. N., Tai, T. T., Adachi, Y., Kawazoe, A., Mu, A., et al. (2014). P53 directly regulates the transcription of the human frataxin gene and its lack of regulation in tumor cells decreases the utilization of mitochondrial iron. *Gene*. 551:1. doi: 10.1016/j.gene.2014.08.043

Shimomura, I., Shimano, H., Korn, B. S., Bashmakov, Y., and Horton, J. D. (1998). Nuclear sterol regulatory element-binding proteins activate genes responsible for the entire program of unsaturated fatty acid biosynthesis in transgenic mouse liver. *J. Biol. Chem.* 273:52. doi: 10.1074/jbc.273.52.35299

Smith, S., Witkowski, A., and Joshi, A. K. (2003). Structural and functional organization of the animal fatty acid synthase. *Prog. Lipid Res.* 42:4. doi: 10.1016/S0163-7827(02)00067-X

Su, X., Gi, Y. J., Chakravarti, D., Chan, I. L., Zhang, A., Xia, X., et al. (2012). TAp63 is a master transcriptional regulator of lipid and glucose metabolism. *Cell Metab.* 16:4. doi: 10.1016/j.cmet.2012.09.006

Su, X., Paris, M., Gi, Y. J., Tsai, K. Y., Cho, M. S., Lin, Y. L., et al. (2009). TAp63 Prevents Premature Aging by Promoting Adult Stem Cell Maintenance. *Cell Stem Cell*. 5:1. doi: 10.1016/j.stem.2009.04.003

Suh, E. K., Yang, A., Kettenbach, A., Bamberger, C., Michaelis, A. H., Zhu, Z., et al. (2006). P63 Protects the Female Germ Line During Meiotic Arrest. *Nature*. 444:7119. doi: 10.1038/nature05337

Tarangelo, A., and Dixon, S. (2018). The p53-p21 pathway inhibits ferroptosis during metabolic stress. *Oncotarget*. 9:37. doi: 10.18632/oncotarget.25362

Thompson, E. A., and Siiteri, P. K. (1974). The involvement of human placental microsomal cytochrome P 450 in aromatization. *J. Biol. Chem.* 249:17. doi: 10.1016/s0021-9258(20)79736-x

Tomasini, R., Tsuchihara, K., Wilhelm, M., Fujitani, M., Rufini, A., Cheung, C. C., et al. (2008). TAp73 knockout shows genomic instability with infertility and tumor suppressor functions. *Genes Dev.* 22:19. doi: 10.1101/gad.1695308

Trink, B., Okami, K., Wu, L., Sriuranpong, V., Jen, J., and Sidransky, D. (1998). A new human p53 homologue. *Nat. Med.* 4:7. doi: 10.1038/nm0798-747

Tsurusaki, S., Tsuchiya, Y., Koumura, T., Nakasone, M., Sakamoto, T., Matsuoka, M., et al. (2019). Hepatic ferroptosis plays an important role as the trigger for initiating inflammation in nonalcoholic steatohepatitis. *Cell Death Dis.* 10:6. doi: 10.1038/s41419-019-1678-y

Venkatesh, D., O'Brien, N. A., Zandkarimi, F., Tong, D. R., Stokes, M. E., Dunn, D. E., et al. (2020). MDM2 and MDMX promote ferroptosis by PPARα-mediated lipid remodeling. *Genes Dev.* 34, 7–8. doi: 10.1101/gad.334219.119

Volz, K. (2008). The functional duality of iron regulatory protein 1. *Curr. Opin. Struct. Biol.* 18:1. doi: 10.1016/j.sbi.2007.12.010

Waldvogel-Abramowski, S., Waeber, G., Gassner, C., Buser, A., Frey, B. M., Favrat, B., et al. (2014). Physiology of iron metabolism. *Transfus. Med. Hemotherapy.* 41:3. doi: 10.1159/000362888

Wallace, D. F. (2019). Regulation of Folate Homeostasis. *Clin. Biochem.* 37:2. doi: 10.1515/9783110856262-175

Wang, G. X., Tu, H. C., Dong, Y., Skanderup, A. J., Wang, Y., Takeda, S., et al. (2017). ΔNp63 Inhibits Oxidative Stress-Induced Cell Death, Including Ferroptosis, and Cooperates with the BCL-2 Family to Promote Clonogenic Survival. *Cell Rep.* 21:10. doi: 10.1016/j.celrep.2017.11.030

Wang, S. J., Yu, G., Jiang, L., Li, T., Lin, Q., Tang, Y., et al. (2013). P53-dependent regulation of metabolic function through transcriptional activation of pantothenate kinase-1 gene. *Cell Cycle.* 12:5. doi: 10.4161/cc.23597

Wang, X., Zhao, X., Gao, X., Mei, Y., and Wu, M. (2013). A new role of p53 in regulating lipid metabolism. *J. Mol. Cell Biol.* 5:2. doi: 10.1093/jmcb/mjs064

Wardman, P., and Candeias, L. P. (1996). Fenton Chemistry: An Introduction. *Source Radiat. Res.* Vol. 145:3579270.

Weizer-Stern, O., Adamsky, K., Margalit, O., Ashur-Fabian, O., Givol, D., Amariglio, N., et al. (2007). Hepcidin, a key regulator of iron metabolism, is transcriptionally activated by p53. *Br. J. Haematol.* 138:2. doi: 10.1111/j.1365-2141.2007.06638.x

Wilhelm, M. T., Rufini, A., Wetzel, M. K., Tsuchihara, K., Inoue, S., Tomasini, R., et al. (2010). Isoform-specific p73 knockout mice reveal a novel role for ΔNp73 in the DNA damage response pathway. *Genes Dev.* 24:6. doi: 10.1101/gad.1873910

Wise, E. M., and Ball, E. G. (1964). Malic Enzyme and Lipogenesis. *Proc. Natl. Acad. Sci. U S.* 52:1933. doi: 10.1073/pnas.52.5.1255

Xie, Y., Zhu, S., Song, X., Sun, X., Fan, Y., Liu, J., et al. (2017). The Tumor Suppressor p53 Limits Ferroptosis by Blocking DPP4 Activity. *Cell Rep.* 20:7. doi: 10.1016/j.celrep.2017.07.055

Yahagi, N., Shimano, H., Matsuzaka, T., Najima, Y., Sekiya, M., Nakagawa, Y., et al. (2003). P53 Activation in Adipocytes of Obese Mice. *J. Biol. Chem.* 278:28. doi: 10.1074/jbc.M302364200

Yamauchi, Y., Iwamoto, N., Rogers, M. A., Abe-Dohmae, S., Fujimoto, T., Chang, C. C. Y., et al. (2015). Deficiency in the lipid exporter ABCA1 impairs retrograde sterol movement and disrupts sterol sensing at the endoplasmic reticulum. *J. Biol. Chem.* 290:39. doi: 10.1074/jbc.M115.662668

Yan, W., and Chen, X. (2006). GPX2, a direct target of p63, inhibits oxidative stress-induced apoptosis in a p53-dependent manner. *J. Biol. Chem.* 281:12. doi: 10.1074/jbc.M512655200

Yang, A., Kaghad, M., Wang, Y., Gillett, E., Fleming, M. D., Dötsch, V., et al. (1998). P63, a P53 Homolog At 3Q27-29, Encodes Multiple Products With Transactivating, Death-Inducing, and Dominant-Negative Activities. *Mol. Cell.* 2:3. doi: 10.1016/S1097-2765(00)80275-0

Yang, A., Schweitzer, R., Sun, D., Kaghad, M., Walker, N., Bronson, R. T., et al. (1999). P63 Is Essential for Regenerative Proliferation in Limb, Craniofacial and Epithelial Development. *Nature.* 398:6729. doi: 10.1038/19539

Yang, A., Walker, N., Bronson, R., Kaghad, M., Oosterwegel, M., Bonnin, J., et al. (2000). P73-Deficient mice have neurological, pheromonal and inflammatory defects but lack spontaneous tumours. *Nature.* 404:6773. doi: 10.1038/35003607

Ye, X., Zhou, X. J., and Zhang, H. (2018). Exploring the role of autophagy-related gene 5 (ATG5ATG5) yields important insights into autophagy in autoimmune/autoinflammatory diseases. *Front. Immunol.* 9:2334. doi: 10.3389/fimmu.2018.02334

Yin, H., Xu, L., and Porter, N. A. (2011). Free radical lipid peroxidation: Mechanisms and analysis. *Chem. Rev.* 111:10. doi: 10.1021/cr200084z

Yin, Y., Stephen, C. W., Luciani, M. G., and Fåhraeus, R. (2002). P53 Stability and Activity Is Regulated By Mdm2-Mediated Induction of Alternative P53 Translation Products. *Nat. Cell Biol.* 4:6. doi: 10.1038/ncb801

Zaidi, N., Swinnen, J. V., and Smans, K. (2012). ATP-citrate lyase: A key player in cancer metabolism. *Cancer Res.* 72:15. doi: 10.1158/0008-5472.CAN-11-4112

Zhang, F., Wang, W., Tsuji, Y., Torti, S. V., and Torti, F. M. (2008). Post-transcriptional modulation of iron homeostasis during p53-dependent growth arrest. *J. Biol. Chem.* 283:49. doi: 10.1074/jbc.M806432200

Zhang, J., Kong, X., Zhang, Y., Sun, W., Wang, J., Chen, M., et al. (2020). FDXR regulates TP73 tumor suppressor via IRP2 to modulate aging and tumor suppression. *J. Pathol.* 251:3. doi: 10.1002/path.5451

Zhang, Q., He, X., Chen, L., Zhang, C., Gao, X., Yang, Z., et al. (2012). Synergistic regulation of p53 by Mdm2 and Mdm4 is critical in cardiac endocardial cushion morphogenesis during heart development. *J. Pathol.* 228:3. doi: 10.1002/path.4077

Zhang, Y. Y., Fu, Z. Y., Wei, J., Qi, W., Baituola, G., Luo, J., et al. (2018). A LIMA1 variant promotes low plasma LDL cholesterol and decreases intestinal cholesterol absorption. *Science* 360:6393. doi: 10.1126/science.aao6575

Zhang, Y., Feng, X., Zhang, J., and Chen, X. (2020). Iron regulatory protein 2 exerts its oncogenic activities by suppressing TAp63 expression. *Mol. Cancer Res.* 18:7. doi: 10.1158/1541-7786.MCR-19-1104

Zhang, Y., Qian, Y., Zhang, J., Yan, W., Jung, Y. S., Chen, M., et al. (2017). Ferredoxin reductase is critical for p53-dependent tumor suppression via iron regulatory protein 2. *Genes Dev.* 31:12. doi: 10.1101/gad.299388.117

Zhu, J., Zhang, S., Jiang, J., and Chen, X. (2000). Definition of the p53 functional domains necessary for inducing apoptosis. *J. Biol. Chem.* 275:51. doi: 10.1074/jbc.M005676200

Zhu, J., Zhou, W., Jiang, J., and Chen, X. (1998). Identification of a novel p53 functional domain that is necessary for mediating apoptosis. *J. Biol. Chem.* 273:21. doi: 10.1074/jbc.273.21.13030

Conflict of Interest: The authors declare that the research was conducted in the absence of any commercial or financial relationships that could be construed as a potential conflict of interest.

p73α1, a p73 C-terminal isoform, regulates tumor suppression and the inflammatory response via Notch1

Kyra Nicole Laubach[a], Wensheng Yan[a,1], Xiangmudong Kong[a], Wenqiang Sun[a], Mingyi Chen[b], Jin Zhang[a,2], and Xinbin Chen[a,2]

Edited by Carol Prives, Columbia University, New York, NY; received December 22, 2021; accepted April 11, 2022

p73, a p53 family member, undergoes alternative splicing at the 3′ end to produce multiple isoforms, but their expression and activity are largely unknown. Thus, CRISPR was used to knock out exon 12 (*E12*) in human cancer cell lines and mice, leading to isoform switch from p73α to isoform p73α1. We found that p73α1 is naturally expressed and induced by DNA damage. We also found that knockout of *E12* suppresses cell growth and migration in H1299 and MIA PaCa-2 cells and promotes cellular senescence in mouse embryonic fibroblasts. Similarly, ectopic expression of p73α1 suppresses cell proliferation, whereas knockdown of p73α1 restores the cell proliferative and migratory capacities of $E12^{-/-}$ cells. Consistently, we found that $E12^{+/-}$ mice are not prone to spontaneous tumors. Instead, $E12^{+/-}$ mice are prone to systemic inflammation and exhibit elevated TNFα expression in inflamed tissues. Moreover, we found that Notch1, a master regulator of the inflammatory response, is regulated by p73α1 and highly expressed in $E12^{-/-}$ cells and inflamed $E12^{+/-}$ mouse tissues. Furthermore, through knockdown of p73α1 and/or Notch1 in $E12^{-/-}$ cells, we found that Notch1 is necessary for p73α1-mediated growth suppression. Together, these data suggest that p73α1 plays a critical role in tumor suppression and the inflammatory response via Notch1.

p53 family | p73 | p73 C-terminal isoforms | Notch1 pathway | tumor suppressor

Significance

p73 is expressed as multiple C-terminal isoforms, but their expression and activity are largely unknown. Here, we identified p73α1 as a p73 C-terminal isoform that results from exon 12 (*E12*) exclusion. We showed that *E12* deficiency in mice leads to systemic inflammation but not spontaneous tumors. We also showed that Notch1 is regulated by p73α1 and plays a critical role in p73-dependent tumor suppression and systemic inflammation.

p53 is a master transcriptional regulator and plays an integral role in tumor suppression. This feat is achieved through the ability of p53 to tightly regulate a multitude of activities, such as the cell cycle and apoptosis, in response to various genomic stressors (1). Over two decades ago, two homologs of *TP53* were discovered, and termed *TP63* (2–4) and *TP73* (5, 6). These three proteins, better known as the p53 family, exhibit significant homology in their transactivation domain (TAD), DNA-binding domain (DBD), and oligomerization domain (OD). The discovery of p73 fueled efforts to determine whether this protein has similar functions to that of p53. Total p73-knockout (p73-KO) mice were not prone to spontaneous tumors but rather had major developmental abnormalities (7). p73-KO mice exhibited reproductive impairments due to pheromone-sensing defects (7) and profound neurological malformations due to abrogated p73 signaling in Cajal–Retzius cells (7–9). These mice also displayed signs of chronic inflammation and infection in the respiratory tract, which were later explained by the indispensable role for p73 in regulating multiciliogenesis of airway epithelia (10, 11).

TP73 is expressed as two N-terminal isoforms through the use of two promoters. Promoter 1 gives rise to the TA (transactivation) isoforms that contain the conventional TAD (12), and Promoter 2 produces the N-terminally truncated ΔN isoforms (7). While ΔNp73 was originally thought to be transcriptionally inactive, it was later found to contain a group of amino acids in the N terminus that function as a unique TAD (13). Specific TAp73- or ΔNp73-KO mouse models revealed that the N terminus of p73 is important for regulating tumor suppression and oncogenesis. Like p53-KO mice, TAp73-KO mice were prone to spontaneous tumors (14), indicating that TAp73 functions as a tumor suppressor. As such, TAp73 was found to induce cell cycle arrest and apoptosis through p21 (15) and PUMA (16), two common p53 targets. Moreover, TAp73 was shown to maintain genome stability through the Bub family proteins (17). On the other hand, ΔNp73-KO mice exhibited neurological defects but were not prone to spontaneous tumors (18). Later studies demonstrated that ΔNp73 functions as an oncogene by forming hetero-oligomers with TAp73 and wild-type (WT) p53 to inhibit their transactivation function (19). Furthermore, ΔNp73 was shown to promote metastasis and invasion (20) and is up-regulated in a variety of cancers (19, 21, 22).

While the p73 N-terminal isoforms are well studied, the C-terminal isoforms remain largely unexplored. Alternative pre-messenger RNA (mRNA) splicing of exons 11 through 13 gives rise to seven known C-terminal isoforms (α, β, γ, δ, ε, ζ, η) (7, 23, 24). Notably, the TAD, DBD, and OD are not contained in exons 11, 12, or 13, but

Author affiliations: [a]Comparative Oncology Laboratory, Schools of Medicine and Veterinary Medicine, University of California, Davis, CA 95616; and [b]Department of Pathology, University of Texas Southwestern Medical Center, Dallas, TX 75390

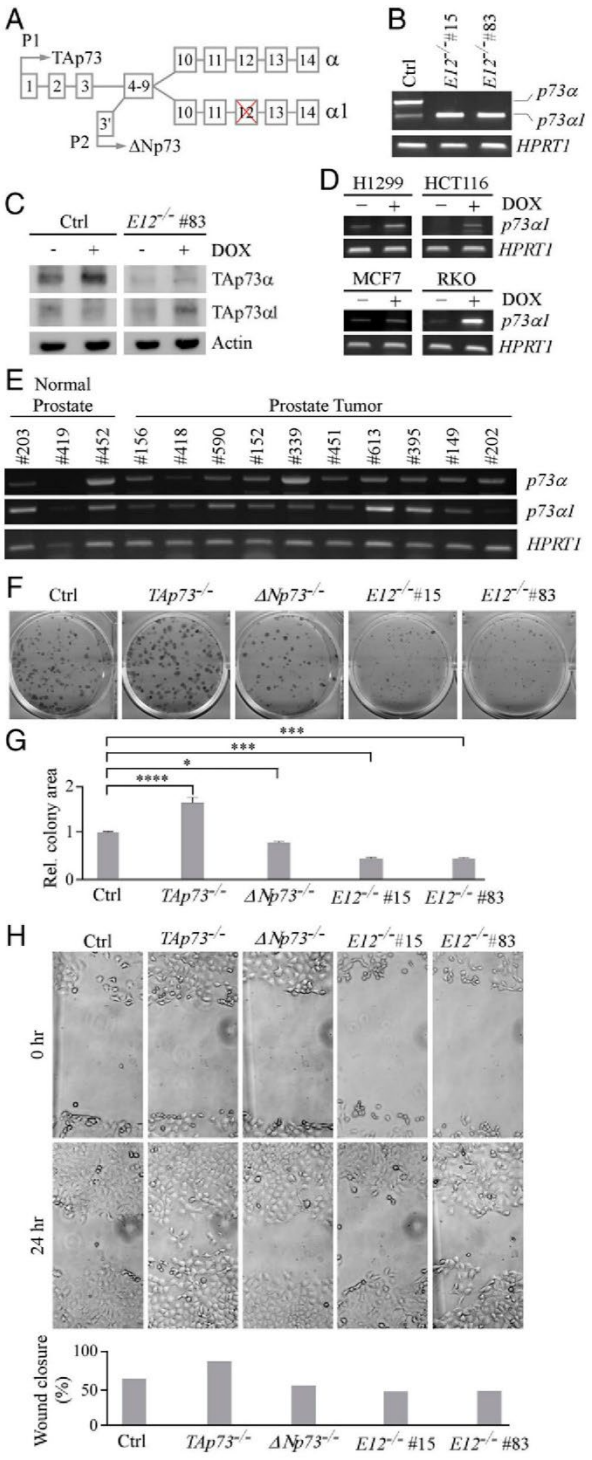

Fig. 1. Isoform switch from p73α to p73α1 inhibits cell growth and migration in H1299 cells. (*A*) Schematic representation of *TP73 E12* exclusion that leads to isoform switch from p73α to p73α1. (*B*) The level of *p73α*, *p73α1*, and *HPRT1* transcripts was measured in isogenic control and $E12^{-/-}$ H1299 cells. (*C*) The level of TAp73α, TAp73α1, and actin proteins was measured in isogenic control and $E12^{-/-}$ H1299 cells treated with (+) or without (−) 0.25 μM DOX. (*D*) The level of *p73α1* and *HPRT1* transcripts was measured in H1299, HCT116, MCF7, and RKO cells treated with (+) or without (−) 0.25 μM DOX. (*E*) The level of *p73α*, *p73α1*, and *HPRT1* transcripts was measured in normal human and tumor prostate tissues. (*F*) Colony formation assay was performed with isogenic control, $TAp73^{-/-}$, $\Delta Np73^{-/-}$, and $E12^{-/-}$ H1299 cells. (*G*) Quantification of colony formation assay shown in *F* using relative colony area. The relative colony area in isogenic control cells was arbitrarily set as 1.0. Data are presented as the mean ± SEM of three independent experiments. One-way ANOVA was used to calculate *P* values. $^{*}P < 0.05$; $^{***}P < 0.001$; $^{****}P < 0.0001$. (*H*) Isogenic control, $TAp73^{-/-}$, $\Delta Np73^{-/-}$, and $E12^{-/-}$ H1299 cells were used for scratch assays. Microscopic images were taken immediately after scratch (0 h) and 24 h later to monitor cell migration. Wound closure percentages were quantified and presented below. Ctrl, control; Rel., relative.

overexpression analyses showed that the C terminus modulates p73 transcriptional activity (25). Studies suggest the differential transactivation strengths are attributed to the presence of the sterile alpha motif (SAM) (26–28) and C-inhibitory domain (TID) (29) in exons 12 through 14. These domains are present only in full-length p73α, although a few shorter isoforms contain truncated versions of the SAM and/or TID. In normal tissues, p73α and p73β are ubiquitously expressed, but p73α is the predominant isoform (26, 27). The other isoforms appear to have a more tissue-specific expression pattern (26, 27). Recently, it was discovered that p73α is necessary for proper hippocampal development in mice, and a loss of p73α produces a neurodegenerative phenotype that is highly similar to the one observed in p73-KO mice (28). On the other hand, the same group showed that an isoform switch from p73α to p73β did not impair multiciliogenesis in airway epithelia (30), suggesting that some C-terminal isoforms have overlapping functions. While p73 is rarely mutated in cancer, overexpression is common (31–34). Interestingly, cancers with p73 overexpression exhibit a shift in isoform expression, from p73α to the less abundant isoforms (35). However, the function of these C-terminal isoforms in tumor suppression or oncogenesis remains uncertain.

To explore the implication of the p73 C-terminal isoforms in cancer, we generated exon 12 knockout (E12-KO) cancer cell lines and an *E12*-deficient mouse model. Loss of *E12* leads to the expression of two isoforms, namely, p73α1 and p73β1, from p73α and p73β, respectively. Because p73α is overwhelmingly the major isoform, we focused on characterizing the function of p73α1. We found that p73α1 is expressed in multiple cancer cell lines and normal human and tumor prostate tissue. We also found that E12-KO leads to decreased cell proliferation and migration in H1299 and MIA PaCa-2 cells but increased cellular senescence in *E12*-deficient mouse embryonic fibroblasts (MEFs) and mouse tissues. Moreover, we found that *Exon* $12^{+/-}$ ($E12^{+/-}$) mice were prone to systemic inflammation but not spontaneous tumors. Furthermore, we found that Notch1 is highly expressed in E12-KO cells and inflamed $E12^{+/-}$ mouse tissues, regulated by p73α1, and plays an important role in p73α1-mediated growth suppression. Collectively, we identify p73α1 as a naturally occurring isoform that plays a critical role in tumor suppression and the inflammatory response via Notch1.

Results

Knockout of *E12* Leads to Isoform Switch from p73α to p73α1, Decreased Colony Formation and Cell Migration, and Increased Cellular Senescence. To determine the biological function of the p73 C-terminal isoforms, CRISPR was used to generate multiple E12-KO H1299 and MIA PaCa-2 cell lines (Fig. 1*A* and *SI Appendix*, Fig. S1 *A* and *B*). Two E12-KO clones from each cell line were chosen for subsequent experiments. DNA sequencing (DNA-seq) showed a 105-nucleotide (nt) deletion in intron 11 and 45-nt deletion in *E12* in H1299 E12-KO #15, and 105-nt deletion in intron 11 and 48-nt deletion in

E12 in H1299 E12-KO #83. Thus, *E12* would be excluded due to the lack of the *E12* splice acceptor site. RT-PCR showed that *p73α* and a low level of *p73α1* were detected in isogenic control H1299 cells (Fig. 1*B*). In contrast, *p73α1*, but not *p73α*, was detected in E12-KO H1299 cells (Fig. 1*B*), suggesting that the isoform switch from p73α to p73α1 was initiated through the deletion of the splice acceptor site. Similarly, knockout of *E12* in MIA PaCa-2 cells led to a p73α-to-p73α1 isoform switch (*SI Appendix*, Fig. S2*A*). DNA-seq showed a 105-nt deletion in intron 11 and 45-nt deletion in *E12* in both E12-KO MIA PaCa-2 #47 and #61. To detect p73α1 protein expression, isogenic control and E12-KO H1299 cells were treated with doxorubicin (DOX), which is known to enhance p73 protein stability for easy detection (36). p73α was detected in isogenic control cells and stabilized by DOX (Fig. 1*C*). However, p73α1, but not p73α, was detected and stabilized by DOX in E12-KO cells (Fig. 1*C*).

Because aberrant splicing is a hallmark of cancer, we speculated that p73α1 would be expressed in tumors. To test this, RT-PCR was used to specifically amplify *p73α1*, which contains a unique DNA sequence at the junction of *E11* and *E13* (*SI Appendix*, Fig. S2*B*). We found that various levels of *p73α1* were expressed in nine different tumor cell lines, including H1299 and MIA PaCa-2 cells (Fig. 1*D* and *SI Appendix*, Fig. S2*C*). Additionally, we found that *p73α1* expression was increased following DOX treatment in H1299, HCT116, MCF7, and RKO cells (Fig. 1*D*), consistent with previous studies in which p73 transcription was induced by DNA damage (37, 38). Moreover, DNA-seq showed that the amplified complementary DNA (cDNA) was indeed *p73α1*. To confirm these findings, H1299 and MCF7 cells were treated with small interfering RNA (siRNA) against *p73α1* to specifically knock down the *p73α1* transcript (*SI Appendix*, Fig. S2*E*, *Left*). We found that upon treatment with si-p73α1, the *p73α1* transcript was markedly decreased in these cells (*SI Appendix*, Fig. S2*F*). These data indicate that the isoform p73α1 is naturally expressed in multiple cancer cell lines.

We then wanted to determine whether p73α1 is expressed in normal human and tumor tissues. First, we analyzed *p73α1* expression in normal and tumor prostate samples. We found that *p73α1* was present in both normal and tumor samples (Fig. 1*E* and *SI Appendix*, Fig. S2*D*). Next, GTEx Portal was used to analyze RNA sequencing (RNA-seq) data mapping to *TP73* in 54 different normal human tissues. Interestingly, it appeared that *E12* was not transcribed in amygdala tissue, suggesting that TAp73α1 and/or ΔNp73α1 are highly expressed in normal tissues in a tissue-dependent manner.

Given that p73α1 was detected in cancer cell lines, normal tissues, and prostate tumors, we wanted to explore why a p73α-to-p73α1 isoform switch might occur. First, RNA-seq was performed to compare the gene expression pattern between isogenic control and E12-KO H1299 cells. We found that the loss of *E12* led to down-regulation of numerous heterogeneous nuclear ribonucleoprotein (hnRNP) genes, which are important splicing factors (39) (*SI Appendix*, Fig. S3*A*). Second, we cross interrogated our RNA-seq data with that of prostate cancer in the The Cancer Genome Atlas (TCGA) database. We found that SNRNP200, HNRNPL, and HNRNPAB were significantly up-regulated in prostate tumors compared to normal prostate tissue (*SI Appendix*, Fig. S3*B*). SNRNP200 is associated with increased prostate cancer severity and metastasis (40), and HNRNPL is critical for prostate cancer cell growth (41). Third, the acceptor site at the junction of intron 11 and *E12* for p73α expression was compared to the one at intron 12 and *E13* for p73α1 expression. We found that the nucleotide sequence in the beginning of *E12* (GCCCCG) was completely different from the one in the beginning of E13 (TTTTTT), although the consensus AG nucleotides were conserved in introns 11 and 12 (*SI Appendix*, Fig. S3*C*). Fourth, we found that the number and composition of intronic splicing enhancer motifs in introns 11 and 12 were quite different. Enhancer motifs are bound by splicing factors and dictate the outcome of alterative splicing (42). Since some splicing factors are up- or down-regulated in tumors, a p73α-to-p73α1 isoform switch is likely induced by preferential usage of one acceptor site over the other.

To determine whether the p73α-to-p73α1 isoform switch has an effect on growth suppression, colony formation and wound healing assays were performed with E12-KO H1299 and MIA PaCa-2 cells along with the respective isogenic controls, namely, TAp73-KO and ΔNp73-KO cells. We showed that TAp73-KO promoted, whereas ΔNp73-KO inhibited, cell growth and migration (Fig. 1 *F*–*H* and *SI Appendix*, Fig. S4 *A*–*C*), consistent with previous observations that TAp73 is a tumor suppressor and ΔNp73 is necessary for cell survival (14, 22). Interestingly, we found that E12-KO suppressed cell proliferation and migration in both H1299 and MIA PaCa-2 cells (Fig. 1 *F*–*H* and *SI Appendix*, Fig. S4 *A*–*C*), suggesting that p73α1 not only compensates for the loss of p73α but also may have stronger growth-suppressive effects than p73α. To directly demonstrate the growth-suppressive activity of p73α1, we generated multiple H1299 cell lines that inducibly express TAp73α1 under the control of a tetracycline-inducible promoter (*SI Appendix*, Fig. S4*D*). We showed that upon induction of TAp73α1, cell proliferation was markedly decreased (*SI Appendix*, Fig. S4*E*).

To determine whether the loss of *E12* in murine *Trp73* leads to a p73α-to-p73α1 isoform switch and subsequently inhibits cell growth, CRISPR was used to generate an *E12*-deficient mouse model (*SI Appendix*, Fig. S5 *A* and *B* and Table S3). By intercrossing $E12^{+/-}$ mice, a cohort of WT, $E12^{+/-}$, and $E12^{-/-}$ MEFs were produced. We found that deletion of *E12* led to an isoform switch from p73α to p73α1 in mice (Fig. 2*A*). We also found that *E12-deficicency* in MEFs increased cellular senescence evidenced by an elevated expression of senescence-associated (SA)-β-galactosidase and senescent markers (PML, p130, and p21) (Fig. 2 *B* and *C*). Moreover, we showed that E12-KO suppressed MEF cell proliferation (Fig. 2*D*). We then examined the effect of *E12* deficiency on cellular senescence in vivo and found that the loss of *E12* led to an increased expression of senescent markers p21 and p16 in liver and kidney tissues and increased SA-β-galactosidase staining in kidney tissue as compared to age- and sex-matched WT tissues (Fig. 2 *E*–*G*). These results indicate that the p73α-to-p73α1 isoform switch and the accompanying growth-suppressive effects are conserved between human and mouse.

p73α1 Is Responsible for Growth Suppression in E12-KO Cells. To demonstrate whether the growth-suppressive effects by E12-KO are due to p73α1 activity, si-p73α1 was designed and used to specifically knock down *p73α1*, whereas si-E11 #1 and #2 were designed and used to knock down both *p73α* and *p73α1* (*SI Appendix*, Fig. S2*E*). As expected, treatment with si-E11 #2, but not si-p73α1, led to a decreased expression of *p73α* in isogenic control H1299 cells (Fig. 3 *A* and *B*, *Left* column). Consistently, cell viability and migration were increased in isogenic control H1299 cells treated with si-E11 #2, but not si-p73α1 (Fig. 3 *C*–*H*, *Left* column). We would like to note that the low level of *p73α1* in isogenic control H1299 cells was further decreased by treatment with si-E11 #2 (Fig. 3*B*). We also

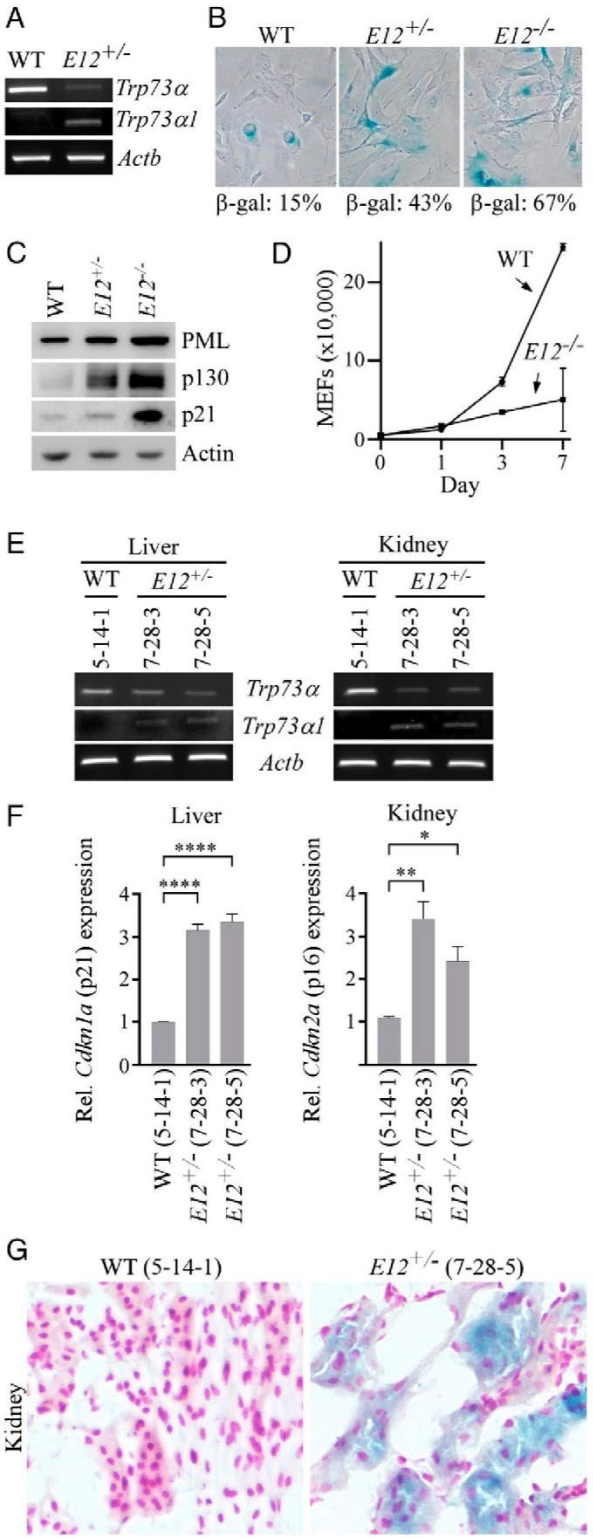

Fig. 2. The loss of *E12* in MEFs and mouse tissues leads to increased cellular senescence. (*A*) The level of *Trp73α*, *Trp73α1*, and *Actb* transcripts was measured in WT and $E12^{+/-}$ MEFs. (*B*) SA-β-galactosidase staining was performed with WT, $E12^{+/-}$, and $E12^{-/-}$ MEFs. The percentage of SA-β-gal-positive cells was shown in each panel. (*C*) The level of PML, p130, p21, and actin proteins was measured in WT, $E12^{+/-}$, and $E12^{-/-}$ MEFs. (*D*) Growth curves were performed with WT and $E12^{-/-}$ MEFs over 7 d. (*E*) The level of *Trp73α*, *Trp73α1*, and *Actb* transcripts was measured in liver and kidney tissues from age- and sex-matched WT and $E12^{+/-}$ mice (100 wk; Female). (*F*) qPCR was used to analyze relative *Cdkn1a* (p21) and *Cdkn2a* (p16) expression in liver and kidney tissues from age- and sex-matched WT and $E12^{+/-}$ mice (100 wk; Female). One-way ANOVA was used to calculate *P* values. **P* < 0.05; ***P* < 0.01; *****P* < 0.0001. (*G*) SA-β-galactosidase staining was performed with kidney tissues from age- and sex-matched WT and $E12^{+/-}$ mice (100 wk; Female).

showed that *p73α1* was knocked down in E12-KO H1299 cells upon treatment with either si-E11 #2 or si-p73α1 (Fig. 3 *A* and *B*, *Central* and *Right* columns). Consistently, cell viability and migration were restored in E12-KO H1299 cells upon knockdown of *p73α1* (Fig. 3 *C–H*, *Central* and *Right* columns), suggesting that p73α1 is responsible for the growth-suppressive effect in E12-KO cells.

$E12^{+/-}$ Mice Are Prone to Systemic Inflammation But Not Spontaneous Tumors. To determine how the isoform switch from p73α to p73α1 alters p73 biological activity, a cohort of $E12^{+/-}$, $E12^{-/-}$, and $Trp73^{+/-}$ mice were generated and monitored throughout their lifespan. To reduce the number of animals used, 55 WT and 26 $Trp73^{+/-}$ mice, which were generated and used for our earlier studies (*SI Appendix*, Tables S1 and S2) (43, 44), were used as controls. All previously generated mice were of the same genetic background and housed in the same facility as $E12^{+/-}$ mice. Initial observations revealed that $E12^{-/-}$ mice were runty and had a substantially shortened lifespan (*SI Appendix*, Fig. S5*C*). As such, $E12^{+/-}$ mice were characterized to determine p73α1 activity.

We showed that like $Trp73^{+/-}$ mice, $E12^{+/-}$ mice had a shorter lifespan than WT mice (Fig. 4*A*). However, unlike $Trp73^{+/-}$ mice, $E12^{+/-}$ mice were not prone to spontaneous tumors (Fig. 4*B*). These findings were likely due in part to increased p21 and p16 expression and increased cellular senescence in $E12^{+/-}$ mice (Fig. 2 *F* and *G*). Previous studies have found that a loss of *Trp73* leads to systemic inflammation (7), and our data yielded similar results wherein $Trp73^{+/-}$ mice exhibited inflammation in three or more organs as compared to WT mice (*SI Appendix*, Fig. S6 *A* and *B*). Interestingly, $E12^{+/-}$ mice had widespread systemic inflammation, as evidenced by a majority of mice displaying inflammation in five or more organs (Fig. 4 *C* and *D* and *SI Appendix*, Fig. S6*C*). Due to the prevalence of widespread systemic inflammation in the $E12^{+/-}$ cohort, TNFα, a common proinflammatory cytokine, was measured and compared in age- and sex-matched WT and $E12^{+/-}$ liver and salivary gland tissues. We found that TNFα was significantly increased in $E12^{+/-}$ tissues compared to both WT and $Trp73^{+/-}$ liver tissues (Fig. 4*E* and *SI Appendix*, Fig. S6*F*). Consistently, TNFα expression was significantly increased in E12-KO H1299 cells (Fig. 4*F*). Additional abnormalities observed in $E12^{+/-}$ mice included splenic hyperplasia and extramedullary hematopoiesis (EMH) (*SI Appendix*, Fig. S6 *D* and *E*). These data demonstrate that a loss of one *E12* allele in vivo leads to increased systemic inflammation but decreased tumor formation, the latter of which is consistent with the observation that E12-KO leads to growth suppression (Figs. 1 and 2).

Notch1 Is a Target of p73α1 and Plays a Critical Role in p73α1-Dependent Growth Suppression and Inflammation. To identify potential targets of p73α1 responsible for tumor suppression and inflammation in *E12*-deficient mice, RNA-seq data were analyzed to compare the differential gene expression profiles between isogenic control and E12-KO H1299 cells. Knockout of *E12* was found to modulate multiple genes involved in cell growth

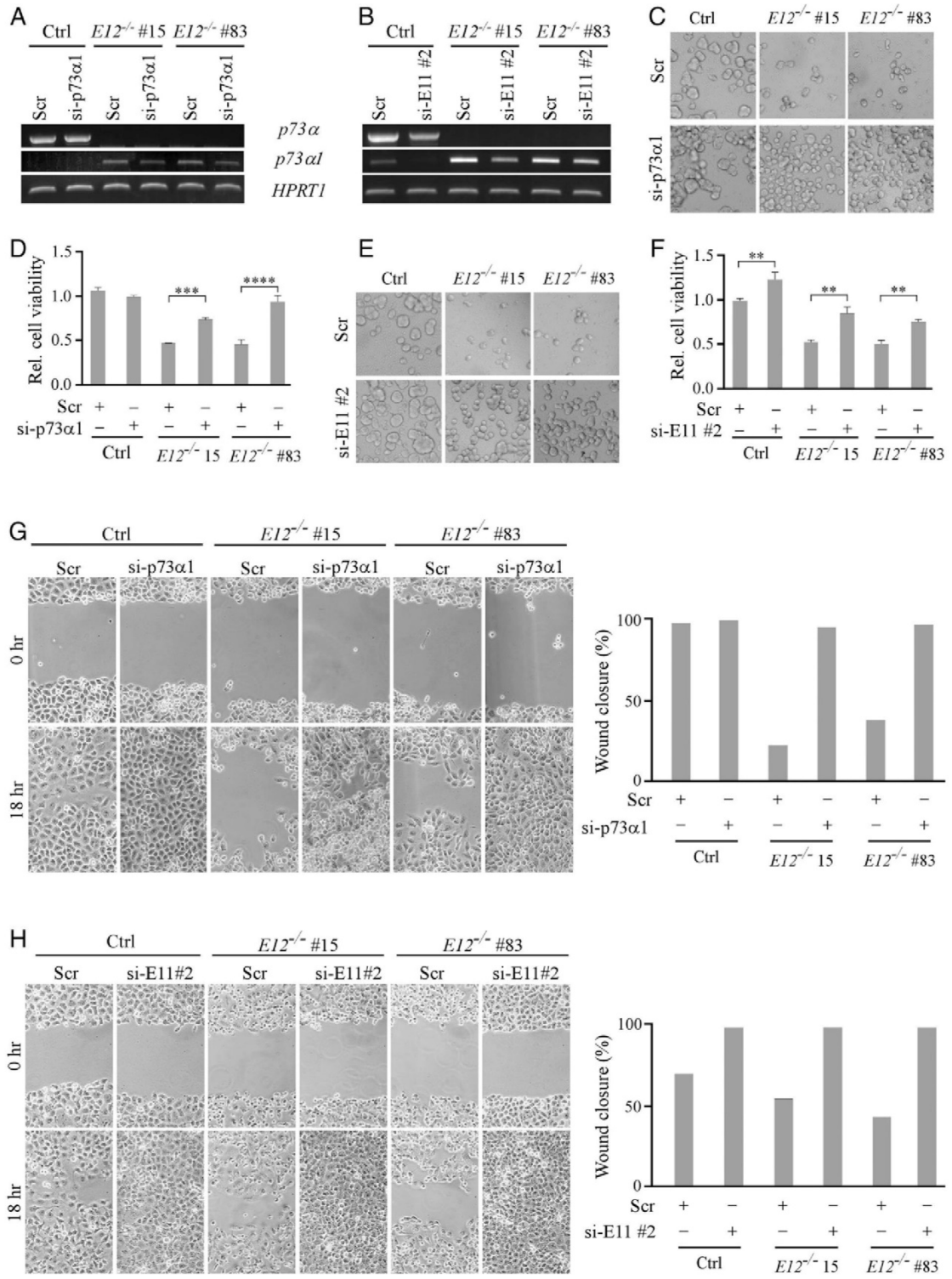

Fig. 3. p73α1 inhibits cell growth and migration in *E12*$^{-/-}$ H1299 cells. (*A* and *B*) The level of *p73α*, *p73α1*, and *HPRT1* transcripts was measured in isogenic control and *E12*$^{-/-}$ H1299 cells transiently transfected with (*A* and *B*) scrambled siRNA (Scr), (*A*) si-p73α1, or (*B*) si-E11#2 for 3 d. (*C* and *D*) Cells were treated as in *A* and used to perform a three-dimensional spheroid assay, followed by (*C*) microscopic images of spheroids and (*D*) measurement of cell viability using CellTiter-Glo 2.0 kit. The relative cell viability in isogenic control cells was arbitrarily set as 1.0. Data are presented as the mean ± SEM of three independent experiments. One-way ANOVA was used to calculate *P* values. ***$P < 0.001$; ****$P < 0.0001$. (*E* and *F*) The experiments were performed the same as in *C* and *D* except that si-E11#2 was used. One-way ANOVA was used to calculate *P* values. **$P < 0.01$. (*G*) Isogenic control and *E12*$^{-/-}$ H1299 cells were transiently transfected with Scr or si-p73α1 for 3 d and used for scratch assays. Microscopic images were taken immediately after scratch (0 h) and 18 h later to monitor cell migration. Wound closure percentages were calculated and shown to the right. (*H*) The experiments were performed same as in *G* except that si-E11#2 was used.

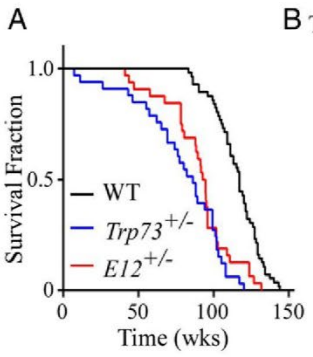

WT vs $Trp73^{+/-}$: p < 0.0001
WT vs $E12^{+/-}$: p < 0.0001
$Trp73^{+/-}$ vs $E12^{+/-}$: p = 0.0396

B Tumor spectra in WT, $Trp73^{+/-}$, and $E12^{+/-}$ mice

Tumor	WT (n = 51)*	$Trp73^{+/-}$ (n = 27)*	$E12^{+/-}$ (n = 33)
DLBCL	6	4	10
T-LBL	2	1	0
Unclassified LM	3	7	0
Sarcoma	1	1	0
Carcinoma	0	0	2
Adenoma	0	1	0
Hemangioma	0	1	0
Hepatoma	0	1	0
Penetrance	11/51	13/27	12/33

WT vs $Trp73^{+/-}$: p = 0.008
WT vs $E12^{+/-}$: p = 0.077
$Trp73^{+/-}$ vs $E12^{+/-}$: p = 0.434

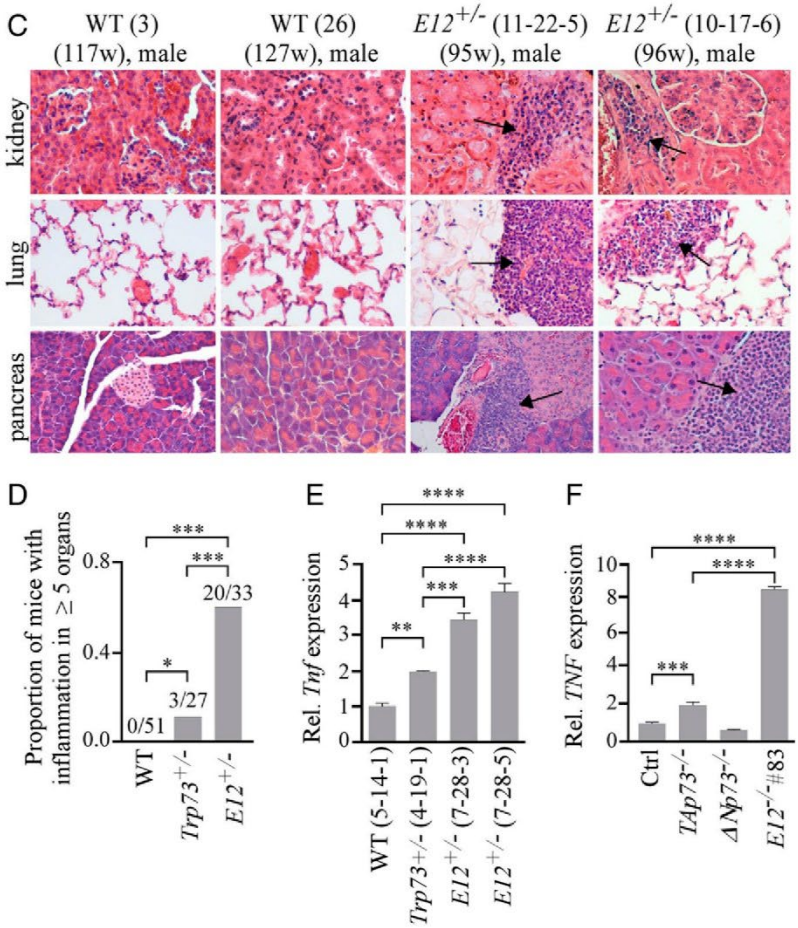

Fig. 4. $E12^{+/-}$ mice are prone to systemic inflammation, but not spontaneous tumors. (*A*) Kaplan–Meier survival curves of WT (n = 56), $Trp73^{+/-}$ (n = 27), and $E12^{+/-}$ (n = 33) mice. Median survival time was 117 wk for WT mice, 86 wk for $Trp73^{+/-}$ mice, and 93.5 wk for $E12^{+/-}$ mice. The log-rank test was used to calculate P values. (*B*) Tumor spectra in WT, $Trp73^{+/-}$, and $E12^{+/-}$ mice. The asterisk (*) indicates that found dead/hydrocephalus mice were excluded. Fisher's exact test was used to calculate P values. DLBCL, diffuse large B cell lymphoma; T-LBL, T-lymphoblastic lymphoma; LM, lymphoma. (*C*) Representative images of hematoxylin and eosin-stained kidney, lung, and pancreas tissues from sex-matched WT and $E12^{+/-}$ mice. Arrows indicate the inflammation site. (*D*) Proportion of WT, $Trp73^{+/-}$, and $E12^{+/-}$ mice with chronic inflammation in five or more organs. Fisher's exact test was used to calculate P values. *P < 0.05; ***P < 0.001. (*E*) qPCR was used to analyze relative *Tnf* (TNFα) expression in liver tissue from age- and sex-matched WT, $Trp73^{+/-}$, and $E12^{+/-}$ mice (100 wk; Female). One-way ANOVA was used to calculate P values. **P < 0.01; ***P < 0.001; ****P < 0.0001. (*F*) qPCR was used to analyze relative *TNF* (TNFα) expression in isogenic control, $TAp73^{-/-}$, $\Delta Np73^{-/-}$, and $E12^{-/-}$ H1299 cell lines. One-way ANOVA was used to calculate P values. ***P < 0.001; ****P < 0.0001.

(*CDKN1A*, *PERP*, *MAP2K1*, and *ERK*) (*SI Appendix*, Fig. S7*A*) and the inflammatory response (*NF-κB2*, *IL1R1*, *SOCS3*, and *NFKRIB*) (*SI Appendix*, Fig. S7*B*). Notably, we found that E12-KO led to up-regulation of *NOTCH1*, along with its ligands (*JAG1* and *JAG2*) and targets (*HES1* and *HEY1*) (*SI Appendix*, Fig. S7 *A* and *B*). Since Notch1 is known to mediate both cell growth (45) and inflammation (46), the genes associated with the Notch1 pathway were chosen for further investigation.

Notch1, a transmembrane receptor, is cleaved at both the extracellular and intracellular regions when bound to a ligand (47). The Notch1 Intracellular Domain (NICD) is then translocated to the nucleus where it cooperates with transcription factor CSL to regulate gene expression (47). To confirm the RNA-seq data, *NOTCH1* and *HES1* mRNAs were measured and shown to be highly induced in E12-KO H1299 and MIA PaCa-2 cells compared to TAp73-KO cells and, to a lesser extent, isogenic control cells (Fig. 5*A* and *SI Appendix*, Fig. S8*A*). This suggests that Notch1 can be induced by TAp73α1, and to a lesser extent by TAp73α (*SI Appendix*, Fig. S8*C*). We would like to note that *NOTCH1* and *HES1* mRNAs were slightly induced in ΔNp73-KO cells (Fig. 5*A* and *SI Appendix*, Fig. S8*A*). Since ΔNp73 is known to suppress TAp73 activity through hetero-oligomerization (19), a loss of ΔNp73 would increase TAp73 transcriptional activity, leading to an increased expression of *NOTCH1* and *HES1*. Similarly, we found that Notch1 NTM (transmembrane/intracellular region), NICD, and Hes1 proteins were increased in E12-KO H1299 and MIA PaCa-2 cells (Fig. 5*B* and *SI Appendix*, Fig. S8*B*). To validate that p73α1 was responsible for Notch1 induction, *NOTCH1* and *HES1* mRNAs were measured in $E12^{-/-}$ cells wherein p73α1 was knocked down by siRNA. We found that knockdown of p73α1 led to a decreased expression of *NOTCH1* and *HES1* (Fig. 5*C*).

Previous studies showed that the *NOTCH1* promoter contains a putative p53-response element (p53-RE) (48, 49). Since p73 is known to bind p53-RE to regulate its target gene expression, a chromatin immunoprecipitation (ChIP) assay was performed and showed that the *NOTCH1* promoter DNA fragment was detected in anti-TAp73 immunoprecipitates from both isogenic control and E12-KO H1299 cells (Fig. 5*D*). These results suggest that like p53, both TAp73α and TAp73α1 are capable of binding to the Notch1 promoter to regulate its expression. To determine whether the induction of Notch1 is correlated with inflammation in $E12^{+/-}$ mouse tissues, the levels of *Notch1* and *Hes1* mRNAs were measured and found to be significantly up-regulated in inflamed $E12^{+/-}$ liver, salivary gland, and spleen tissues compared to age- and sex-matched WT counterparts (Fig. 5 *E*–*G* and *SI Appendix*, Fig. S8*D*). These findings suggest that the isoform switch from p73α to p73α1 leads to an increased expression of Notch1, thus contributing to the widespread systemic inflammation in $E12^{+/-}$ mice.

In addition to promoting the inflammatory response, Notch1 is a context-dependent tumor suppressor (45). Thus, p73α1 might activate Notch1 to induce growth suppression, making $E12^{+/-}$ mice less tumor prone. To test this, colony formation and wound healing assays were performed with isogenic control and E12-KO H1299 cells in which Notch1 was knocked down by siRNA (Fig. 6*A*). As expected, knockdown of Notch1 had little if any effect on cell proliferation and migration in isogenic control cells (Fig. 6*B* and *SI Appendix*, Fig. S9), suggesting that knockdown of a low basal level of NICD would not have a measurable effect on cell growth. In contrast, we found that knockdown of Notch1 restored cell proliferation and migration in E12-KO cells (Fig. 6*B* and *SI Appendix*, Fig. S9). To confirm that Notch1 is necessary for p73α1-mediated tumor suppression, p73α1 was knocked down alone or together with Notch1 in E12-KO cells (Fig. 6 *C* and *D*). We showed that knockdown of p73α1 or Notch1 led to increased cell proliferation, which was not significantly further increased by a combined knockdown of p73α1 and Notch1 in E12-KO H1299 cells (Fig. 6*E*). Taken together, these data provide evidence that Notch1 plays a role in p73α1-dependent tumor suppression.

Discussion

p73α is the most abundant p73 isoform in human/mouse tissues and primarily responsible for p73-associated phenotypes. TAp73α is widely recognized as a tumor suppressor, as demonstrated by p73- and TAp73-KO mouse models. The complete and partial loss of p73 in mice is associated with increased tumor formation (44, 50–52). Consistently, TAp73-KO, but not ΔNp73-KO, mice are prone to genomic instability and spontaneous tumors (14, 18). Moreover, a loss of p73 is associated with tumor dissemination and transformation in multiple types of cancer (53–57). A recent study showed that isoform switch from p73α to p73β leads to profound neurological defects, but its effect on tumorigenesis was not analyzed (28). In the present study, we showed that isoform switch from p73α to p73α1 does not increase tumor formation, suggesting that TAp73α1 compensates for the loss of TAp73α and therefore functions as a tumor suppressor. Moreover, we speculate that p73α1 has a stronger transactivation activity than p73α due to differences at the extreme C terminus. p73α has a relatively low transactivation potential (25) and is the only isoform that contains both inhibitory domains SAM (58–60) and TID (29). SAM and TID can block the binding of coactivators p300/CBP to p73 TAD, therefore attenuating the transactivation potential of p73α (29). These data indicate that despite its relatively low abundance, TAp73α1 has a strong transactivation potential and plays an important role in p73-dependent tumor suppression.

It is well defined that p73α regulates tumor suppression through both common and distinct p53 family targets, such as p21, PUMA, and HIF-1α (15, 61, 62). Similarly, RNA-seq analysis showed that p73α1 regulates several p53 family targets, such as *CDKN1A* and *PERP*, suggesting that p73α1 has a similar mode of tumor suppression as other p53 family members. However, since *E12*-deficient mice are prone to inflammation but not spontaneous tumors, we speculated that a p73 target may have a dual function in growth suppression and inflammation. Indeed, we found that Notch1, a master regulator of inflammatory response, is induced by p73α1 in E12-KO cells and *E12*-deficient mice (Fig. 5). Our data indicate that the induction of Notch1/p21/p16 and cellular senescence by p73α1 plays a role in mitigating the susceptibility of $E12^{+/-}$ mice to spontaneous tumors. This observation is consistent with published studies that Notch1 functions as a tumor suppressor in a p53-dependent manner (48, 49, 63) by suppressing oncogenic kinases (ROCK1/2 and MRCKα) (48) or Wnt signaling (64, 65). Additionally, studies showed that normal levels of Notch1 are necessary for maintaining malignant tumor growth, whereas overexpression of Notch1 inhibits tumor progression (66, 67). Moreover, Notch1 is decreased in late-stage cervical tumors, suggesting that excessive Notch1 signaling impairs tumor invasion and metastasis (68).

Mice deficient in total p73 or TAp73 are prone to chronic inflammation (7, 44, 50–52). Whether or not mice deficient in

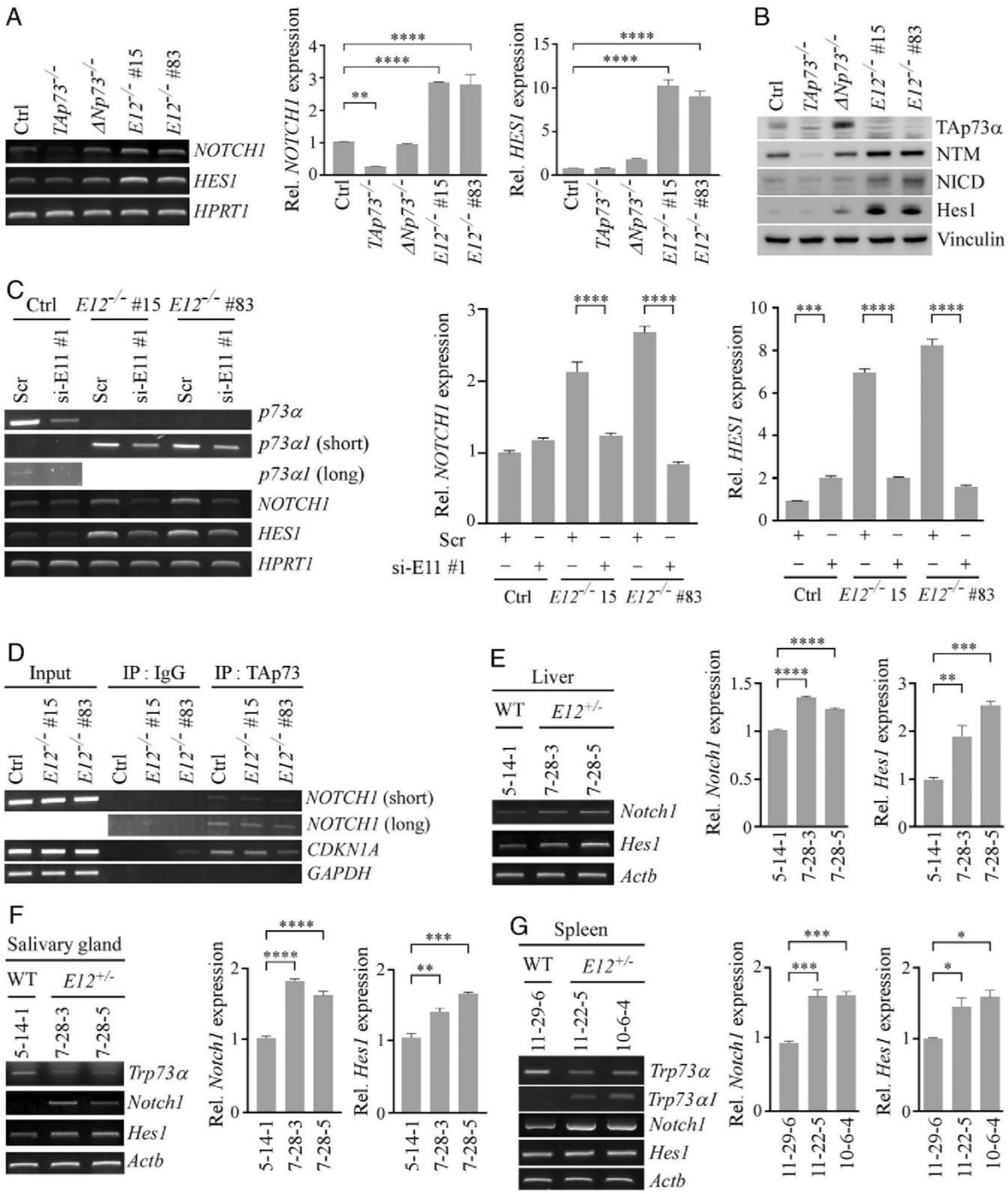

Fig. 5. Notch1 is a direct target of p73α1 and highly expressed in inflamed $E12^{+/-}$ mouse tissues. (*A*) The level of *NOTCH1*, *HES1*, and *HPRT1* transcripts was measured in isogenic control, $TAp73^{-/-}$, $\Delta Np73^{-/-}$, and $E12^{-/-}$ H1299 cells. (*Right*) qPCR was used to analyze relative *NOTCH1* and *HES1* expression. One-way ANOVA was used to calculate *P* values. $^{**}P < 0.01$; $^{****}P < 0.0001$. (*B*) The level of TAp73α, Notch1 NTM, NICD, Hes1, and vinculin proteins was measured in isogenic control, $TAp73^{-/-}$, $\Delta Np73^{-/-}$, and $E12^{-/-}$ H1299 cells. (*C*) The level of *p73α*, *p73α1*, *NOTCH1*, *HES1*, and *HPRT1* transcripts was measured in isogenic control and $E12^{-/-}$ H1299 cells transiently transfected with Scr or si-E11#1 for 3 d. (*Right*) qPCR was used to analyze relative *NOTCH1* and *HES1* expression. One-way ANOVA was used to calculate *P* values. $^{***}P < 0.001$; $^{****}P < 0.0001$. (*D*) ChIP analysis was performed with isogenic control and $E12^{-/-}$ H1299 cells. Cell lysates were immunoprecipitated with control IgG or anti-TAp73 overnight to bring down the DNA-protein immunocomplex, and the DNA fragments were visualized by PCR with primers for *NOTCH1*, *CDKN1A*, and *GAPDH* promoters. (*E*) The levels of *Notch1*, *Hes1*, and *Actb* transcripts were measured in liver tissue from age- and sex-matched WT and $E12^{+/-}$ mice (100 wk; Female). (*Right*) qPCR was used to analyze relative *Notch1* and *Hes1* expression. One-way ANOVA was used to calculate *P* values. $^{**}P < 0.01$; $^{***}P < 0.001$; $^{****}P < 0.0001$. (*F*) The level of *Trp73α*, *Notch1*, *Hes1*, and *Actb* transcripts was measured in salivary gland tissue from age- and sex-matched WT and $E12^{+/-}$ mice (100 wk; Female). (*Right*) qPCR was used to analyze relative *Notch1* and *Hes1* expression. $^{**}P < 0.01$; $^{***}P < 0.001$; $^{****}P < 0.0001$. One-way ANOVA was used to calculate *P* values. (*G*) The level of *Trp73α*, *Trp73α1*, *Notch1*, *Hes1*, and *Actb* transcripts was measured in spleen tissue from age- and sex-matched WT and $E12^{+/-}$ mice (100 wk; Male). (*Right*) qPCR was used to analyze relative *Notch1* and *Hes1* expression. One-way ANOVA was used to calculate *P* values. $^{*}P < 0.05$; $^{***}P < 0.001$.

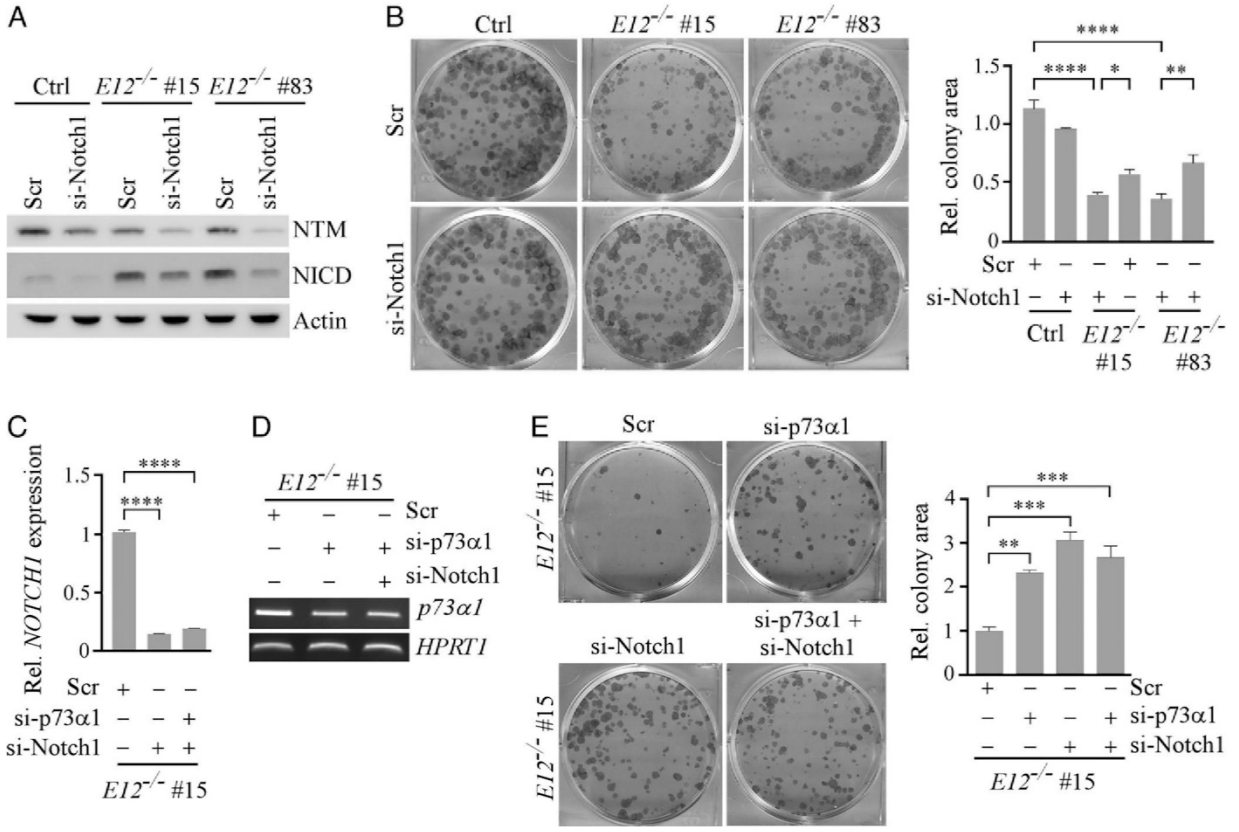

Fig. 6. Notch1 is necessary for p73α1-mediated growth suppression in H1299 cells. (*A*) The level of Notch1 NTM, NICD, and vinculin proteins was measured in isogenic control and *E12*$^{-/-}$ H1299 cells transiently transfected with Scr or si-Notch1 for 3 d. (*B*) Cells were treated as in *A* and used for the colony formation assay. (*Right*) Quantification of colony formation assay using relative colony area. The relative colony area in isogenic control cells treated with Scr was arbitrarily set as 1.0. Data are presented as the mean ± SEM of three independent experiments. One-way ANOVA was used to calculate *P* values. **P* < 0.05; ***P* < 0.01; *****P* < 0.0001. (*C*) qPCR was used to analyze relative *NOTCH1* expression in *E12*$^{-/-}$ H1299 cells transiently transfected with Scr, si-Notch1, or si-p73α1 and si-Notch1 for 3 d. One-way ANOVA was used to calculate *P* values. *****P* < 0.0001. (*D*) The level of *p73α1* and *HPRT1* transcripts was measured in *E12*$^{-/-}$ H1299 cells transiently transfected with Scr, si-p73α1, or si-p73α1 and si-Notch1 for 3 d. (*E*) Colony formation assay was performed with *E12*$^{-/-}$ H1299 cells transiently transfected with Scr, si-p73α1, si-Notch1, or both for 3 d. (*Right*) Quantification of colony formation assay using relative colony area. The relative colony area in *E12*$^{-/-}$ cells treated with Scr was arbitrarily set as 1.0. Data are presented as the mean ± SEM of three independent experiments. One-way ANOVA was used to calculate *P* values. ****P* < 0.001; *****P* < 0.0001.

ΔNp73 or *E13* (p73α to p73β isoform switch) are susceptible to chronic inflammation has not been reported (18, 28, 30). Here, we found that mice deficient in *E12* are prone to multiorgan inflammation along with an increased expression of TNFα in inflamed tissues. Mechanistically, our studies revealed three possible pathways by which p73α1 promotes systemic inflammation. First, the RNA-seq analysis showed that E12-KO leads to an induction of *NOTCH1*, its ligands (*JAG1* and *JAG2*), and its targets (*HES1* and *HEY1*). Previous studies showed that *JAG1* and *JAG2* are regulated by the p53 family proteins (69, 70). Thus, induction of *NOTCH1* and its ligands by p73α1 would amplify the potency of Notch1 to promote proinflammatory cytokine production (71), leading to systemic inflammation. Second, we showed that MEFs and mouse tissues deficient in *E12* are prone to cellular senescence. Despite their growth-arrested state, senescent cells are metabolically active and secrete an array of proteins that constitute the senescence-associated secretory phenotype (SASP). SASP includes growth factors and cytokines, such as IL-1β, IL-6, and IFN-γ. Thus, increased cytokine production by senescent cells may contribute to p73α1-mediated inflammation. Third, our RNA-seq analysis showed that E12-KO modulates several pro- and anti-inflammatory pathways, including NF-κB and SOCS3 (72, 73). While much work is needed to validate these RNA-seq data, it is likely that some of these alterations may directly, or together with Notch1 and SASP, promote p73α1-dependent systemic inflammation.

In summary, we identified p73α1 as a naturally expressed C-terminal isoform. Despite its relatively low abundance, p73α1 has a strong transactivation potential due to a lack of C-terminal inhibitory domains and can compensate for the loss of TAp73α in tumor suppression. We also revealed that p73α1 regulates tumor suppression and the inflammatory response in part through Notch1. Considering that the function of multiple p73 C-terminal isoforms is unclear, exon exclusion by CRISPR to induce isoform switch should be further explored to determine how p73 exerts its activity in tumor suppression.

Materials and Methods

Reagents. Anti-Actin (catalog number [Cat#] sc-47778, 1:2,000), anti-p130 (Cat# sc-374521, 1:3,000), anti-p21 (Cat# sc-53870, 1:3,000), anti-p130 (Cat# sc-374521, 1:3,000), and anti-PML (Cat# sc-377390, 1:3,000) were purchased from Santa Cruz Biotechnology. Anti-TAp73 (Cat# A300-126A, 1:1,000) was purchased from Bethyl Laboratories, Inc. Anti-HA (Cat# 901513, 1:2,000) was purchased from BioLegend. Anti-Cleaved Notch1 (Cat# 4741, 1:1,000), anti-Notch1

(Cat# 4380T, 1:1,000), and anti-Hes1 (Cat# 11988S, 1:800) were purchased from Cell Signaling Technology. WesternBright ECL HRP substrate (Cat# K-12043-D20) was purchased from Advansta. Scrambled siRNA (5′-GGC CGA UUG UCA AAU AAU U-3′), sip73α1 siRNA (5′-ACC UGG GGC CCG UGG UUU-3′), siE11 siRNA#1 (5′-GCA CAG UUC GGC AGC UAC A-3′), siE11 siRNA#2 (5′-UCC UCU CGC CCA UGA ACA A-3′), and siNotch1 siRNA (5′-ACA AAG AUA UGC AGA ACA A-3′) were purchased from Horizon Discovery Biosciences Limited. RNAiMax (Cat# 13778150, Invitrogen), Protease Inhibitor Mixture (Cat# 78438), Magnetic Protein A/G beads (Cat# 78609), RevertAid RT Reverse Transcription Kit (Cat# K1691), and DreamTaq DNA Polymerase (Cat# EP0702) were all purchased from ThermoFisher. All reagents were used according to the manufacturer's protocol.

Plasmid Generation. The pSpCas9(BB)-2A-Puro expression vector was generated by the Zhang Lab (74) and purchased from Addgene. To generate a vector expressing a single guide RNA (sgRNA) that targets TAp73, ΔNp73, or *E12*, two 25-nt oligos were annealed and cloned into the pSpCas9(BB)-2A-Puro expression vector via BbsI. To generate the pcDNA4 vector expressing HA-tagged TAp73α1, a 620-bp cDNA fragment was amplified from H1299 $E12^{-/-}$ cells and then used to replace the C terminus of the previously generated HA-TAp73α vector (29) via EcoRI and XhoI. All primer sequences were listed in *SI Appendix*, Table S4.

Cell Culture and Cell Line Generation. H1299 cells and their derivatives, HCT116 cells, MCF7 cells, and RKO cells were cultured in Dulbecco's Modified Eagle Medium (DMEM) supplemented with 10% fetal bovine serum (FBS) (Gibco, Cat# A4766801). H1299, HCT116, MCF7, and RKO cell lines were purchased from ATCC;tested negative for mycoplasma; and used at passage 20 or lower. We did not authenticate the cell lines used in this study because ATCC has thoroughly authenticated these cell lines. To generate $TAp73^{-/-}$, $\Delta Np73^{-/-}$, and $E12^{-/-}$ cell lines using CRISPR/Cas9, H1299 cells were transfected with a pSpCas9(BB)-2A-Puro vector expressing a sgRNA, and subsequently selected with puromycin (0.66 μM) for 2 to 3 wk. Individual clones were picked ,and the appropriate knockout cell lines were confirmed via Sanger DNA sequencing and/or Western blot analysis. HA-TAp73α inducible H1299 cell lines were generated previously (75). To generate HA-TAp73α1 inducible H1299 cell lines, H1299 cells expressing a tetracycline repressor were transfected with a pcDNA4-HA-TAp73α1 vector. Cells were selected with zeocin (33 μM) for 2 to 3 wk, and individual clones were picked and confirmed via Western blot analysis. To induce TAp73α or TAp73α1 expression, 1 μM tetracycline was added to the media for 24 h.

Mouse Model Generation. WT and $Trp73^{+/-}$ mice were generated as described previously (53). The E12-KO strategy was outlined in *SI Appendix*, Fig. S4*A*. E12-KO mice were generated by the Mouse Biology Program at University of California Davis. All animals and use protocols were approved by University of California Davis Institutional Animal Care and Use Committee. All genotyping primers were listed in *SI Appendix*, Table S5.

MEF Isolation. To generate WT, $E12^{+/-}$, and $E12^{-/-}$ MEFs, $E12^{+/-}$ mice were crossbred and MEFs were isolated from mouse embryos that were 12.5 to 13.5 d postcoitum, as described previously (76). MEFs were cultured in DMEM supplemented with 10% FBS, 55 μM β-mercaptoethanol, and 1× non-essential amino acids (Gibco, Cat# 11140050).

Histological Analysis. Mouse tissue was fixed in 10% (wt/vol) neutral buffered formalin, processed, and embedded in paraffin blocks. Tissues blocks were sectioned at 6 μm and stained with Modified Meyer's Hematoxylin (Richard Allan Scientific, Cat# 22-110-639) and Eosin-Y (Richard Allan Scientific, Cat# 22-110-637).

RNA Isolation, RT-PCR, and qPCR. Total RNA was isolated with the TRIzol reagent according to the manufacturer's manual, followed by cDNA synthesis using RevertAid Reverse Transcriptase. The PCR program used for amplification was 1) 94 °C for 5 min, 2) 94 °C for 30 s, 3) 60 to 63 °C for 30 s, 4) 72 °C for 30 s, and 5) 72 °C for 10 min. Steps 2 to 4 were repeated for 25 cycles to amplify ATCB, HPRT1, and GAPDH or 28 to 35 times to amplify other genes of interest. For qPCR, PowerUp Syber Green Master Mix (Applied Biosystems, Cat# A25742) was used according to the manufacturer's protocol. All primers used for RT-PCR and qPCR were listed in *SI Appendix*, Table S5.

Western Blot Analysis. Western blot analysis was performed as previously described (77). Briefly, the whole-cell lysate was harvested with 1× sodium dodecyl-sulfate (SDS) lysis buffer. Proteins were separated in a 8 to 10% SDS polyacrylamide gel, transferred to a nitrocellulose membrane, and probed with the indicated primary and secondary antibodies. The proteins were visualized by enhanced chemiluminescence using VisionWorksLS software.

ChIP Assay. The ChIP assay was performed as previously described (78). Briefly, chromatin was cross-linked in 1% formaldehyde in phosphate-buffered saline (PBS). Chromatin lysates were sonicated to yield ∼200- to 1,000-base pair DNA fragments and immunoprecipitated with 1 μg of control IgG or anti-TAp73 antibody at 4 °C overnight. The protein–DNA immunocomplex was reverse cross-linked and purified using ChIP DNA Clean & Concentrator (Cat# 50-44-363) from Zymo Research. PCR was used to amplify the DNA fragments. Primers used for ChIP assays were listed in *SI Appendix*, Table S5.

Colony Formation Assay. A total of 10^3 cells was seeded per well in a six-well plate and cultured for 15 d. At the end point, cells were fixed by methanol/glacial acetic acid (7:1, vol/vol) and then stained with 0.1% crystal violet solution. Relative colony area was quantified using ColonyArea from ImageJ (79).

Spheroid Assay. Cells were resuspended in MammoCult (Cat# 05620) (StemCell) and mixed with Matrigel (Cat# 354234) (Corning) in a 3:4 ratio. A total of 15 μL of cell/Matrigel mixture was plated in a ring-like shape in a well of 96-well plate and incubated at 37 °C for 20 min followed by the addition of 100 μL of MammoCult to the each well. At 72 h, cells were washed with PBS and treated with 50 μL of Dispase (5 mg/mL) (Corning, Cat# 354235) at 37 °C for 1.5 h. Cell viability was measured using the CellTiter-Glo 2.0 Cell Viability Assay kit (Cat# G9241) (Promega) according to the manufacturer's protocol. The assay was performed in triplicates to ensure proper statistical analyses.

Wound Healing Assay. Cells were seeded at a density of 4×10^5 in a 6-well plate and allowed to grow into monolayers. The monolayered cells were scraped with a P2 micropipette tip and washed two times with PBS. Microscopic images were taken at the indicated time points with phase contrast microscopy. Wound closure percentage was quantified using the ImageJ plugin MRI Wound Healing Tool.

Senescence Assay. The senescence assay was performed as described previously (80). Briefly, 5×10^4 primary MEFs at passage five were seeded in one well of a 6-well plate for 24 h. Cells were washed with PBS, fixed with a solution of 2% formaldehyde/0.2% glutaraldehyde for 15 min at room temperature, and then incubated with an SA-β-galactosidase staining solution (1 mg/mL 5-bromo-4-chloro-3-indolyl-β-d-galactopyranoside, 40 mm citric acid/sodium phosphate [pH 6.0], 5 mm potassium ferrocyanide, 5 mm potassium ferricyanide, 150 mm NaCl, and 2 mm $MgCl_2$) at 37 °C overnight. The percentage of senescent cells was calculated by dividing the number of SA-β-galactosidase-positive cells by the total number of cells counted. For SA-β-galactosidase staining on tissue, fresh-frozen tissue was embedded in Tissue Plus O.C.T. (optimal cutting temperature) Compound (Fisher Healthcare, Cat# 23-730-571), cryo-sectioned at 10 μm, stained according to the protocol mentioned above, and counter stained with Nuclear Fast Red Solution (RICCA, Cat# R5463200-500A).

Growth Rate Determination. To determine the rate of cell growth, $5x10^3$ WT, $E12^{+/-}$, and $E12^{-/-}$ MEFs were seeded in 60 mm diameter plates. At the time points indicated, two plates were rinsed two times with PBS to remove dead cells and debris. Live cells on the plates were trypsinized and collected separately. Cells from each plate were counted four times with the Coulter cell counter. The average number of cells from the plates was used to determine growth rate.

Statistical Analysis. The Log-rank test was used for Kaplan–Meier survival analysis. Fisher's exact test was used to determine statistical significance for the proportion of mice with inflammation, splenic hyperplasia, and EMH. One-way ANOVA was used to determine statistical significance in colony formation and tumor sphere assays and qPCR analysis. $P < 0.05$ was considered as statistically significant.

Data Availability. All study data are included in the article and/or *SI Appendix*.

ACKNOWLEDGMENTS. This work was supported in part by National Institutes of Health R01 grants (CA081237 and CA224433) and UC Davis Cancer Center Core Support Grant CA093373 to X. Chen, by TRDRP T31IP1727 to J.Z., and T32 HL007013 to K.N.L. The authors would like to graciously thank Dr. Yanhong Zhang for her technical support, and the members of the Chen Lab for their suggestions.

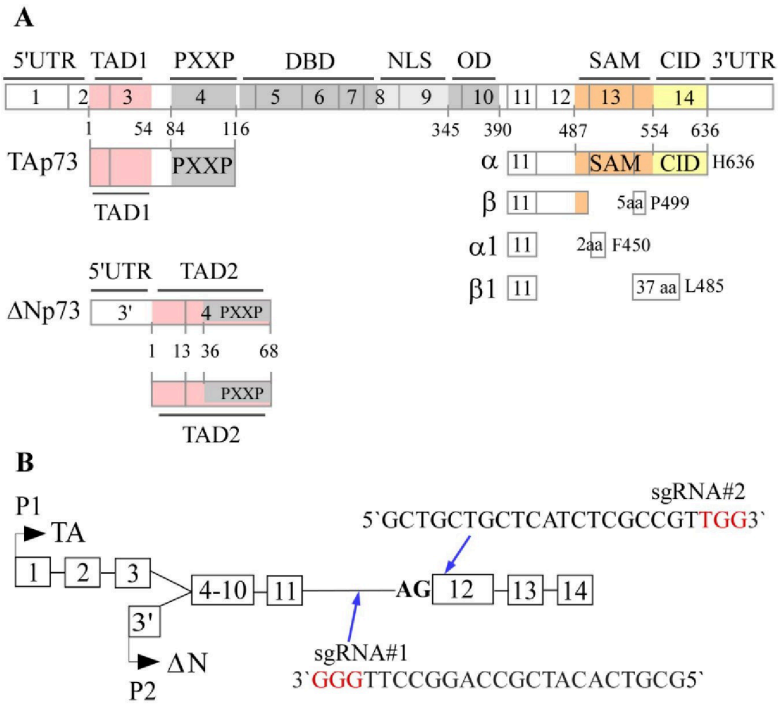

Fig. S1. p73 functional domains and gene structure.
(**A**) p73 functional domains. TAD1: Transactivation Domain 1. TAD2: Transactivation Domain 2. PXXP: Proline-rich Domain. DBD: DNA-Binding Domain. NLS: Nuclear Localization Signal. OD: Oligomerization Domain. SAM: Sterile Alpha Motif. CID: C-terminal Inhibitory Domain.

(**B**) Schematic representation of sgRNA #1 and #2 used to generate *E12*$^{-/-}$ cell lines.

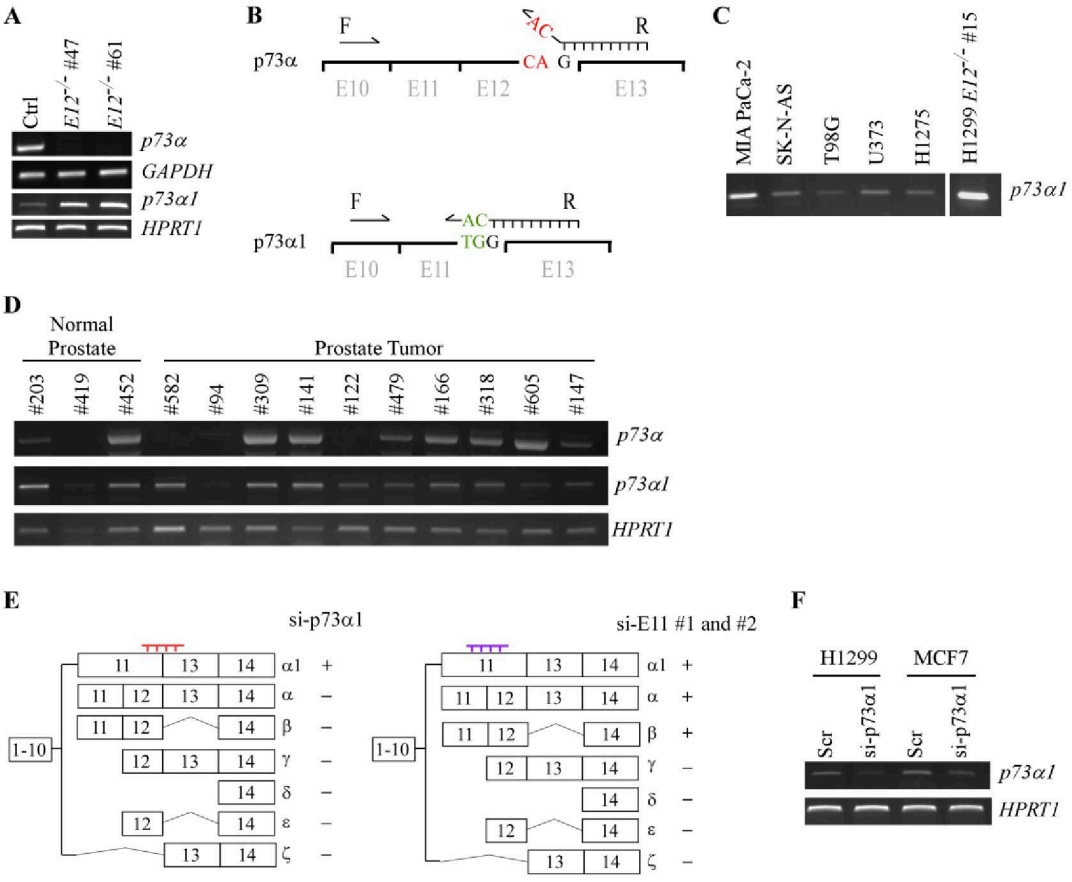

Fig. S2. Endogenous expression of *p73α1*.

(**A**) The level of *p73α*, *p73α1*, *GAPDH*, and *HPRT1* transcripts was measured in isogenic control and *E12*$^{-/-}$ MIA PaCa-2 cells.

(**B**) Schematic diagram of the reverse primer that specifically amplifies p73α1, but not p73α.

(**C**) The level of *p73α1* transcript was measured in MIA PaCa-2, SK-N-AS, T98G, U373, H12975, and H1299 *E12*$^{-/-}$ cells.

(D) The level of *p73α*, *p73α1*, and *HPRT1* transcripts was measured in normal human and tumor prostate tissues.

(**E**) Diagram of the locations targeted by si-p73α1 and si-E11 #1 and 2 and the effect on each p73 isoform. + : knockdown; - : no effect.

(**F**) The level of *p73α1* and *HPRT1* transcripts was measured in H1299 and MCF7 cells transiently transfected with Scrambled siRNA (Scr) or si-p73α1 for 3 days.

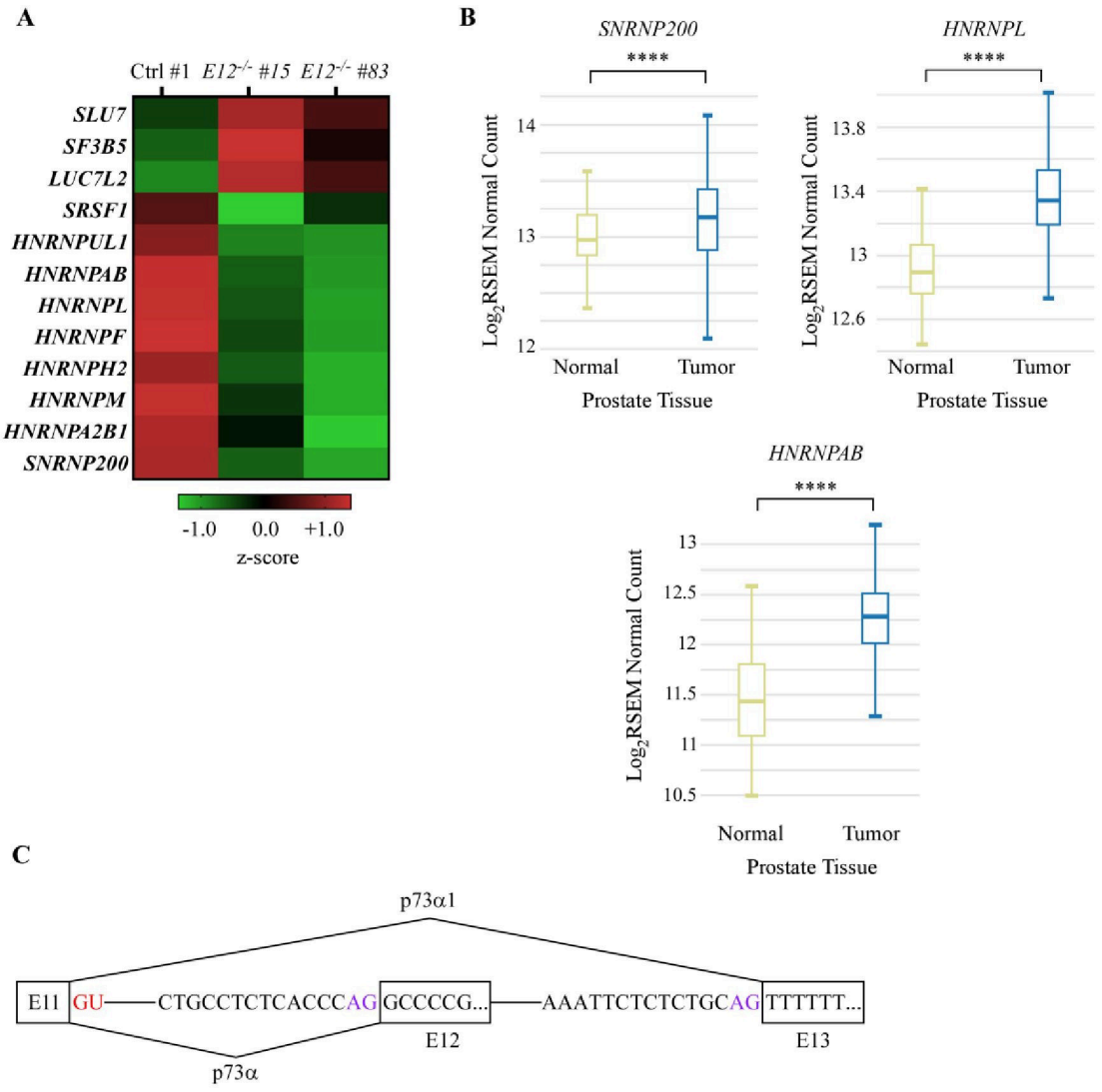

Fig. S3. E12-KO differentially regulates splicing-associated genes.

(**A**) Heatmap of splicing-associated genes and their differential expression in isogenic control and *E12*$^{-/-}$ H1299 cells.

(B) RSEM values of *SNRNP200*, *HNRNPL*, and *HNRNPAB* in normal human and prostate cancer samples from GTEx and TCGA databases, respectively. Data was analyzed using UCSC Xena Browser (TCGA Target GTEx).

(C) Diagram showing donor splice site (red) in intron 11 and the splice acceptor sites (purple) in introns 11 and 12.

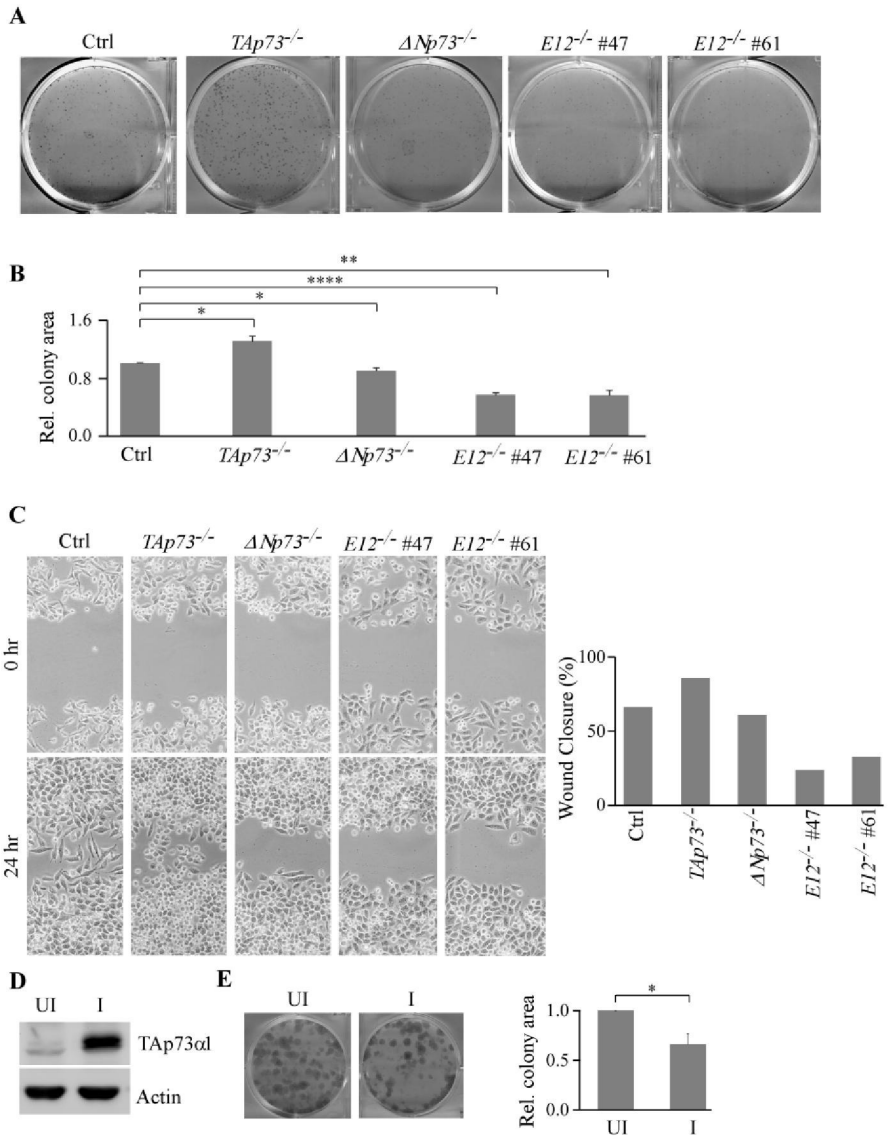

Fig. S4. p73α1 inhibits cell growth and migration.

(**A**) Colony formation assay was performed in isogenic control, *TAp73*$^{-/-}$, *ΔNp73*$^{-/-}$, and *E12*$^{-/-}$ MIA PaCa-2 cells.

(**B**) Quantification of colony formation assay shown in (A) using relative colony area. The relative colony area in isogenic control cells was arbitrarily set as 1.0. Data are presented as the mean ± SEM of three independent experiments. One-way ANOVA was used to calculate p-values. * $p < 0.05$; ** $p < 0.01$; **** $p < 0.0001$.

(**C**) Isogenic control, *TAp73*$^{-/-}$, *ΔNp73*$^{-/-}$, and *E12*$^{-/-}$ MIA PaCa-2 cells were used for scratch assays. Microscopic images were taken immediately after scratch (0 hr) and 24 hr later to monitor cell migration. Wound closure percentages were calculated and presented to the right.

(**D**) The level of TAp73α1 and actin proteins was examined in H1299 cells that were uninduced (UI) or induced (I) to express TAp73α1 for 24 hr.

(**E**) Colony formation assay was performed with H1299 cells that were uninduced (UI) or induced (I) to express TAp73α1 for 24 hr. (Right) Quantification of colony formation assay by using relative colony area. The relative colony area in UI cells was arbitrarily set as 1.0. Data are presented as the mean ± SEM of three independent experiments. Student's t-test was used to calculate p-values. * $p < 0.05$.

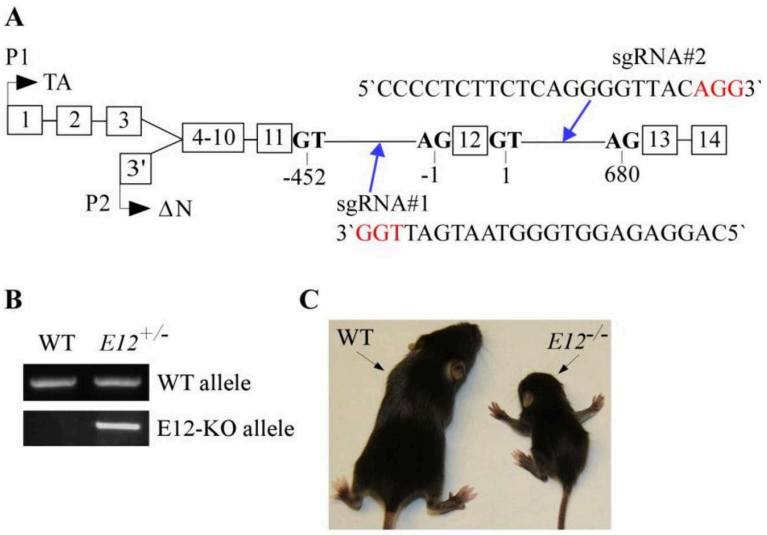

Fig. S5. Generation of *E12*-deficient mice.
(**A**) Schematic representation of *Trp73* gene structure and the locations of sgRNA #1 and #2 used to generate *E12*-deficient mice.

(**B**) Genotype of WT and $E12^{+/-}$ mice.

(**C**) Image of WT and $E12^{-/-}$ littermates at 13 weeks of age.

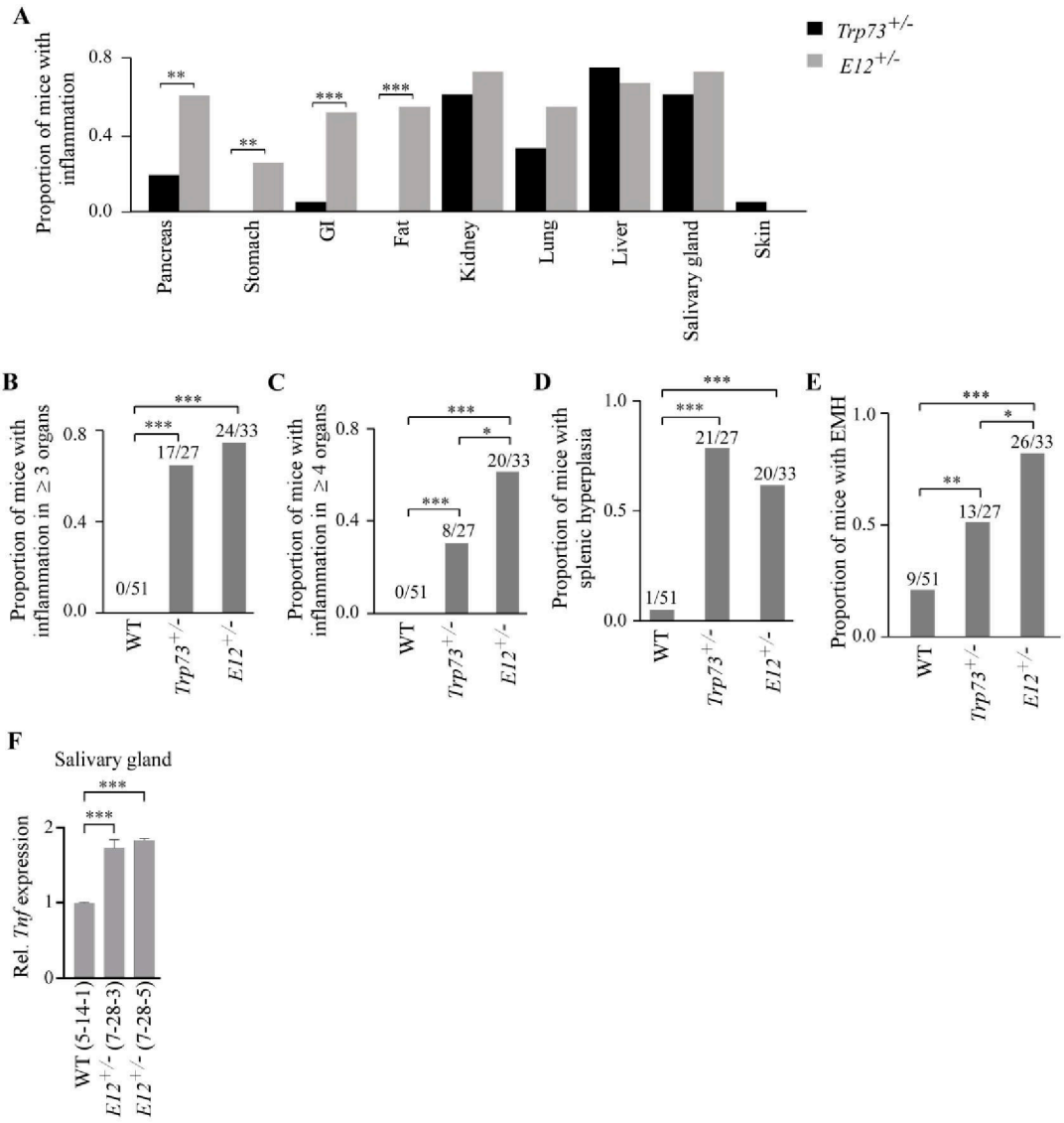

Fig. S6. *E12*$^{+/-}$ mice exhibit widespread systemic inflammation.
(**A**) Proportion of *Trp73*$^{+/-}$ and *E12*$^{+/-}$ with inflammation in the indicated organs. Fisher's exact test was used to calculate p-values. ** $p < 0.01$; *** $p < 0.001$.

(**B**) Proportion of WT, *Trp73*$^{+/-}$, and *E12*$^{+/-}$ with inflammation in three or more organs. Fisher's exact test was used to calculate p-values. *** $p < 0.001$.

(**C**) Proportion of WT, *Trp73*$^{+/-}$, and *E12*$^{+/-}$ with inflammation in four or more organs. Fisher's exact test was used to calculate p-values. * $p < 0.05$; *** $p < 0.001$.

(**D**) Proportion of WT, *Trp73*$^{+/-}$, and *E12*$^{+/-}$ with splenic hyperplasia. Fisher's exact test was used to calculate p-values. *** $p < 0.001$.

(**E**) Proportion of WT, *Trp73*$^{+/-}$, and *E12*$^{+/-}$ with EMH. Fisher's exact test was used to calculate p-values. * $p < 0.05$; ** $p < 0.01$; *** $p < 0.001$.

(**F**) qPCR was used to quantify relative *Tnf* expression in salivary gland tissue from age- and sex-matched WT and *E12*$^{+/-}$ mice (100 wks; F). One-way ANOVA was used to calculate p-values. *** $p < 0.001$.

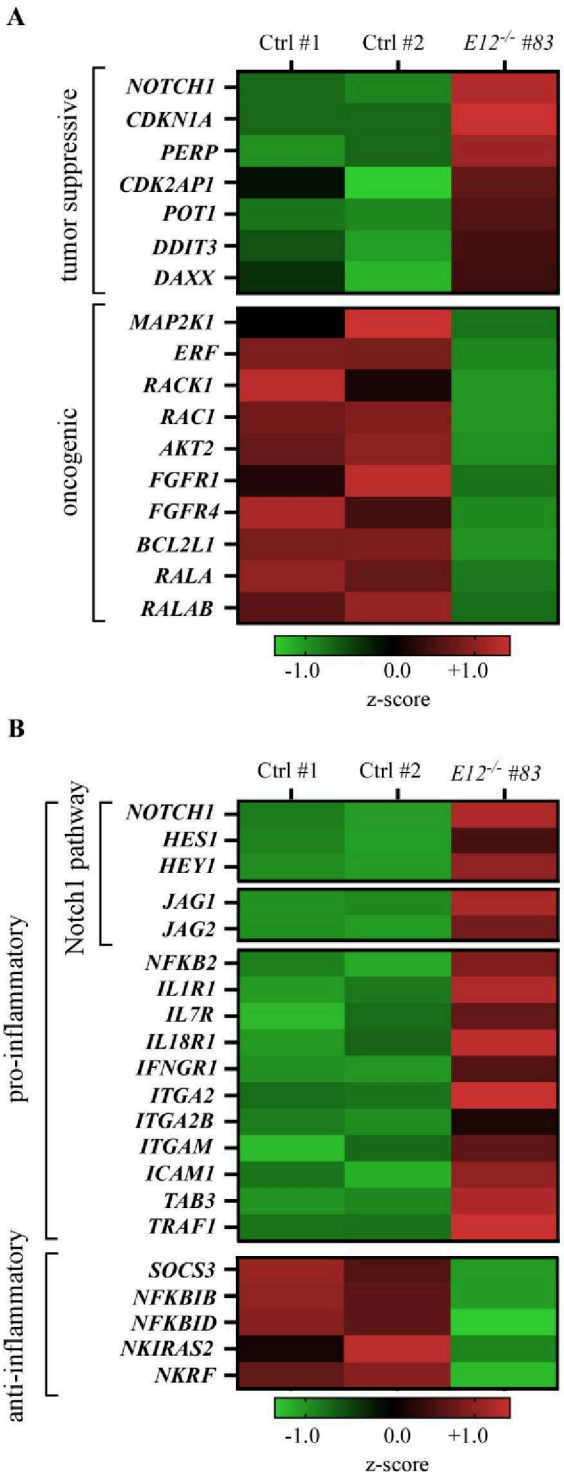

Fig. S7. E12-KO differentially regulates cancer- and inflammation-associated genes.

(**A**) Heatmap of cancer-associated genes and their differential expression in isogenic control and *E12*$^{-/-}$ H1299 cells.

(**B**) Heatmap of inflammation-associated genes and their differential expression in isogenic control and *E12*$^{-/-}$ H1299 cells.

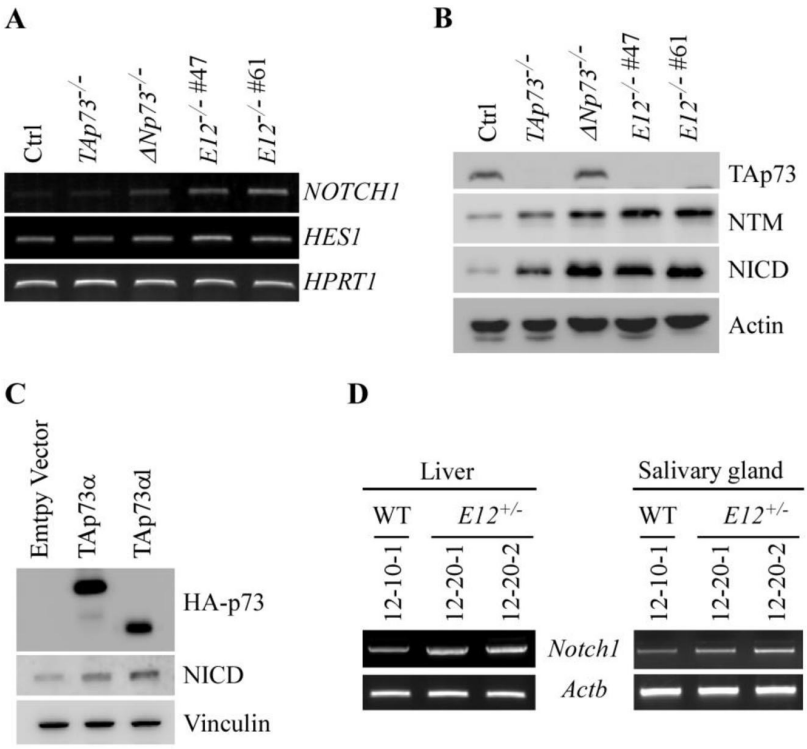

Fig. S8. p73α1 regulates the Notch1 pathway.
(**A**) The level of *NOTCH1*, *HES1*, and *HPRT1* transcripts were measured in isogenic control, *TAp73*$^{-/-}$, *ΔNp73*$^{-/-}$, and *E12*$^{-/-}$ MIA PaCa-2 cells.

(**B**) The level of TAp73, Notch1 transmembrane/intracellular region (NTM), Notch1 intracellular domain (NICD), and actin proteins was measured in isogenic control, *TAp73*$^{-/-}$, *ΔNp73*$^{-/-}$, and *E12*$^{-/-}$ MIA PaCa-2 cells.

(**C**) H1299 cells were transfected with HA-TAp73α or TAp73α1 plasmids and then subjected to Western blot analysis to detect HA-tagged p73, Notch1 intracellular domain (NICD), and vinculin proteins.

(**D**) The level of *Notch1* and *Actb* transcripts was measured in liver and salivary gland tissue from age- and sex-matched WT and *E12*$^{+/-}$ mice (78 wks; F).

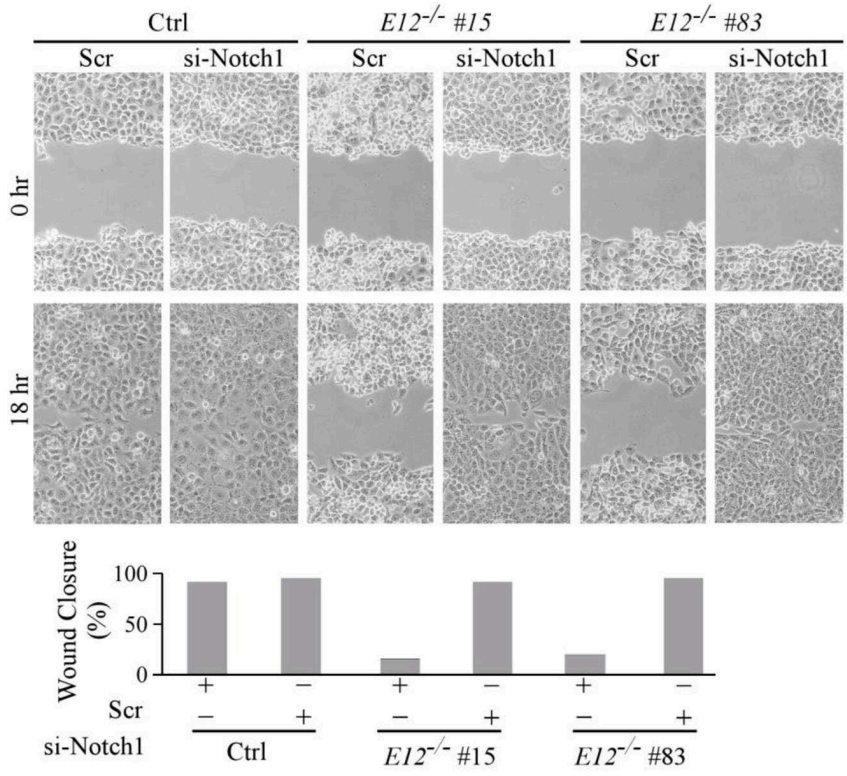

Fig. S9. p73α1 mediates Notch1 to inhibit cell migration in H1299 cells.
Isogenic control and *E12*$^{-/-}$ H1299 cells were transiently transfected with Scrambled siRNA (Scr) or si-Notch1 for 3 days and used for scratch assays. Microscopic images were taken immediately after scratch (0 hr) and 18 hr later to monitor cell migration. Wound closure percentages were quantified and presented below.

Table S1. Wild type (WT) mice (n=56) survival time, tumor spectrum, inflammation, and other abnormalities

ID	Gender	Survival (wks)	Tumor	Inflammation	Other abnormalities
5	F	134	-	-	-
7	F	117	-	-	-
16	F	100	-	-	-
22	F	109	-	-	-
25	F	109	-	-	-
44	F	90	-	-	-
55	F	104	T-LBL	-	-
64	F	120	-	-	-
2	M	127	-	-	-
3	M	117	-	Liver	-
12	M	127	-	-	-
13	M	127	-	-	-
20	M	122	-	-	-
23	M	122	-	-	-
26	M	127	-	Liver/Salivary gland	-
34	M	124	DLBCL	-	-
37	M	134	-	-	-
62	M	128	-	-	-
45	M	133	-	-	-
49	M	117	-	-	-
50	M	113	T-LBL/ DLBCL	-	-
56	M	117	DLBCL	-	-
59	M	119	DLBCL	-	-
65	M	106	-	-	-
69	M	102	DLBCL	-	Spleenic hyperplasia
70	M	103	-	-	Thymic hyperplasia
71	M	90	-	-	-
1-24-2	M	83	-	-	Steatosis
2-15-2	F	140	Lymphoma	-	EMH in liver
2-19-6	M	132	-	Pancreas	EMH in Spleen
2-19-2	F	143	-	-	EMH in Spleen
3-11-3	M	129	-	-	-
3-28-5	F	85	-	-	EMH in spleen/Steatosis
3-9-7	M	129	-	-	-
5-12-3	F	99	Lymphoma	-	EMH in Spleen
7-9-9	F	116	-	-	-
8-2-6	M	120	-	-	-
10-24-7	F	130	-	Pancreas	EMH in spleen
10-26-6	F	129	Histiocytic sarcoma	-	EMH in spleen/liver
11-10-7	M	121	-	-	-
11-7-3	F	121	-	-	-
11-29-2	F	144	-	-	EMH in spleen/Steatosis
12-2-4	F	113	-	-	-
12-20-7	F	115	-	-	EMH in Spleen
11-9-6	F	96	DLBCL	Skin	-
1-19-1	F	86	-	Skin	-
11-10-15	F	105	-	Skin/Pancreas	-
12-25-6	M	111	-	-	Hepatocirrhosis
1-19-5	F	109	Lymphoma	-	-
7-22-4	M	86	-	-	-
7-22-7	M	126	-	Kidney	-
11	M	111	N/A		Found dead
42	M	111	N/A		Found dead
43	M	107	N/A		Found dead
46	M	117	N/A		Found dead
52	M	101	N/A		Found dead

These mice were from published studies (Yang et al, 2017, PNAS, 114 (43) 11500-11505; Zhang et al, 2017, Genes & Dev, 31:1243-56)
T-LBL: Thymic lymphoblastic lymphoma; DLBCL: Diffuse large B-cell lymphoma; N/A: not applicable; EMH: Extramedullary hematopoiesis
5-14-1 (F, 105 wks), 11-29-6 (M, 110 wks), 12-10-1 (F, 80 wks)

Table S2. *Trp73*$^{+/-}$ mice (n=32) survival time, tumor spectrum, steatosis, inflammation, and other abnormalities

ID#	Gender	Survival (Wks)	Tumor	Steatosis	Inflammation	Other abnormalities
1-30-11	F	82	-	-	Liver/Salivary gland/Kidney/Pancreas	SWPH/EMH
6-7-14	M	43	-	-	Liver/Lung/Kidney/Salivary gland/Skin	SWPH/EMH/TH
9-23-1	F	77	Hepatoma	-	Liver/Pancreas/Kidney	SWPH
12-14-3	F	46	-	-	Skin/Lung/Kidney/Liver/Salivary gland	SWPH/EMH
5-27-14	M	65	-	-	Liver/Salivary gland	SWPH/EMH
9-13-11	F	69	-	-	Liver/Salivary gland/Lung/Kidney	SWPH/EMH
11-6-1	F	55	TLBCL	-	Liver/Kidney/Salivary gland/Pancreas/Lung	SWPH/EMH
5-3-5	F	105	-	Y	Kidney/Liver/Pancreas/Salivary gland	SWPH/EMH/TH
11-6-5	F	88	DLBCL/Hemangioma	Y	Liver/Salivary gland	SWPH/EMH/TH
5-13-2	M	117	-	Y	Liver/Salivary gland/Kidney	SWPH/EMH/TH
11-13-1/5	M	99	-	-	Liver/Salivary gland	-
10-13-12	F	89	Lymphoma	-	-	-
11-5-7	F	102	DLBCL/Lymphoma	-	Kidney/Liver/Cecum	SWPH
6-11-6	M	108	Lymphoma	-	Liver	SWPH
10-3-11	F	99	-	-	Liver/Salivary gland/Lung	SWPH/TH
10-22-4	F	86	Histiocytic sarcoma	-	Kidney/Salivary gland	-
5-28-16	F	120	Lymphoma	-	-	-
11-13-4	F	74	Lymphoma	-	-	-
12-14-1	F	103	-	-	Liver/Pancreas/Salivary gland	SWPH
1-25-4	F	94	DLBCL	-	-	-
1-15-8	F	69	-	-	Liver/Kidney/Salivary gland	SWPH
10-31-4	F	88	Lymphoma	-	Liver/Kidney/Lung/Salivary gland	SRPH/EMH
11-6-4	F	62	Gastric Adenoma	-	Lung/Salivary gland/Liver/Kidney	SRPH/EMH
9-16-5	F	76	-	-	Kidney/Liver/Salivary gland	SRPH/EMH Liver multifocal necrosis
6-22-4	F	80	-	-	Kidney/Lung/liver	SRPH/EMH Liver multifocal necrosis
4-19-1	F	102	-	-	Liver/Heart	SWPH/FH
10-31-5	F	99	DLBCL	Y	Kidney/Lung/Salivary Gland	-
1-2-5	M	7	-	-		Hydrocephalus
11-13-2	M	11	-	-		Hydrocephalus
10-9-2	M	101	N/A			Found dead
2-10-3	M	57	N/A			Found dead
3-10-3	M	108	N/A			Found dead

These mice were from published studies (Zhang et al., 2019, PNAS, 116 (48) 24259-24267)
DLBCL: Diffuse large B-cell lymphoma; EMH: Extramedullary hematopoiesis; SWPH: Spleen white pulp hyperplasia; SRPH: Spleen red pulp hyperplasia; TH: Thymic hyperplasia; LBCL: Large B-cell lymphoma; FH: Follicular hyperplasia

Table S3. *E12*$^{+/-}$ mice (n=33) survival time, tumor spectrum, steatosis, inflammation, and other abnormalities.

ID	Sex	Survival (wks)	Tumor	Steatosis	Inflammation	Other Abnormalities
9-16-12	M	43.57	-	-	Salivary gland	SWPH/EMH
4-14-1	F	78.86	-	-	Kidney/Lung/Liver/Stomach/GI/Fat/Salivary gland	EMH/SWPH
6-21-1	F	91.57	-	-	Liver	EMH/SWPH/FH
9-18-3	F	80.14	DLBCL	-	Kidney/Salivary gland	-
9-13-7	F	89.43	-	-	Kidney/Lung/Pancreas/Liver/Stomach/GI/Fat/Salivary gland	EMH/FH
10-6-1	M	91.00	DLBCL	-	Salivary gland	EMH/TH
9-13-6	F	95.86	AC	-	Kidney/Pancreas/Liver/GI/Fat/Salivary gland	EMH/SWPH
9-13-3	M	95.86	DLBCL	-	-	EMH
4-7-9	F	67.43	DLBCL	-	-	EMH
11-22-1	M	87.71	HCC	-	Kidney/Lung/Liver/GI/Fat/Salivary gland	-
10-17-6	M	95.86	-	-	Kidney/Lung/Pancreas/Liver/GI/Fat/Salivary gland	EMH/SWPH
4-14-4	F	126.71	-	-	Kidney/Lung/Pancreas/GI/Fat/Salivary gland	SWPH
11-22-5	M	95.00	-	-	Kidney/Lung/Pancreas/Liver/Stomach/GI/Fat/Salivary gland	EMH/SWPH
10-6-4	M	101.71	-	-	Kidney/Lung/Pancreas/Liver/Stomach/GI/Fat/Salivary gland	EMH/SWPH
1-8-1	M	88.29	DLBCL	-	Kidney/Pancreas/Liver/GI/Salivary gland	EMH/SWPH
10-6-3	M	101.71	DLBCL	-	Kidney/Pancreas/Liver	-
11-8-2	F		-	-	Kidney/Lung/Pancreas/Liver/GI/Fat/Salivary gland	EMH/SWPH/TH
4-7-8	M	131.57	-	-	Lung/Pancreas/Liver/Stomach/GI/Fat/Salivary gland	SWPH
9-13-5	F	108.86	-	-	Kidney/Lung/Pancreas/Liver/GI/Salivary gland	EMH/SWPH
8-25-2	F	123.57	DLBCL	-	Stomach/GI	-
8-25-3	F	123.57	DLBCL	-	Kidney/Liver/Fat	-
5-11-12	F	92.57	DLBCL	-	Kidney/Pancreas/GI	EMH
3-15-11	F	102.57	DLBCL	-	-	EMH
3-15-7	M	110.71	-	-	Kidney/Lung/Pancreas/Liver/Stomach/GI/Fat/Salivary gland	EMH/SWPH
3-2-3	F	40.86	-	-	Lung/Pancreas/Liver/Stomach/GI/Fat/Salivary gland	EMH/SWPH
15	F	57.57	-	-	Kidney/Lung/Pancreas/Liver/GI/Salivary gland	EMH/SWPH
1		46.86	-	-	Kidney/Salivary gland	EMH/TH
7-28-3	F	94.43	-	-	Kidney/Heart/Lung/Pancreas/Liver/Fat/Salivary gland	EMH/SWPH
7-28-5	F	94.71	-	-	Kidney/Heart/Lung/Pancreas/Liver/Salivary gland	EMH/SWPH
7-28-8	F	94.43	-	Y	Kidney/Heart/Lung/Pancreas/Liver/Fat/Salivary gland	EMH/SWPH
12-20-1	F	78	-	Y	Kidney/Heart/Lung/Pancreas/Liver/Fat/Salivary gland	EMH/SWPH/TH
12-20-2	F	78	-	-	Kidney/Heart/Lung/Pancreas/Liver/Fat/Salivary gland	EMH/SWPH
12-20-3	F	78	-	-	Kidney/Fat/Salivary gland	EMH/SWPH

DLBCL: Diffuse large B-cell lymphoma; AC: Adenocarcinoma; HCC: Hepatocellular carcinoma; EMH: Extramedullary hematopoiesis; SWPH: Spleen white pulp hyperplasia; TH: thymic hyperplasia

Table S4. Primers used to generate expression vectors

Name	Oligonucleotide	Sequence
TAp73-sgRNA-1	Sense	5`-ACCGCTTCCCCACGCCGGCCTCCG-3`
	Antisense	5`-AAACCGGAGGCCGGCGTGGGGAAGC-3`
TAp73-sgRNA-2	Sense	5`-CACCGTCAAACGTGGTGCCCCCATC-3`
	Antisense	5`-AAACGATGGGGGCACCACGTTTGAC-3`
ΔNp73-sgRNA-1	Sense	5`-CACCGTACAGCATGGTAGGCGCCG-3`
	Antisense	5`-AAACCGGCGCCTACCATGCTGTAC-3`
ΔNp73-sgRNA-2	Sense	5`-CACCGCGTCACACCTACCGTGGCG-3`
	Antisense	5`-AAACCGCCACGGTAGGTGTGACGC-3`
p73-E12-gRNA-1	Sense	5`-CACCGCGTCACATCGCCAGGCCTT-3`
	Antisense	5`-AAACAAGGCCTGGCGATGTGACGC-3`
p73-E12-gRNA-2	Sense	5`-CACCGCTGCTGCTCATCTCGCCGT-3`
	Antisense	5`-AAACACGGCGAGATGAGCAGCAGC-3`
HA-TAp73α1	Sense	5`-ACGGAATTCACCACCATCCTG-3`
	Antisense	5`-CTCGAGTTAAAAAACCACGGGCCCCAG-3`
HA-TAp73β1	Sense	5`-ACGGAATTCACCACCATCCTG-3`
	Antisense	5`-CTCGAGCTAGAGCGGAGCAGCTGCTG-3`

Table S5. Primers used for RT-PCR, qPCR, and ChIP

Name	Oligonucleotide	Sequence
TP73-all-isoforms (human)	Sense	5'-ACCGCTTCCCCACGCCGGCCTCCG-3'
	Antisense	5`-AAACCGGAGGCCGGCGTGGGGAAGC-3`
TP73α1 (human)	Sense	5`-CACCGTCAAACGTGGTGCCCCCATC-3`
	Antisense	5`-AAACGATGGGGGCACCACGTTTGAC-3`
NOTCH1 (human)	Sense	5`-CACCGTACAGCATGGTAGGCGCCG-3`
	Antisense	5`-AAACCGGCGCCTACCATGCTGTAC-3`
HES1 (human)	Sense	5`-CACCGCGTCACACCTACCGTGGCG-3`
	Antisense	5`-AAACCGCCACGGTAGGTGTGACGC-3`
TNF (human)	Sense	5`-ACCACCACTTCGAAACCTGG-3`
	Antisense	5`-GGCCTAAGGTCCACTTGTGT-3`
HPRT1 (human)	Sense	5`-CACCGCGTCACATCGCCAGGCCTT-3`
	Antisense	5'-AAACAAGGCCTGGCGATGTGACGC-3`
GAPDH (human)	Sense	5`-CACCGCTGCTGCTCATCTCGCCGT-3`
	Antisense	5`-AAACACGGCGAGATGAGCAGCAGC-3`
Tnf (mouse)	Sense	5`-TGGCCTCCCTCTCATCAGTT-3`
	Antisense	5`-ACAAGGTACAACCCATCGGC-3`
Cdkn1a (mouse)	Sense	5`-CCCGTGGACAGTGAGCAGT-3`
	Antisense	5`-CAGCAGGGCAGAGGAAGTA-3`
Cdkn2a (mouse)	Sense	5`-AGGTTCTTGGTCACTGTGAGG-3`
	Antisense	5`-ACAACATGTTCACGAAAGCCAG-3`
Actb (mouse)	Sense	5`-TCCATCATGAAGTGTGACGT-3`
	Antisense	5`-TGATCCACATCTGCTGGAAG-3`
Notch1 (mouse)	Sense	5`-CAATCAGGGCACCTGTGAGCCCACAT-3`
	Antisense	5`-TAGAGCGCTTGATTGGGTGCTTGCGC-3`
Notch1 (mouse qPCR)	Sense	5`-TGTGGCTTCCTTCTACTGCG-3`
	Antisense	5`-CTTTGCCGTTGACAGGGTTG-3`
Trp73α/α1 (mouse)	Sense	5`-GTCAACAAACTGCCCTCCGTC-3`
	Antisense	5`-CCTTGGGAAGTGAAGCACTCG-3`
Hes1 (mouse)	Sense	5`-GAAGAGGCGAAGGGCAAGAATAAATG-3`
	Antisense	5`-CAGGAAGCGGGTCACCTCGTTC-3`
NOTCH1-ChIP (human)	Sense	5`-TGACCGAGGAGCGTGTCGA-3`
	Antisense	5`-AGAGTGGCCTAGCCGTGTGT-3`
CDKN1A-ChIP (human)	Sense	5`-GGTCTGCTACTGTGTCCTCC-3`
	Antisense	5`-CATCTGAACAGAAATCCCAC-3`
GAPDH-ChIP (human)	Sense	5`-AAAAGCGGGGAGAAAGTAGG-3`
	Antisense	5`-AAGAAGATGCGGCTGACTGT-3`

1. L. J. Ko, C. Prives, p53: Puzzle and paradigm. *Genes Dev.* **10**, 1054–1072 (1996).
2. H. Schmale, C. Bamberger, A novel protein with strong homology to the tumor suppressor p53. *Oncogene* **15**, 1363–1367 (1997).
3. B. Trink *et al.*, A new human p53 homologue. *Nat. Med.* **4**, 747–748 (1998).
4. M. Osada *et al.*, Cloning and functional analysis of human p51, which structurally and functionally resembles p53. *Nat. Med.* **4**, 839–843 (1998).
5. M. Kaghad *et al.*, Monoallelically expressed gene related to p53 at 1p36, a region frequently deleted in neuroblastoma and other human cancers. *Cell* **90**, 809–819 (1997).
6. C. A. Jost, M. C. Marin, W. G. Kaelin Jr., p73 is a human p53-related protein that can induce apoptosis. *Nature* **389**, 191–194 (1997).
7. A. Yang *et al.*, p73-deficient mice have neurological, pheromonal and inflammatory defects but lack spontaneous tumours. *Nature* **404**, 99–103 (2000).
8. G. Meyer, C. G. Perez-Garcia, H. Abraham, D. Caput, Expression of p73 and Reelin in the developing human cortex. *J. Neurosci.* **22**, 4973–4986 (2002).
9. H. Abraham, G. Meyer, Reelin-expressing neurons in the postnatal and adult human hippocampal formation. *Hippocampus* **13**, 715–727 (2003).
10. C. B. Marshall *et al.*, p73 is required for multiciliogenesis and regulates the Foxj1-associated gene network. *Cell Rep.* **14**, 2289–2300 (2016).
11. A. Nemajerova *et al.*, TAp73 is a central transcriptional regulator of airway multiciliogenesis. *Genes Dev.* **30**, 1300–1312 (2016).
12. C. H. Arrowsmith, Structure and function in the p53 family. *Cell Death Differ.* **6**, 1169–1173 (1999).
13. G. Liu, S. Nozell, H. Xiao, X. Chen, DeltaNp73β is active in transactivation and growth suppression. *Mol. Cell. Biol.* **24**, 487–501 (2004).
14. R. Tomasini *et al.*, TAp73 knockout shows genomic instability with infertility and tumor suppressor functions. *Genes Dev.* **22**, 2677–2691 (2008).
15. J. Zhu, J. Jiang, W. Zhou, X. Chen, The potential tumor suppressor p73 differentially regulates cellular p53 target genes. *Cancer Res.* **58**, 5061–5065 (1998).
16. G. Melino *et al.*, p73 Induces apoptosis via PUMA transactivation and Bax mitochondrial translocation. *J. Biol. Chem.* **279**, 8076–8083 (2004).
17. P. Vernole *et al.*, TAp73α binds the kinetochore proteins Bub1 and Bub3 resulting in polyploidy. *Cell Cycle* **8**, 421–429 (2009).
18. M. T. Wilhelm *et al.*, Isoform-specific p73 knockout mice reveal a novel role for delta Np73 in the DNA damage response pathway. *Genes Dev.* **24**, 549–560 (2010).
19. A. I. Zaika *et al.*, DeltaNp73, a dominant-negative inhibitor of wild-type p53 and TAp73, is up-regulated in human tumors. *J. Exp. Med.* **196**, 765–780 (2002).
20. M. Steder *et al.*, DNp73 exerts function in metastasis initiation by disconnecting the inhibitory role of EPLIN on IGF1R-AKT/STAT3 signaling. *Cancer Cell* **24**, 512–527 (2013).
21. N. Concin *et al.*, Transdominant DeltaTAp73 isoforms are frequently up-regulated in ovarian cancer. Evidence for their role as epigenetic p53 inhibitors in vivo. *Cancer Res.* **64**, 2449–2460 (2004).
22. M. Müller *et al.*, TAp73/Delta Np73 influences apoptotic response, chemosensitivity and prognosis in hepatocellular carcinoma. *Cell Death Differ.* **12**, 1564–1577 (2005).
23. V. De Laurenzi *et al.*, Two new p73 splice variants with different transcriptional activity. *J. Exp. Med.* **188**, 1763–1768 (1998).
24. V. D. De Laurenzi *et al.*, Additional complexity in p73: Induction by mitogens in lymphoid cells and identification of two new splicing variants ε and ζ. *Cell Death Differ.* **6**, 389–390 (1999).
25. Y. Ueda, M. Hijikata, S. Takagi, T. Chiba, K. Shimotohno, New p73 variants with altered C-terminal structures have varied transcriptional activities. *Oncogene* **18**, 4993–4998 (1999).
26. A. Rufini *et al.*, p73 in cancer. *Genes Cancer* **2**, 491–502 (2011).
27. F. Grespi, I. Amelio, P. Tucci, M. Annicchiarico-Petruzzelli, G. Melino, Tissue-specific expression of p73 C-terminal isoforms in mice. *Cell Cycle* **11**, 4474–4483 (2012).
28. I. Amelio *et al.*, The C terminus of p73 is essential for hippocampal development. *Proc. Natl. Acad. Sci. U.S.A.* **117**, 15694–15701 (2020).
29. G. Liu, X. Chen, The C-terminal sterile α motif and the extreme C terminus regulate the transcriptional activity of the α isoform of p73. *J. Biol. Chem.* **280**, 20111–20119 (2005).
30. N. Buckley *et al.*, P73 C-terminus is dispensable for multiciliogenesis. *Cell Cycle* **19**, 1833–1845 (2020).
31. A. I. Zaika, S. Kovalev, N. D. Marchenko, U. M. Moll, Overexpression of the wild type p73 gene in breast cancer tissues and cell lines. *Cancer Res.* **59**, 3257–3263 (1999).
32. A. Yokomizo *et al.*, Overexpression of the wild type p73 gene in human bladder cancer. *Oncogene* **18**, 1629–1633 (1999).
33. C.-L. Chen, S.-M. Ip, D. Cheng, L.-C. Wong, H. Y. S. Ngan, P73 gene expression in ovarian cancer tissues and cell lines. *Clin. Cancer Res.* **6**, 3910–3915 (2000).
34. H. Pan, S.-J. Liao, W.-Y. Lai, H.-C. Lu, K.-M. Hsiao, Overexpression but lack of mutation and methylation of p73 in hepatocellular carcinoma. *Acta Oncol.* **41**, 550–555 (2002).
35. P. Vikhreva, G. Melino, I. Amelio, p73 alternative splicing: Exploring a biological role for the C-terminal isoforms. *J. Mol. Biol.* **430**, 1829–1838 (2018).
36. X. Chen, Y. Zheng, J. Zhu, J. Jiang, J. Wang, p73 is transcriptionally regulated by DNA damage, p53, and p73. *Oncogene* **20**, 769–774 (2001).
37. M. Marabese, F. Vikhanskaya, C. Rainelli, T. Sakai, M. Broggini, DNA damage induces transcriptional activation of p73 by removing C-EBPalpha repression on E2F1. *Nucleic Acids Res.* **31**, 6624–6632 (2003).
38. M. Urist, T. Tanaka, M. V. Poyurovsky, C. Prives, p73 induction after DNA damage is regulated by checkpoint kinases Chk1 and Chk2. *Genes Dev.* **18**, 3041–3054 (2004).
39. A. M. Krecic, M. S. Swanson, hnRNP complexes: Composition, structure, and function. *Curr. Opin. Cell Biol.* **11**, 363–371 (1999).
40. J. M. Jiménez-Vacas *et al.*, Dysregulation of the splicing machinery is directly associated to aggressiveness of prostate cancer. *EBioMedicine* **51**, 102547 (2020).
41. T. Fei *et al.*, Genome-wide CRISPR screen identifies HNRNPL as a prostate cancer dependency regulating RNA splicing. *Proc. Natl. Acad. Sci. U.S.A.* **114**, E5207–E5215 (2017).
42. Y. Wang, M. Ma, X. Xiao, Z. Wang, Intronic splicing enhancers, cognate splicing factors and context-dependent regulation rules. *Nat. Struct. Mol. Biol.* **19**, 1044–1052 (2012).
43. H. J. Yang *et al.*, Ninjurin 1 has two opposing functions in tumorigenesis in a p53-dependent manner. *Proc. Natl. Acad. Sci. U.S.A.* **114**, 11500–11505 (2017).
44. Y. Zhang *et al.*, Ferredoxin reductase is critical for p53-dependent tumor suppression via iron regulatory protein 2. *Genes Dev.* **31**, 1243–1256 (2017).
45. G. P. Dotto, Notch tumor suppressor function. *Oncogene* **27**, 5115–5123 (2008).
46. Y. Shang, S. Smith, X. Hu, Role of Notch signaling in regulating innate immunity and inflammation in health and disease. *Protein Cell* **7**, 159–174 (2016).
47. F. Radtke, K. Raj, The role of Notch in tumorigenesis: Oncogene or tumour suppressor? *Nat. Rev. Cancer* **3**, 756–767 (2003).
48. K. Lefort *et al.*, Notch1 is a p53 target gene involved in human keratinocyte tumor suppression through negative regulation of ROCK1/2 and MRCKalpha kinases. *Genes Dev.* **21**, 562–577 (2007).
49. T. Yugawa *et al.*, Regulation of Notch1 gene expression by p53 in epithelial cells. *Mol. Cell. Biol.* **27**, 3732–3742 (2007).
50. J. Zhang *et al.*, FDXR regulates TP73 tumor suppressor via IRP2 to modulate aging and tumor suppression. *J. Pathol.* **251**, 284–296 (2020).
51. J. Zhang *et al.*, Mutant p53 antagonizes p63/p73-mediated tumor suppression via Notch1. *Proc. Natl. Acad. Sci. U.S.A.* **116**, 24259–24267 (2019).
52. E. R. Flores *et al.*, Tumor predisposition in mice mutant for p63 and p73: Evidence for broader tumor suppressor functions for the p53 family. *Cancer Cell* **7**, 363–373 (2005).
53. P. Loukopoulos *et al.*, Genome-wide array-based comparative genomic hybridization analysis of pancreatic adenocarcinoma: Identification of genetic indicators that predict patient outcome. *Cancer Sci.* **98**, 392–400 (2007).
54. A. Nemajerova, O. Petrenko, L. Trümper, G. Palacios, U. M. Moll, Loss of p73 promotes dissemination of Myc-induced B cell lymphomas in mice. *J. Clin. Invest.* **120**, 2070–2080 (2010).
55. A. Nemajerova, G. Palacios, N. J. Nowak, S. Matsui, O. Petrenko, Targeted deletion of p73 in mice reveals its role in T cell development and lymphomagenesis. *PLoS One* **4**, e7784 (2009).
56. J. Johnson *et al.*, p73 loss triggers conversion to squamous cell carcinoma reversible upon reconstitution with TAp73alpha. *Cancer Res.* **67**, 7723–7730 (2007).
57. S.-G. Chi *et al.*, Elevated and biallelic expression of p73 is associated withprogression of human bladder cancer. *Cancer Res.* **59**, 2791–2793 (1999).
58. C. D. Thanos, J. U. Bowie, p53 Family members p63 and p73 are SAM domain-containing proteins. *Protein Sci.* **8**, 1708–1710 (1999).
59. S. W. Chi, A. Ayed, C. H. Arrowsmith, Solution structure of a conserved C-terminal domain of p73 with structural homology to the SAM domain. *EMBO J.* **18**, 4438–4445 (1999).
60. T. Ozaki *et al.*, Deletion of the COOH-terminal region of p73α enhances both its transactivation function and DNA-binding activity but inhibits induction of apoptosis in mammalian cells. *Cancer Res.* **59**, 5902–5907 (1999).
61. E. Bálint, A. C. Phillips, S. Kozlov, C. L. Stewart, K. H. Vousden, Induction of p57(KIP2) expression by p73β. *Proc. Natl. Acad. Sci. U.S.A.* **99**, 3529–3534 (2002).
62. M. Stantic *et al.*, TAp73 suppresses tumor angiogenesis through repression of proangiogenic cytokines and HIF-1α activity. *Proc. Natl. Acad. Sci. U.S.A.* **112**, 220–225 (2015).
63. F. Alimirah, R. Panchanathan, F. J. Davis, J. Chen, D. Choubey, Restoration of p53 expression in human cancer cell lines upregulates the expression of Notch1: Implications for cancer cell fate determination after genotoxic stress. *Neoplasia* **9**, 427–434 (2007).
64. M. Nicolas *et al.*, Notch1 functions as a tumor suppressor in mouse skin. *Nat. Genet.* **33**, 416–421 (2003).
65. V. Devgan, C. Mammucari, S. E. Millar, C. Brisken, G. P. Dotto, p21WAF1/Cip1 is a negative transcriptional regulator of Wnt4 expression downstream of Notch1 activation. *Genes Dev.* **19**, 1485–1495 (2005).
66. J. Yao, L. Duan, M. Fan, J. Yuan, X. Wu, Notch1 induces cell cycle arrest and apoptosis in human cervical cancer cells: Involvement of nuclear factor kappa B inhibition. *Int. J. Gynecol. Cancer* **17**, 502–510 (2007).
67. L. Wang *et al.*, Overexpressed active Notch1 induces cell growth arrest of HeLa cervical carcinoma cells. *Int. J. Gynecol. Cancer* **17**, 1283–1292 (2007).
68. C. Talora, D. C. Sgroi, C. P. Crum, G. P. Dotto, Specific down-modulation of Notch1 signaling in cervical cancer cells is required for sustained HPV-E6/E7 expression and late steps of malignant transformation. *Genes Dev.* **16**, 2252–2263 (2002).
69. Y. Sasaki *et al.*, The p53 family member genes are involved in the Notch signal pathway. *J. Biol. Chem.* **277**, 719–724 (2002).
70. N. E. Buckley *et al.*, BRCA1 is a key regulator of breast differentiation through activation of Notch signalling with implications for anti-endocrine treatment of breast cancers. *Nucleic Acids Res.* **41**, 8601–8614 (2013).
71. M. Colombo *et al.*, Cancer cells exploit notch signaling to redefine a supportive cytokine milieu. *Front. Immunol.* **9**, 1823 (2018).
72. B. Carow, M. E. Rottenberg, SOCS3, a major regulator of infection and inflammation. *Front. Immunol.* **5**, 58 (2014).
73. P. P. Tak, G. S. Firestein, NF-kappaB: A key role in inflammatory diseases. *J. Clin. Invest.* **107**, 7–11 (2001).
74. F. A. Ran *et al.*, Genome engineering using the CRISPR-Cas9 system. *Nat. Protoc.* **8**, 2281–2308 (2013).
75. M. Dohn, S. Nozell, A. Willis, X. Chen, "Tumor suppressor gene-inducible cell lines" in *Methods in Molecular Biology, W. S. El-Deiry, Ed.* (Humana Press, 2003), pp. 221–235.
76. A. Scoumanne, S. J. Cho, J. Zhang, X. Chen, The cyclin-dependent kinase inhibitor p21 is regulated by RNA-binding protein PCBP4 via mRNA stability. *Nucleic Acids Res.* **39**, 213–224 (2011).
77. X. Chen, J. Bargonetti, C. Prives, p53, through p21 (WAF1/CIP1), induces cyclin D1 synthesis. *Cancer Res.* **55**, 4257–4263 (1995).
78. G. Liu, T. Xia, X. Chen, The activation domains, the proline-rich domain, and the C-terminal basic domain in p53 are necessary for acetylation of histones on the proximal p21 promoter and interaction with p300/CREB-binding protein. *J. Biol. Chem.* **278**, 17557–17565 (2003).
79. C. Guzmán, M. Bagga, A. Kaur, J. Westermarck, D. Abankwa, ColonyArea: An ImageJ plugin to automatically quantify colony formation in clonogenic assays. *PLoS One* **9**, e92444 (2014).
80. G. P. Dimri *et al.*, A biomarker that identifies senescent human cells in culture and in aging skin in vivo. *Proc. Natl. Acad. Sci. U.S.A.* **92**, 9363–9367 (1995).

p73α1, an Isoform of the p73 Tumor Suppressor, Modulates Lipid Metabolism and Cancer Cell Growth via Stearoyl-CoA Desaturase-1

Zachary Rabow [1,†], Kyra Laubach [2,†], Xiangmudong Kong [2], Tong Shen [1], Shakur Mohibi [2], Jin Zhang [2,*], Oliver Fiehn [1,*] and Xinbin Chen [2,*]

[1] West Coast Metabolomics Center, University of California, Davis, CA 95616, USA
[2] Comparative Oncology Laboratory, Schools of Medicine and Veterinary Medicine, University of California, Davis, CA 95616, USA
* Correspondence: jinzhang@ucdavis.edu (J.Z.); ofiehn@ucdavis.edu (O.F.); xbchen@ucdavis.edu (X.C.); Tel.: +1-530-752-8725 (J.Z.); +1-530-754-8258 (O.F.); +1-530-754-8404 (X.C.)
† These authors contributed equally to this work.

Abstract: Altered lipid metabolism is a hallmark of cancer. p73, a p53 family member, regulates cellular processes and is expressed as multiple isoforms. However, the role of p73 in regulating lipid metabolism is not well-characterized. Previously, we found that loss of p73 exon 12 (*E12*) leads to an isoform switch from p73α to p73α1, the latter of which has strong tumor suppressive activity. In this study, comprehensive untargeted metabolomics was performed to determine whether p73α1 alters lipid metabolism in non-small cell lung carcinoma cells. RNA-seq and molecular biology approaches were combined to identify lipid metabolism genes altered upon loss of *E12* and identify a direct target of p73α1. We found that loss of *E12* leads to decreased levels of phosphatidylcholines, and this was due to decreased expression of genes involved in phosphatidylcholine synthesis. Additionally, we found that E12-knockout cells had increased levels of phosphatidylcholines containing saturated fatty acids (FAs) and decreased levels of phosphatidylcholines containing monounsaturated fatty acids (MUFAs). We then found that p73α1 inhibits cancer cell viability through direct transcriptional suppression of Stearoyl-CoA Desaturase-1 (SCD1), which converts saturated FAs to MUFAs. Finally, we showed that p73α1-mediated suppression of SCD1 leads to increased ratios of saturated FAs to MUFAs.

Keywords: p73 isoforms; the p53 family; Stearoyl-CoA Desaturase; lipid metabolism; Kennedy pathway

1. Introduction

Lipids are key building blocks in cells that are essential for membrane formation, energy storage, and cell signaling. In particular, glycerophospholipids are the primary component of cell membranes and are composed of a phosphate head group attached to a diacylglycerol (DG) backbone and two fatty acids (FAs) [1]. There are multiple classes of glycerophospholipids, but phosphatidylcholines (PCs) are the most abundant class within eukaryotic cell membranes, contributing up to 50% of the total phospholipid content [2]. PC biosynthesis occurs through the Kennedy pathway (consisting of the CDP-choline and CDP-ethanolamine branches), the Lands Cycle, or the phosphatidylethanolamine methyltransferase (PEMT) pathway [3–5]. The Kennedy pathway is initiated by intracellular choline import via choline transporters (CTLs and CHTs), where choline is quickly converted to phosphocholine (P-choline) by choline kinases in the cytosol [6]. P-choline is then converted to CDP-choline by CDP-choline synthetase in the nucleus or cytosol. Finally, the choline head group is linked to a DG backbone by choline/ethanolamine phosphotransferase to form PCs [3]. In the Lands Cycle, phospholipases cleave PCs to form lysophosphatidylcholines (LPCs) and FAs [7]. LPCs can then be converted back to PCs through lysophospholipid acyltransferases. The PEMT pathway, occurring in the liver, methylates

phosphatidylethanolamines (PEs), through the methyl donor S-adenosylmethionine, to form PCs [8]. Various PC metabolites exist due to differences in fatty acyl chain length and saturation [9].

Traditionally thought of as membrane lipids, the role of PCs in energy metabolism, cell signaling, and lipoprotein transport is becoming more apparent [10].

Altered lipid metabolism has become a consequential hallmark of tumorigenesis [11]. Carcinogenic cells can increase lipid synthesis and/or uptake to sustain their rapidly dividing state [12]. Evidence shows that increased levels of PCs and other choline-containing metabolites are associated with oncogenesis [13]. Cancer cells maintain high levels of PC synthesis through increased choline import and the formation of PC intermediates [14–16]. An abundance of PCs and choline-containing metabolites confers cancer cell survival in metabolically demanding conditions [17]. PCs can also be modified to form signaling lipids, such as arachidonic acid, phosphatidic acid, and DGs. These signaling lipids activate a myriad of oncogenic pathways to promote tumorigenesis [18,19]. For example, phosphatidic acid activates the mTOR pathway to inhibit apoptosis and promote cancer cell survival [20]. Similarly, arachidonic acid and its derivatives have been shown to promote angiogenesis, and tumor cell proliferation and invasion [21]. As such, altered PC metabolism is undoubtedly critical for driving tumorigenesis.

p73, a member of the p53 family of tumor suppressors, is a transcription factor and regulates many cellular processes [22,23]. The p73 gene structure affords the formation of multiple isoforms with varying functions. The N-terminal isoforms arise from two promoters, denoted P1 and P2, located upstream of exon 1 and in intron 3, respectively [24]. Transcription initiation from the P1 promoter leads to the expression of TAp73 isoforms [24], which have a tumor suppressive function similar to that of p53 [25–28]. Conversely, the P2 promoter produces ΔNp73 isoforms [29] that promote cell survival and can function as oncoproteins [30–32]. At the 3′ end, alternative splicing of exons 11, 12 and 13 gives rise to several known C-terminal isoforms [29,33,34]. p73α is the major isoform expressed in most human and mouse tissues and the most well-studied [35,36]. Previously, we found that exclusion of exon 12 (*E12*) leads to an isoform switch from p73α to a novel isoform that we termed p73α1 [37]. We found that p73α1 was endogenously expressed in multiple cancer cell lines, as well as normal and cancerous human prostate tissues [37]. Additionally, we found that p73α1 inhibits cancer cell viability in vitro, and mice deficient in *E12* are not prone to spontaneous tumors [37]. To further investigate the biological function of p73α1, we wanted to explore whether p73α1 regulates lipid metabolism.

In the present study, we investigated the effect of p73α1 expression on the lipidome in non-small cell lung carcinoma (H1299) cells, which do not express p53. We found that loss of *E12* leads to decreased levels of PCs, PEs, and their derivatives. RNA-seq analysis showed that E12-knockout (E12-KO) cells had decreased expression of several enzymes involved in PC and PE synthesis, but choline import appeared unchanged. Furthermore, we found that loss of *E12* led to increased levels of PCs containing saturated FAs and decreased levels of PCs containing mono-unsaturated FAs (MUFAs). We then discovered that p73α1 directly inhibits Stearoyl-CoA Desaturase-1 (SCD1) expression, which converts saturated FAs to MUFAs. Finally, we found that p73α1-mediated suppression of *SCD1* inhibits cancer cell viability and leads to an increased ratio of saturated FAs to MUFAs.

2. Materials and Methods

2.1. Cell Culture and Cell Line Generation

H1299 cells (non-small cell lung carcinoma, ATCC; Manassas, VA, USA; Cat# CRL-5803) were cultured in DMEM (Gibco; Waltham, MA, USA; Cat# 12100-61) supplemented with 10% FBS (Gibco; Waltham, MA, USA; Cat# A4766801) and Antibiotic-Antimycotic solution (Gibco; Waltham, MA, USA; Cat# 15240-062). H1299 cell lines tested negative for mycoplasma and were used at passage 20 or lower. $E12^{-/-}$ H1299 cell lines were generated as described previously [37].

2.2. Plasmid Generation

pSpCas9(BB)-2A-Puro expression vector was generated by the Zhang Lab [38] and purchased from Addgene (Watertown, MA, USA; Cat# 48139). A vector expressing a single guide RNA (sgRNA) that targeted *E12* was generated by annealing two 25-nt oligos and cloning the product into the pSpCas9(BB)-2A-Puro expression vector via BbsI. All primer sequences used to generate the corresponding expression vectors were listed in Table S1.

2.3. RNA Isolation and qPCR

Quick-RNA MiniPrep Kit (Zymo Research; Irvine, CA, USA; Cat# 11-327) was used to isolate RNA according to the manufacturer's protocol. RNA was then used for cDNA synthesis using oligo dT (18) primer (Thermo Scientific; Waltham, MA, USA; Cat# FERSO123), random hexamer primer (Thermo Scientific; Waltham, MA, USA; Cat# SO142), dNTP (Cat# FERR0181), RiboLock RNase Inhibitor (Thermo Scientific; Waltham, MA, USA; Cat# EO0381), and RevertAid Reverse Transcriptase (Thermo Scientific; Waltham, MA, USA; Cat# EP0441) according to the manufacturer's protocol. The cDNA was used for qPCR with PowerUp Sybr Green Master Mix (Applied Biosystems, Waltham, MA, USA; Cat# A25742) according to the manufacturer's protocol. All primers used for qPCR were listed in Table S2.

2.4. Western Blot Analysis

Western blot analysis was performed as previously described [39]. Briefly, whole cell lysates were harvested with 1× SDS lysis buffer [62.5 mM Tris-HCl pH 6.5, 10% glycerol (Sigma; St. Louis, MO, USA; Cat# G5516-4L), 2% SDS, 0.71 M 2-mercaptoethanol (Acros Organics; Waltham, MA, USA; Cat# 125470010), and 0.15 mm bromophenol blue (Fisher Bioreagents; Waltham, MA, USA; Cat# BP115-25)] and boiled at 95 °C for 6 min. Proteins were separated on polyacrylamide gel [10% acrylamide/bis-acrylamide (Sigma; St. Louis, MO, USA; Cat# A3574-5L), 0.37 M Tris-HCl pH 8.8, 0.035% ammonium persulfate (VWR; Radnor, PA, USA; Cat# 0486-100G), and 4.6 M TEMED (Acros Organics; Waltham, MA, USA Cat# 138455000)], then transferred to 0.45 mM nitrocellulose membrane (Cytiva; Marlborough, MA, USA; Cat# 10600002). Membranes were probed overnight at 4 °C with the indicated primary antibodies: anti-CD92 (Santa Cruz Biotechnology; Dallas, TX, USA; Cat# 517098), anti-GAPDH (Cell Signaling Technology; Danvers, MA, USA; Cat# 14C10), anti-Vinculin (Cell Signaling Technology; Danvers, MA, USA; Cat# E1E9V), anti-CCTa (Cell Signaling Technology; Danvers, MA, USA; Cat# 6931S), anti-SMPD4 (Novus Biologicals; Littleton, CO, USA; Cat# NBP2-93253), anti-CEPT1 (Invitrogen; Waltham, MA, USA; Cat# PA5-23876) anti-SCD1 (Abcam; Cambridge, United Kingdom; Cat# ab236868). Membranes were then incubated at room temperature for 3 h with either anti-mouse (Bio Rad; Hercules, CA, USA; Cat# 1705047) or anti-rabbit (Bio Rad; Hercules, CA, USA; Cat# 1705046) HRP conjugated secondary antibodies. The proteins were visualized with WesternBright ECL HRP substrate (Advansta; San Jose, CA, USA; Cat# K-12043-D20). VisionWorks®LS software was used to analyze the images.

2.5. ChIP Assay

ChIP assay was performed as previously described [40]. Briefly, chromatin was cross-linked with 1% formaldehyde in phosphate-buffered saline (PBS) and added directly to the media. Cells were lysed in 2× modified RIPA buffer [0.1 M Tris-HCl, 2% NP-40 (USB; Waltham, MA, USA; Cat# 19628), 0.5% deoxycholic acid (Fisher Bioreagents; Waltham, MA, USA; Cat# BP349-100), 2 mm EDTA (Fisher Bioreagents; Waltham, MA, USA; Cat# BP120-1) with protease inhibitor cocktail (Thermo Scientific; Waltham, MA, USA; Cat# 78438). Chromatin lysates were sonicated to yield ~200–1000 base pair DNA fragments and immunoprecipitated with 1 mg of control anti-IgG normal rabbit (EMD Millipore; Burlington, MA, USA; Cat# NI01-100 mg) or anti-TAp73 (Bethyl Laboratories; Waltham, MA, USA; Cat# A300-126A) and captured with protein A/G magnetic agarose beads (Thermo Scientific; Waltham, MA, USA; Cat# 78609) at 4 °C overnight. The DNA-protein

immunocomplexes were reverse cross-linked and purified using ChIP DNA Clean and Concentrator (Zymo Research; Irvine, CA, USA; Cat# 50-44-363). The DNA fragments were amplified with PCR using DreamTaq DNA polymerase (Thermo Scientific; Waltham, MA, USA; Cat# FEREP0713). The PCR program used for amplification was (1) 94 °C for 5 min, (2) 94 °C for 30 s, (3) 60 °C for 30 s, (4) 72 °C for 30 s, and (5) 72 °C for 10 min. Steps 2–4 were repeated for 32 cycles to amplify *GAPDH*, 36 cycles to amplify *SCD1*, or 38 cycles to amplify *CDKN1A*. Primers used for ChIP assay were listed in Table S2.

2.6. siRNA Knockdown

siRNA was purchased from Horizon Discovery Biosciences and resuspended in 5× siRNA Buffer (Thermo Scientific; Waltham, MA, USA; Cat# B-002000-UB-100) to a final concentration of 20 mM. 2×10^5 cells were plated in a 6-well plate. After 24 h, cells were transfected using RNAi Max (Invitrogen; Waltham, MA, USA; Cat# 13778150) according to the manufacturer's protocol with the appropriate siRNA at the indicated concentrations: scrambled siRNA (Scr) (5′-GGC CGA UUG UCA AAU AAU U-3′) (90 nM), si-p73α1 (5′-ACC UGG GGC CCG UGG UUU-3′) (70 nM), or si-SCD1 (5′-GAG AUA AGU UGG AGA CGA UdTdT-′3) (20 nM). After 48 h, cells were trypsinized (VWR; Radnor, PA, USA; Cat# 0458-250G) and either seeded for RNA or protein collection, or for cell viability assay.

2.7. Cell Viability Assay

5×10^3 cells were plated in a 96-well plate. After 96 h, cell viability was measured using CellTiter-Glo 2.0 Cell Viability Assay kit (Promega; Madison, WI, USA; Cat# G9241) according to the manufacturer's protocol. The assay was performed in triplicates to ensure proper statistical analyses.

2.8. Metabolomics and Lipidomics

Lipidomics and metabolomics analysis was performed at the UC Davis West Coast Metabolomics Center. Three million cells were collected into 2 mL Eppendorf tubes (Eppendorf; Hamburg, Germany; Cat# 4036-3352). Samples were randomized and extracted alongside one method blank and one bioreclamation sample per every 10 biological samples. Samples were extracted using the modified Matyash Extraction [41]. 225 µL of ice-cold methanol, with Avanti SPLASHone internal standards (Avanti Polar Lipids; Alabaster, AL, USA; Cat# 330707) was added to each sample. Cells were homogenized for 90 s in methanol with 2 mm stainless steel beads using an SPEX Geno/Grinder (SPEX SamplePrep; Metuchen, NJ, USA). 750 µL MTBE was added to the samples, vortex briefly, and then mixed on an orbital shaker for 5 min at 4 °C. Next, 188 µL water was added to the tubes, vortexed, and then centrifuged for 3 min at 16k RPM. The top organic layer was collected (two, 180 µL fractions) for lipidomics analysis, and the bottom polar fraction (two, 150 µL fractions) was collected for metabolomics. All fractions were dried under vacuum using a rotovap. Lipidomics analysis was performed by resuspending dried fractions in 100 µL Methanol: Toluene (9:1) and analyzed using liquid chromatography (LC) high-resolution mass spectrometry (Q Exactive HF MS/MS). LC conditions were carried out using a Vanquish Focused UHPLC, Waters Acquity UPLC CSH C18 columns (100 mm × 2.1 mm, 1.7 µm particle size) with mobile phase A consisting of 6:4 acetonitrile: water and mobile phase B consisting of 9:1 isopropanol: water, both containing 10 mM ammonium formate and 0.1% formic acid for positive ionization mode, and 10 mM ammonium formate for negative ionization mode analysis. 3 and 5 µLs of pooled samples were injected for positive and negative modes to equilibrate the column prior to analysis. Mobile phase gradient and mass spectrometry parameters were identical, as described previously [42]. Metabolomics was performed by GC-MS as previously described [43] and by high-resolution LC-MS/MS as described previously [44].

2.9. Statistical Analysis

Data are presented as mean ± SEM. Significant difference between two groups was assessed by one-tailed, unpaired Student's *t*-test and comparisons between two or more groups were assessed by one-way ANOVA with Benjamini and Hochberg FDR post-test for multiple comparisons, when appropriate. Statistical analysis was performed with GraphPad Prism 9. Statistical parameters can be found in the figure legends. ChemRICH analysis was performed as previously described [45].

3. Results

3.1. Isoform Switch from p73α to p73α1 Alters the Metabolome in H1299 Cells

To determine the role of p73α1 in regulating lipid metabolism, untargeted metabolomic and lipidomic analyses were performed in isogenic control and E12-KO clone #1 (*E12*$^{-/-}$ #1) H1299 cell lines (Figure 1A). It is important to note that isogenic control cells express mostly p73α and a small amount of p73α1, and E12-KO cells express p73α1 and no p73α (Figure S1A) [37]. 734 lipids and 163 primary metabolites were identified through LC-MS/MS and GC-MS analysis, respectively. Triacylglycerols (TGs), PCs, ether-linked PCs, and PEs were among the classes with the highest lipid counts, and carbohydrates, amino acids, and peptides had the highest primary metabolite counts (Figure 1B). Principal Component Analysis showed the cell lines scattered in the first two principal components, with tight clustering of the pooled quality control samples, indicating excellent analytical precision. The first principal component explains 51% of the total observed biological variance, with the second principal component accounting for nearly 34% of the variance (Figure 1C). Total lipid content was found to be significantly lower in E12-KO cells compared to isogenic control cells (Figure S1B). Consistent with this, the volcano plot displayed a general trend of metabolites and lipids being downregulated in E12-KO cells compared to isogenic control cells (Figure 1D).

To identify class-level lipid changes associated with loss of *E12*, a chemical similarity enrichment analysis (ChemRICH) plot was generated. Using general class-level classifications, the analysis showed that PCs and TGs were the two most significantly altered classes; PCs were decreased, but TGs were increased in E12-KO cells, with a slightly mixed effect for both. The mixed effect for PCs indicated that many of these lipids were decreased in E12-KO cells, while some were increased, compared to isogenic control cells. Conversely, the mixed effect in TGs indicated that most TG lipids were increased in E12-KO cells, while some were decreased, compared to isogenic control cells (Figure 1E). To expand on the broad class-level analysis, a heat map detailing all annotated lipids was generated (Figure 1F). Loss of *E12* led to a considerable decrease in overall FAs compared to isogenic control cells (Figure 1F). Additionally, E12-KO cells exhibited decreased levels of PCs, LPCs, and PEs compared to isogenic control cells (Figure 1F). On the other hand, E12-KO cells elicited a substantial increase in TGs compared to isogenic control cells (Figure 1F). Carnitines and bis(monoacylglycerol)phosphates were significantly decreased in E12-KO cells compared to isogenic control cells, while ether-linked TGs exhibited the opposite trend (Figure S1C). Phosphatidylglycerols, cardiolipins, sphingomyelins, ceramides, and cholesterol esters were not altered between isogenic control and E12-KO cells (Figure S1D).

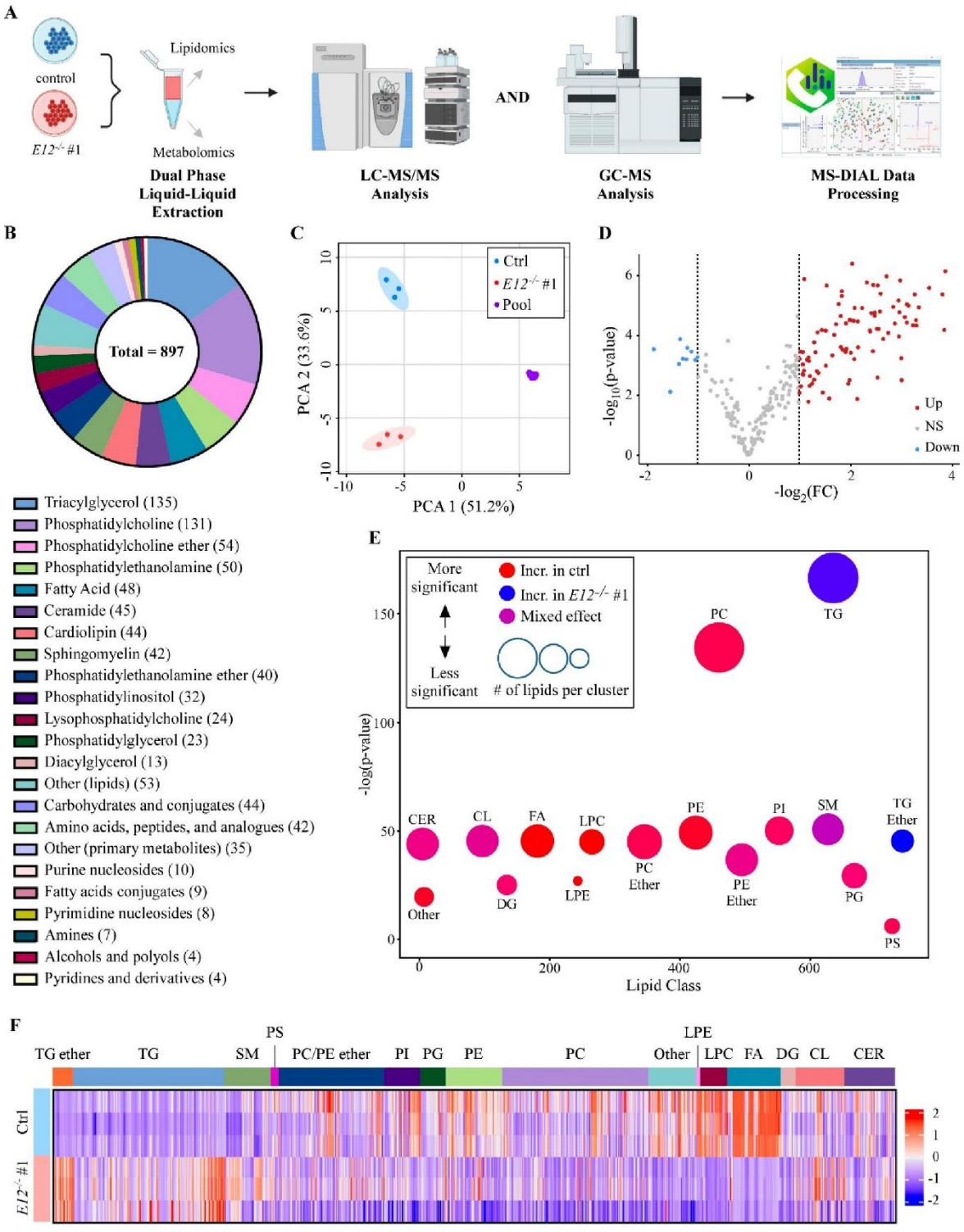

Figure 1. Lipidome overview in isogenic control and E12-KO H1299 cells. (**A**). Schematic of lipidomic and metabolomic analysis workflow in isogenic control and *E12*$^{-/-}$ H1299 cells. (**B**). Class-level overview of metabolites annotated by LC-MS/MS and GC-MS analysis in isogenic control and *E12*$^{-/-}$ H1299 cells. 897 individual metabolites were identified using accurate mass and in-silico libraries (top). Number of metabolites in each class are indicated in the parentheses (bottom). Classes with less than 10 identified lipids or metabolites were grouped together and denoted "Other (lipids)"

or "Other (primary metabolites)". (**C**). Principal component analysis (PCA) of isogenic control, *E12*$^{-/-}$ H1299 cells and pooled quality control samples. (**D**). Volcano plot of isogenic control compared to *E12*$^{-/-}$ H1299 cells. Up indicates lipids and metabolites higher in isogenic control cells. (**E**). Chemical similar enrichment analysis (ChemRICH) of all lipids identified in isogenic control and *E12*$^{-/-}$ H1299 cells. Y-axis represents statistical significance assessed by Kolmogorov-Smirnov test and node size represents total number of lipids per cluster. Classes with less than 10 identified lipids were grouped together and denoted "Other". TG: triacylglycerols; PC: phosphatidylcholines; CER: ceramides; CL: cardiolipins; FA: fatty acids; DG: diacylglycerols; LPE: lysophosphatidylethanolamines; LPC: lysophosphatidylcholines; PE: phosphatidylethanolamines; PI: phosphatidylinositols; PG: phosphatidylglycerols; PS: phosphatidylserines; SM: sphingomyelins. (**F**). Heatmap of all annotated lipids clustered by class in isogenic control and *E12*$^{-/-}$ H1299 cells. Color intensity indicates z-score values of peak heights. CER: ceramides; CL: cardiolipins; DG: diacylglycerols; FA: fatty acids; LPC: lysophosphatidylcholines; LPE: lysophosphatidylethanolamines; PC: phosphatidylcholines; PE: phosphatidylethanolamines; PG: phosphatidylglycerols; PI: phosphatidylinositols; PS: phosphatidylserines; SM: sphingomyelins; TG: triacylglycerols.

3.2. Loss of E12 Leads to Specific Lipidome Changes in H1299 Cells

Lipidome changes between isogenic control and E12-KO cells were further investigated. The top six upregulated (Figure 2A) and downregulated (Figure 2B) compounds were analyzed to determine whether specific lipid classes or pathways were affected by the loss of *E12*. The top six downregulated metabolites were all FAs; three MUFAs (FA 18:1, FA 20:1, FA 26:1) all with fold changes of 0.10, two saturated FAs (FA 16:0, FA 24:0) with fold changes of 0.20 and 0.25, and one poly-unsaturated FA (PUFA) (FA 24:4) with a fold change of 0.14 (Figure 2A). TG species made up four of the top six upregulated metabolites, consisting of three ether-linked TGs (TG-O 48:2, TG-O 54:1, TG-O 46:0) with fold changes of 5, 5 and 10, respectively, and TG 42:0, with a fold change of 10 (Figure 2B). Two polar metabolites, glycerol 3-phosphate and inosine-5-monophosphate with fold changes of 14 and 10, were the other most upregulated metabolites. We hypothesized that the accumulation of glycerol 3-phosphate in E12-KO cells was a result of decreased glycerophospholipid levels, as shown in Figure 1F. Overall, these data indicate that loss of *E12* alters the abundance of certain lipid classes and precursors.

To better understand lipid metabolism alterations in E12-KO cells, the general class-level ChemRICH plot (Figure 1E) was delineated by saturation level (Figure 2C,D). Interestingly, the mixed effect seen in PCs and TGs in Figure 1E was not observed when the broad classes were stratified by saturation status. PCs containing PUFAs were significantly dysregulated (FDR = 3.4×10^{45}), where 70% of all PCs containing PUFAs were altered (67 downregulated and 8 upregulated in E12-KO cells) (Figure 2D). On the other hand, PCs containing MUFAs had a slightly mixed effect, with 9 out of 13 being lower in E12-KO cells, and four out of 13 being higher in the E12-KO cells (Figure 2D). Interestingly, PCs containing saturated FAs were significantly upregulated (FDR = 2.5×10^{8}) in E12-KO cells, with 90% being increased in E12-KO cells (Figure 2C,D). Overall, TGs of all saturation levels were increased in E12-KO cells compared to isogenic control cells (Figure 2C). All TG species containing saturated FAs and MUFAs were increased in E12-KO cells (Figure 2D). While over 90% of TGs containing di-unsaturated fatty acids (DUFAs) and PUFAs were increased in E12-KO cells, there were 4 individual species that were decreased in E12-KO cells (Figure 2D). Similar trends were seen for other lipid classes; however, several classes–ceramides, cardiolipins, sphingomyelins, and ether-linked PEs–showed a mixed effect (Figure 2D).

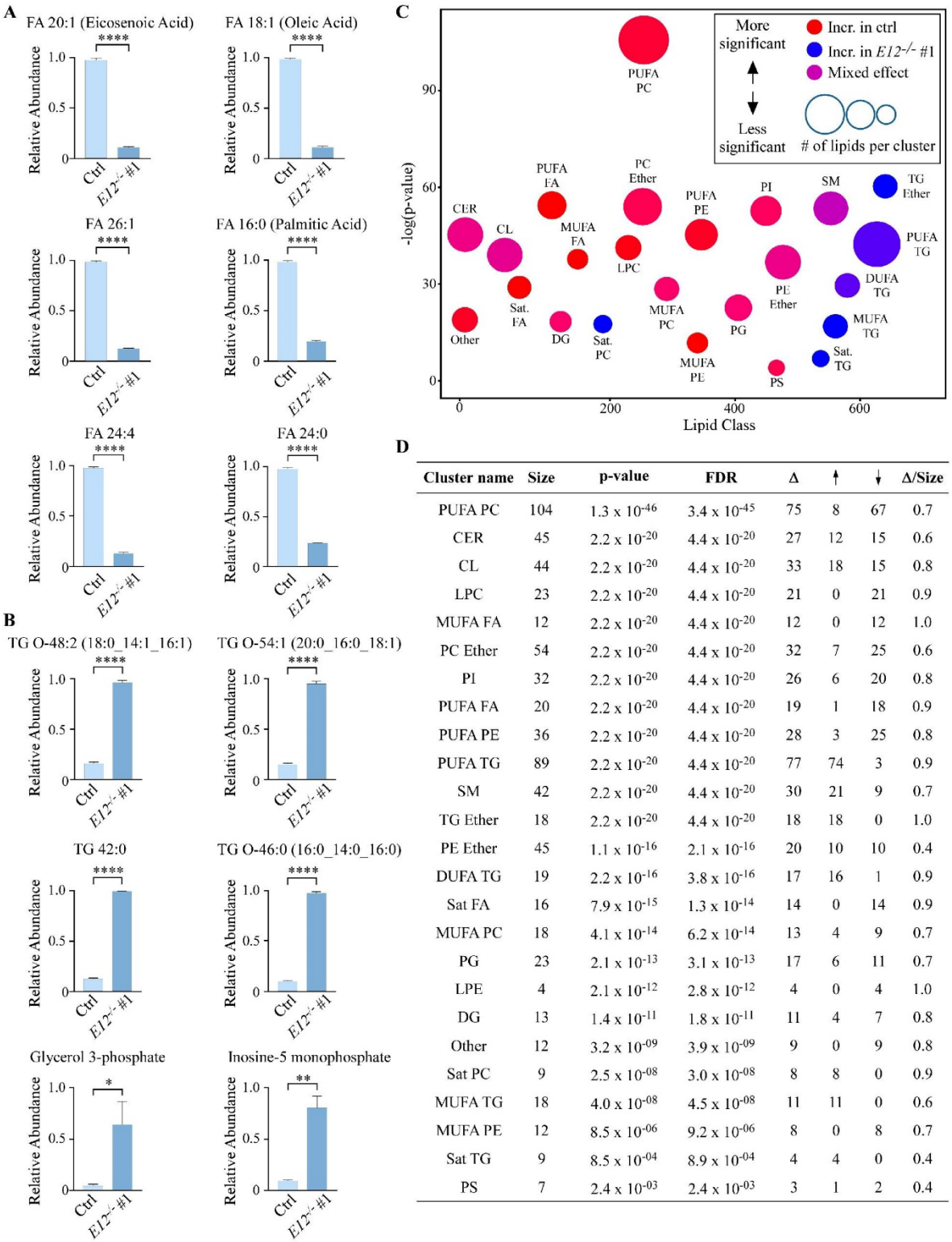

D

Cluster name	Size	p-value	FDR	Δ	↑	↓	Δ/Size
PUFA PC	104	1.3×10^{-46}	3.4×10^{-45}	75	8	67	0.7
CER	45	2.2×10^{-20}	4.4×10^{-20}	27	12	15	0.6
CL	44	2.2×10^{-20}	4.4×10^{-20}	33	18	15	0.8
LPC	23	2.2×10^{-20}	4.4×10^{-20}	21	0	21	0.9
MUFA FA	12	2.2×10^{-20}	4.4×10^{-20}	12	0	12	1.0
PC Ether	54	2.2×10^{-20}	4.4×10^{-20}	32	7	25	0.6
PI	32	2.2×10^{-20}	4.4×10^{-20}	26	6	20	0.8
PUFA FA	20	2.2×10^{-20}	4.4×10^{-20}	19	1	18	0.9
PUFA PE	36	2.2×10^{-20}	4.4×10^{-20}	28	3	25	0.8
PUFA TG	89	2.2×10^{-20}	4.4×10^{-20}	77	74	3	0.9
SM	42	2.2×10^{-20}	4.4×10^{-20}	30	21	9	0.7
TG Ether	18	2.2×10^{-20}	4.4×10^{-20}	18	18	0	1.0
PE Ether	45	1.1×10^{-16}	2.1×10^{-16}	20	10	10	0.4
DUFA TG	19	2.2×10^{-16}	3.8×10^{-16}	17	16	1	0.9
Sat FA	16	7.9×10^{-15}	1.3×10^{-14}	14	0	14	0.9
MUFA PC	18	4.1×10^{-14}	6.2×10^{-14}	13	4	9	0.7
PG	23	2.1×10^{-13}	3.1×10^{-13}	17	6	11	0.7
LPE	4	2.1×10^{-12}	2.8×10^{-12}	4	0	4	1.0
DG	13	1.4×10^{-11}	1.8×10^{-11}	11	4	7	0.8
Other	12	3.2×10^{-09}	3.9×10^{-09}	9	0	9	0.8
Sat PC	9	2.5×10^{-08}	3.0×10^{-08}	8	8	0	0.9
MUFA TG	18	4.0×10^{-08}	4.5×10^{-08}	11	11	0	0.6
MUFA PE	12	8.5×10^{-06}	9.2×10^{-06}	8	0	8	0.7
Sat TG	9	8.5×10^{-04}	8.9×10^{-04}	4	4	0	0.4
PS	7	2.4×10^{-03}	2.4×10^{-03}	3	1	2	0.4

Figure 2. Loss of *E12* leads to lipidome changes in H1299 cells. A-B. (**A**) Top six downregulated and (**B**) upregulated metabolites in $E12^{-/-}$ compared to isogenic control H1299 cells. TG-O indicates triacylglycerols with an ether bond. Statistical significance was determined using Student's *t*-test. Data are presented as mean ± SEM. $n = 3$ independent experiments. * $p < 0.05$, ** $p < 0.01$, **** $p < 0.0001$. (**C**). ChemRICH of all lipids identified in isogenic control and $E12^{-/-}$ H1299 cells. Y-

axis represents statistical significance assessed by Kolmogorov-Smirnov test and node size represents total number of lipids per cluster. MUFA: mono-unsaturated fatty acids; DUFA: di-unsaturated fatty acids; PUFA: poly-unsaturated fatty acids; Sat: saturated. (**D**). Lipid clusters with significant alterations due to loss of *E12* determined by ChemRICH analysis. Δ indicates number of lipids altered in a cluster; ↑ indicates number of increased lipids in $E12^{-/-}$ compared to isogenic control H1299 cells; ↓ indicates number of decreased lipids in $E12^{-/-}$ compared to isogenic control H1299 cells; FDR indicates false discovery rate; Δ/size shows the proportion of significantly altered lipids within each class.

3.3. Kennedy Pathway Metabolites Are Altered upon Loss of E12 in H1299 Cells

As previously discussed, PCs are formed through the Kennedy pathway, the Lands Cycle, or the PEMT pathway (Figure 3A). ChemRICH analyses indicated that the Kennedy pathway was altered, so levels of PCs, LPCs, PEs, and lysophosphatidylethanolamines (LPEs) were further analyzed. Loss of *E12* led to a significant decrease in the four PC synthesis lipids compared to isogenic control cells (Figure 3B,C). Levels of the PEMT pathway methyl donor S-adenosylmethionine were more significantly increased in E12-KO cells, compared to the product of this reaction, S-adenosylhomocysteine (Figure S2A). These data suggest that the PEMT pathway might be inhibited by loss of *E12*, therefore leading to decreased PC production. We then postulated that loss of *E12* was altering the expression of genes involved in PC synthesis, thus explaining the observed lipid changes. To test this, previously generated RNA-seq data was analyzed and showed that several key genes involved in PC synthesis were differentially expressed in E12-KO cells compared to isogenic control cells (Figure 3D). mRNA and protein levels of several of these targets were then confirmed via qPCR and Western blot analysis. CCTα (encoded by *PCYT1A*) and CEPT1, two enzymes directly involved in PC synthesis, were significantly downregulated at the mRNA level and markedly decreased at the protein level in E12-KO cells compared to isogenic control cells (Figure 3E,F). Furthermore, SMPD4, which hydrolyzes sphingomyelin to ceramide and P-choline (Figure 3A), exhibited the same trend at both the mRNA and protein levels (Figure 3G). These data suggest that decreased PC levels in E12-KO cells are partly attributed to decreased expression of enzymes involved in PC synthesis.

DGs are necessary for the final step of PC synthesis and are also converted to TGs through the addition of acyl-CoA, which is catalyzed by diacylglycerol transferases (DGAT) [46] (Figure 3A). Levels of DGs and FAs were found to be significantly decreased in E12-KO cells, but TGs were significantly increased compared to isogenic control cells (Figure 3I). FAs are stored primarily as TGs [47], so increased TGs in E12-KO cells might explain why FAs are lower than in isogenic control cells. Moreover, the RNA-seq data showed that *DGAT1* and *DGAT2* were upregulated in E12-KO cells (Figure 3D), suggesting that DGs were shuttled more towards TG formation, rather than PC synthesis.

As previously mentioned, increased choline import is essential for tumor cells to maintain high levels of PCs. Due to this, it was determined whether decreased choline import was contributing to decreased PC levels in E12-KO cells. mRNA and protein levels of a major choline importer, CTL1 (encoded by *SLC44A1*), were analyzed and found to be unchanged in E12-KO cells compared to isogenic control cells (Figure 3H). Next, LC-MS/MS metabolomics was conducted to investigate intracellular choline and ethanolamine levels, and both were found to be significantly increased in E12-KO cells compared to isogenic control cells (Figure 3J). We hypothesize that the accumulation of choline and ethanolamine in E12-KO cells resulted from the decreased flux of these metabolites through the Kennedy pathway due to decreased expression of downstream genes, as discussed above. Altogether, these findings indicate that loss of *E12* leads to decreased PC levels due to decreased expression of enzymes directly or indirectly involved in PC/PE synthesis, and not due to decreased choline import.

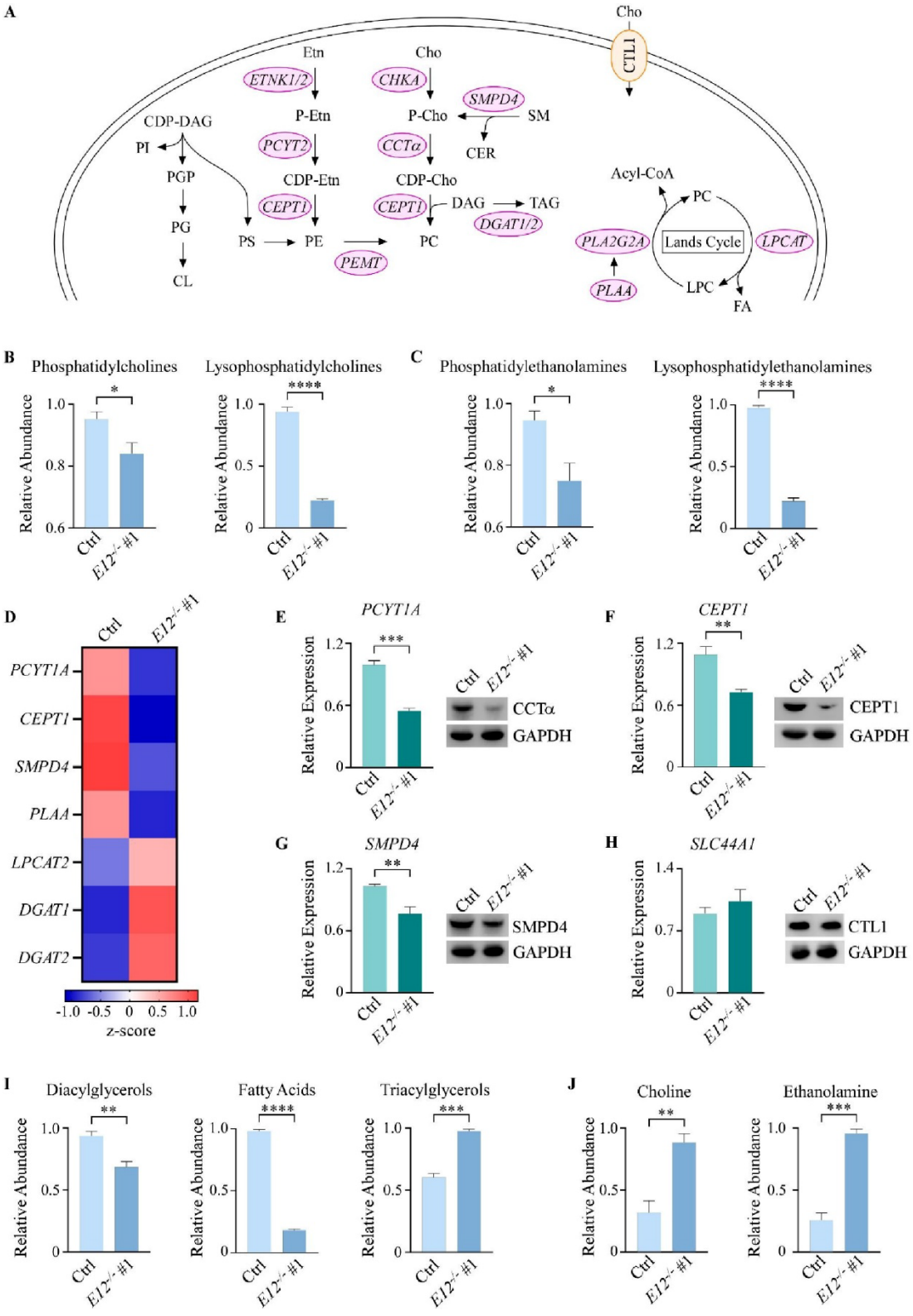

Figure 3. Kennedy pathway metabolites are altered upon knockout of *E12* in H1299 cells. (**A**). Schematic overview of the Kennedy pathway. CDP-DAG: CDP-diacylglycerol; PI: phosphatidylinositol; PG: phosphatidylglycerol; CL: cardiolipin; PS: phosphatidylserine; Cho: choline; P-cho: phosphocholine, (CDP-cho: cytidine diphosphate-choline; Etn: ethanolamine, P-Etn: phosphoethanolamine; CDP-Etn:

cytidine diphosphate-ethanolamine; SM: sphingomyelin; CER: ceramide; DAG: diacylglycerol; TAG: triacylglycerol; FA: fatty acid; CTL1: choline transporter-like protein 1. **B**,**C**). Relative abundance of (**B**) phosphatidylcholines and lysophosphatidylcholines and (**C**) phosphatidylethanolamines and lysophosphatidylethanolamines in isogenic control and $E12^{-/-}$ H1299 cells. Statistical significance was determined using Student's *t*-test. (**D**). Heat map of differentially expressed genes identified by RNA-seq analysis in isogenic control and $E12^{-/-}$ H1299 cell lines. Color density indicating z-score values was displayed below. (**E**–**H**). (Left) qPCR was used to quantify relative mRNA levels of *PCYT1A*, *CEPT1*, *SMPD4*, and *SLC44A1* in isogenic control and $E12^{-/-}$ H1299 cell lines. All values were normalized to *HPRT1* and are presented as relative to isogenic control (light green). Statistical significance was determined using Student's *t*-test. (Right) Western blot analysis was used to determine CCTa, CEPT1, SMPD4, CTL1, and GAPDH protein levels in isogenic control and $E12^{-/-}$ H1299 cell lines. (**I**,**J**). Relative abundance of (**I**) diacylglycerols, fatty acids, and triacylglycerols, and (**E**) choline and ethanolamine in isogenic control and $E12^{-/-}$ H1299 cells. Statistical significance was determined using Student's *t*-test. For B-C and E-J. Data presented as mean ± SEM. $n = 3$ independent experiments. * $p < 0.05$, ** $p < 0.01$, *** $p < 0.001$, **** $p < 0.0001$.

3.4. Loss of E12 Alters PC Chain Length and Saturation in H1299 Cells

Multiple studies show that increased FA chain length and desaturation are associated with malignancy and tumorigenesis [48,49]. In this study, loss of *E12* did not alter levels of long-chain fatty acids (LCFAs), but levels of very long-chain fatty acids (VLCFAs) were significantly decreased compared to isogenic control cells (Figure S2B). Consistent with the data in Figure 2D, a deeper analysis of PC saturation showed that, when compared to isogenic control cells, E12-KO cells had significantly higher levels of PCs containing saturated FAs and lower levels of PCs containing MUFAs, DUFAs, and PUFAs (Figure 4A). These findings suggest that loss of *E12* leads to dysregulation of PC chain length and saturation.

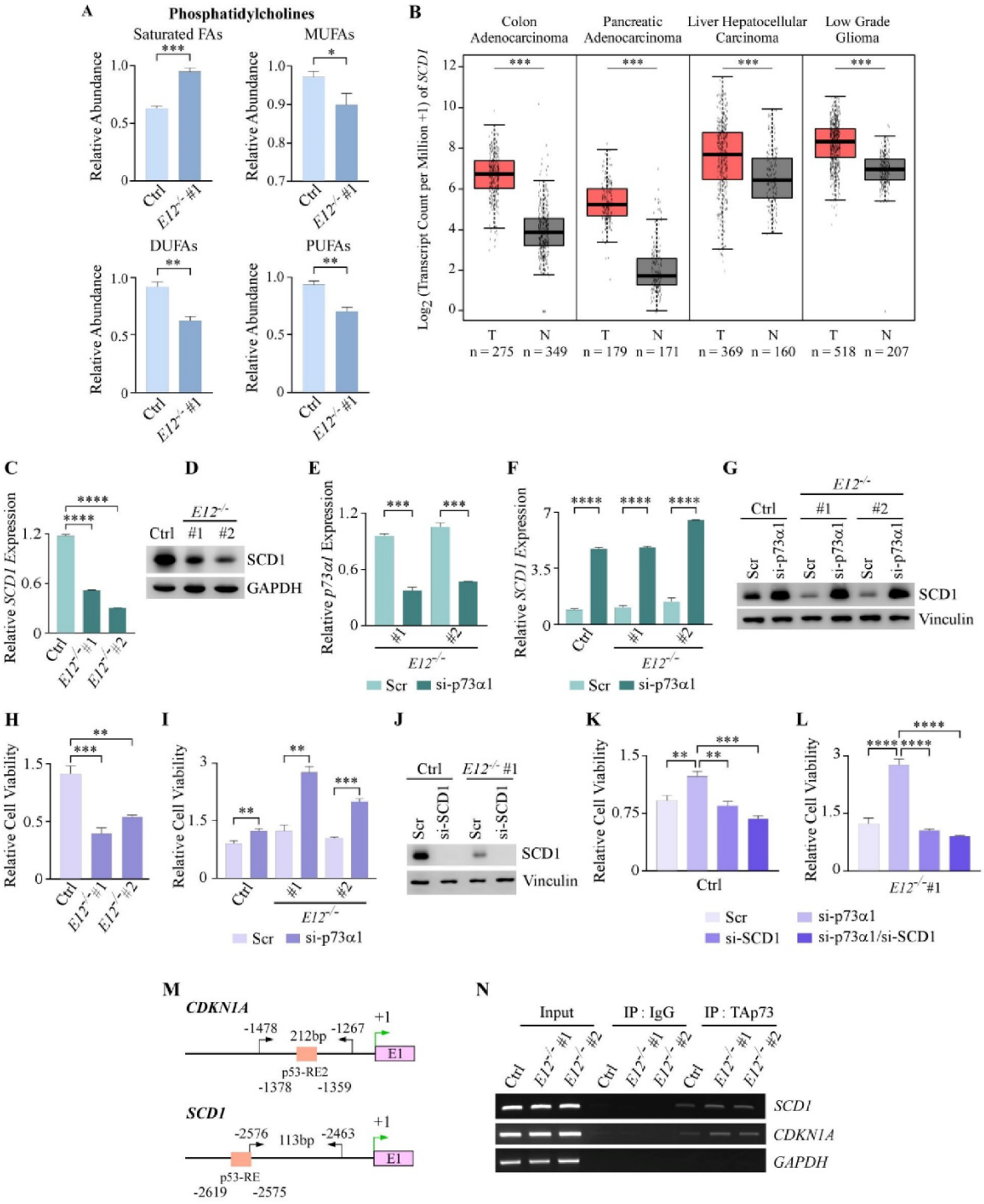

Figure 4. p73α1 suppresses cell viability by directly inhibiting *SCD1* expression. (**A**). Relative abundance of PC saturation level in isogenic control and *E12*$^{-/-}$ H1299 cells. Statistical significance was determined using Student's *t*-test. (**B**). *SCD1* transcript counts in the indicated tumors (data from TCGA) and the matched normal tissues (data from TCGA and GTEx) were analyzed via Gene Expression Profiling Interactive Analysis (GEPIA; http://gepia.cancer-pku.cn/index.html; accessed on 6 May 2022). T: tumor; N: matched normal tissue. (**C**). qPCR was used to quantify relative mRNA levels of *SCD1* in isogenic control and *E12*$^{-/-}$ H1299 cell lines. All values were normalized to *HPRT1* and are presented as relative to isogenic control (light green). Statistical significance was determined

using one-way ANOVA. (**D**). Western blot analysis was used to determine SCD1 and GAPDH protein levels in isogenic control and $E12^{-/-}$ H1299 cell lines. (**E**). qPCR was used to quantify relative mRNA levels of *p73α1* in $E12^{-/-}$ H1299 cells treated with scramble siRNA (Scr) or si-p73α1 for 48 h. All values were normalized to *HPRT1* and are presented as relative to each Scr-treated cell line. Statistical significance was determined using multiple Student's *t*-tests comparing Scr to si-p73α1 treatment for each cell line. (**F**). Cells were treated as in (**C**) and qPCR was used to quantify relative mRNA levels of *SCD1*. All values were normalized to *HPRT1* and are presented as relative to each Scr-treated cell line. Statistical significance was determined using multiple Student's *t*-tests comparing Scr to si-p73α1 treatment for each cell line. (**G**). Cells were treated as in (**C**) and Western blot analysis was used to determine SCD1 and Vinculin protein levels. (**H**). Cells were treated as in (**C**) and cell viability of the Scr-treated cell lines was determined using CellTiter-GLO. Cell viability for $E12^{-/-}$ #1 and #2 (dark purple) were presented as relative to isogenic control cells (light purple). Statistical significance was determined using one-way ANOVA. (**I**). Cells were treated as in (**C**) and cell viability was determined using CellTiter-GLO. Cell viability for isogenic control cells treated with si-p73α1 was presented as relative to isogenic control Scr-treated cells. Cell viability for $E12^{-/-}$ #1 cells treated with si-p73α1 was presented as relative to $E12^{-/-}$ #1 Scr-treated cells. Cell viability for $E12^{-/-}$ #2 cells treated with si-p73α1 was presented as relative to $E12^{-/-}$ #2 Scr-treated cells. Statistical significance was determined using multiple Student's *t*-tests comparing Scr to si-p73α1 treatment for each cell line. (**J**). Western blot analysis of SCD1 and Vinculin proteins in isogenic control and $E12^{-/-}$ H1299 cell lines treated with Scr or si-SCD1 for 48 h. (**K**). Cell viability was determined using CellTiter-GLO in the isogenic control H1299 cell line treated with Scr, si-p73α1, si-SCD1, or si-p73α1 and si-SCD1 for 48 h. Cell viability for isogenic control cells treated with si-p73α1, si-SCD1, or si-p73α1 and si-SCD1 was presented as relative to isogenic control Scr-treated cells. Statistical significance was determined using one-way ANOVA. (**L**). Cell viability was determined using CellTiter-GLO in the $E12^{-/-}$ H1299 cell line treated with Scr, si-p73α1, si-SCD1, or si-p73α1 and si-SCD1 for 48 h. Cell viability for $E12^{-/-}$ cells treated with si-p73α1, si-SCD1, or si-p73α1 and si-SCD1 was presented as relative to $E12^{-/-}$ Scr-treated cells. Statistical significance was determined using one-way ANOVA. (**M**). Diagram of the putative p53-Response Elements (p53-RE) (orange) in the promoter of *CDKN1A* and *SCD1*. Locations of the primers used to amplify the p53-RE in the promoters of *CDKN1A* and *SCD1* are indicated by the black arrows. Green arrows indicate transcription start site; E1 indicates exon 1. (**N**). ChIP analysis was performed with isogenic control and $E12^{-/-}$ H1299 cells. Cell lysates were immunoprecipitated with anti-rabbit IgG or anti-TAp73 to bring down the DNA-protein complex. DNA fragments were visualized by PCR with primers for *SCD1*, *CDKN1A*, and *GAPDH* promoters. For (**A**,**C**,**E**,**F**,**H**,**I**,**K**,**L**). Data are presented as mean ± SEM. $n = 3$ independent experiments. * $p < 0.05$, ** $p < 0.01$, *** $p < 0.001$, **** $p < 0.0001$.

3.5. p73α1 Suppresses Cancer Cell Viability by Directly Inhibiting SCD1 Expression in H1299 Cells

The finding that loss of *E12* led to increased saturated FAs and decreased MUFAs was further explored given the importance of MUFAs in tumorigenesis. There are three human desaturase enzymes (Δ5, Δ6 and Δ9) that are responsible for the formation of MUFAs, DUFAs, and PUFAs [50,51]. The rate-limiting step is the conversion of saturated FAs to MUFAs, which is catalyzed by Δ9 desaturase, or SCD1 [52]. SCD1 primarily catalyzes the formation of palmitoleic acid (FA 16:1) and oleic acid (FA 18:1) from palmitic acid (FA 16:0) and stearic acid (18:0), respectively [53]. Oleic acid and palmitoleic acid are the most abundant intracellular MUFAs and are necessary for the production of many lipids [54]. Interestingly, increased SCD1 expression is highly implicated in a variety of cancer types because of the tumorigenic properties of MUFAs [55–57]. Analysis of The Cancer Genome Atlas and the Genotype-Tissue Expression databases showed that *SCD1* transcript levels were significantly increased in 17 out of 31 tumor types compared to the matched normal tissues (Figure 4B; Figure S3A,B). Previously, p53 was identified as a direct suppressor of *SCD1* expression [58], and it is known that p73 can bind to p53-response elements to regulate target gene expression [59]. Given this, we hypothesized that p73α1 directly inhibits *SCD1* expression, therefore suppressing cancer cell proliferation.

To test this, SCD1 mRNA and protein levels were analyzed in isogenic control and E12-KO H1299 cell lines. mRNA levels were significantly decreased, and protein levels were considerably decreased in E12-KO cells compared to isogenic control cells (Figure 4C,D). Next, p73α1-specific siRNA was used to determine whether p73α1 was responsible for the observed decrease in SCD1 mRNA and protein levels (Figure 4E). Indeed, the data revealed that knockdown of p73α1 in both isogenic control and E12-KO cells led to a significant increase in *SCD1* mRNA levels, and a consistent increase at the protein level (Figure 4F,G). We then wanted to determine whether p73α1-mediated suppression of *SCD1* expression was contributing to the previously described tumor suppressive effects of p73α1. First, it was reiterated that loss of *E12* leads to decreased cell viability (Figure 4H), and that p73α1 was responsible for the growth-suppressive effects (Figure 4I). Next, siRNA targeting p73α1 and SCD1 (Figure 4J) was used to determine whether p73α1-mediated suppression of *SCD1* inhibits cancer cell proliferation. In both isogenic control and E12-KO cells, knockdown of *SCD1*, alone or with p73α1, led to a significant decrease in cell viability compared to knockdown of only p73α1 (Figure 4K,L). Moreover, knockdown of p73α1 and *SCD1* did not elicit a significant difference in cell viability compared to knockdown of *SCD1* alone (Figure 4K,L), confirming that p73α1-mediated suppression of *SCD1* contributes to the decreased cell viability in E12-KO cells.

To determine whether p73α1 was directly inhibiting *SCD1* expression, a chromatin immunoprecipitation (ChIP) assay was performed in isogenic control and E12-KO cell lines (Figure 4M). The data showed that DNA fragments containing the putative p53-response element in the *SCD1* promoter were detected following immunoprecipitation with TAp73 antibody in both isogenic control and E12-KO cell lines (Figure 4N). Taken together, these data identify SCD1 as a direct target of p73α1 and show that p73α1-mediated suppression of *SCD1* expression contributes to the tumor suppressive effects of p73α1.

3.6. p73α1-Mediated Suppression of SCD1 Leads to an Increased Ratio of Stearic Acid to Oleic Acid in H1299 Cells

As previously mentioned, palmitic acid and stearic acid are the major substrates for SCD1, leading to the formation of palmitoleic acid and oleic acid, respectively (Figure 5A). Due to the findings that p73α1 directly suppresses *SCD1* expression, it was determined whether this affected the levels of these four lipids. E12-KO cells had significantly decreased levels of these four FAs compared to isogenic control cells (Figure 5B,C). Next, the ratios of saturated FAs to MUFAs were analyzed because a change in SCD1 expression and/or activity would alter these ratios. Indeed, the data showed that the ratios of palmitic acid to palmitoleic acid and stearic acid to oleic acid were significantly increased in E12-KO cells compared to isogenic control cells (Figure 5D). Additionally, the ratios of saturated FAs to MUFAs of varying chain lengths were analyzed, and 8 out of 9 were significantly increased in E12-KO cells compared to isogenic control cells (Figure 5E).

To confirm that p73α1-mediated suppression of *SCD1* expression leads to an increased ratio of saturated FAs to MUFAs, lipidomic analysis was performed following knockdown of p73α1 or p73α1 and SCD1. The ratio of stearic acid to oleic acid was significantly decreased after knockdown of p73α1, with a similar, albeit not significant, trend seen in the ratio of palmitic acid to palmitoleic acid in E12-KO cells (Figure 5F). Following knockdown of both p73α1 and SCD1 in E12-KO cells, there was a significant increase in the ratio of stearic acid to oleic acid, but not in the ratio of palmitic acid to palmitoleic acid (Figure 5F). A similar trend for both ratios was found in the isogenic control cells (Figure 5G). Taken together, these data identify p73α1 as a transcriptional repressor of *SCD1*, which leads to an increased ratio of stearic to oleic acid.

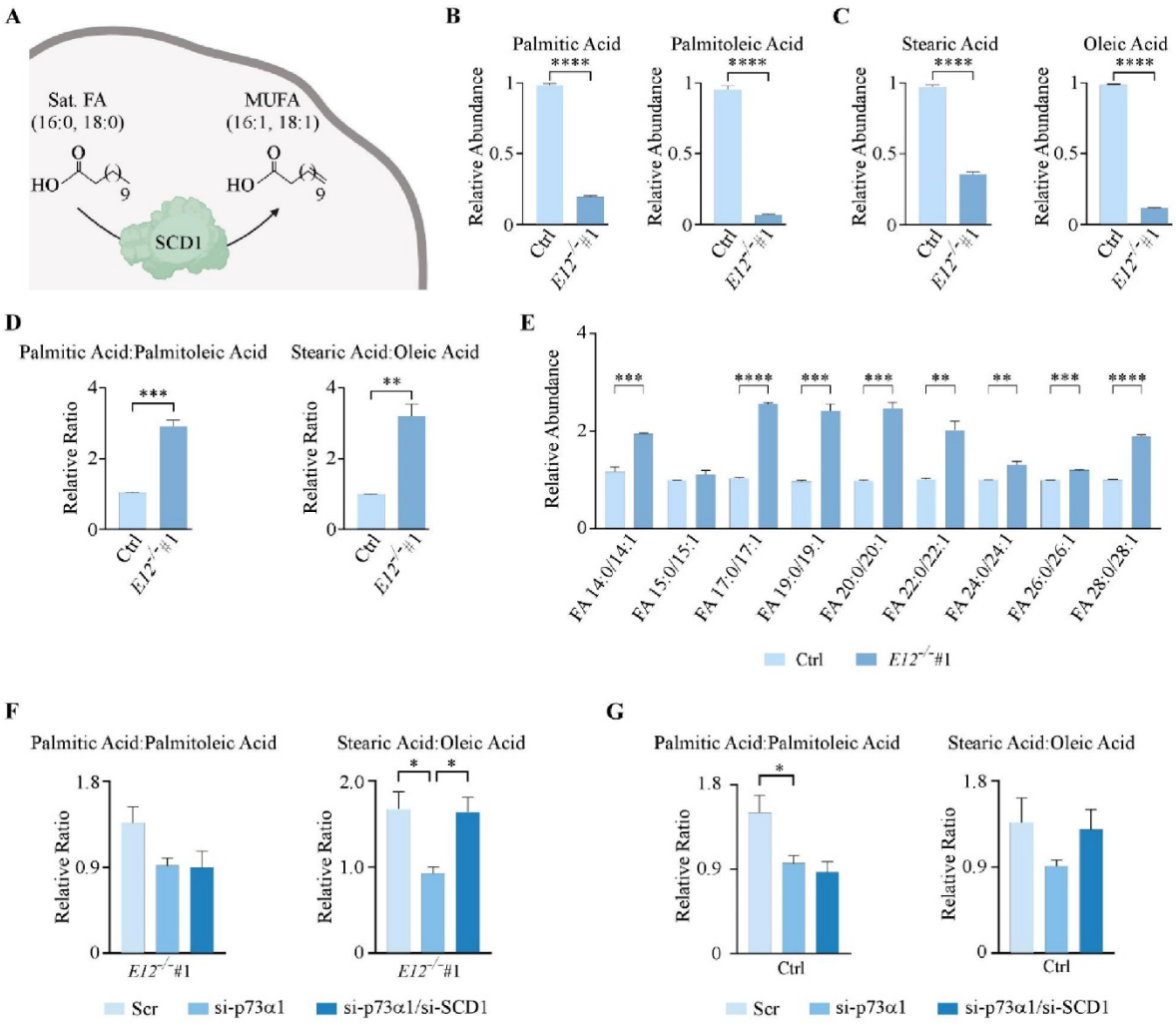

Figure 5. p73α1-mediated suppression of *SCD1* leads to an increased ratio of saturated FAs to MUFAs. (**A**). Schematic representation of SCD1 enzymatic activity. (**B**,**C**). Relative abundance of (**B**) palmitic acid and palmitoleic acid and (**C**) stearic acid and oleic acid in isogenic control and $E12^{-/-}$ H1299 cells. Statistical significance was determined using Student's *t*-test. (**D**). Ratio of (left) palmitic acid to palmitoleic acid and (right) stearic acid to oleic acid in isogenic control and $E12^{-/-}$ H1299 cells. Statistical significance was determined using Student's *t*-test. (**E**). Ratio of saturated FAs to MUFAs for the indicated FA chain length in isogenic control (light blue) and $E12^{-/-}$ (dark blue) H1299 cells. Statistical significance was determined using multiple Student's *t*-tests comparing isogenic control and $E12^{-/-}$ cell lines for each saturated/unsaturated FA pair. (**F**). Ratio of (left) palmitic acid to palmitoleic acid and (right) stearic acid to oleic acid in $E12^{-/-}$ H1299 cells following treatment with Scr, si-SCD1, or si-SCD1 and si-p73α1 for 48 h. Statistical significance was determined using one-way ANOVA. (**G**). Ratio of (left) palmitic acid to palmitoleic acid and (right) stearic acid to oleic acid in isogenic control H1299 cells treated with Scr, sip73α1, or sip73α1 and siSCD1 for 48 h. Statistical significance was determined using one-way ANOVA. For B-G. Data are presented as mean ± SEM. $n = 3$ independent experiments. * $p < 0.05$, ** $p < 0.01$, *** $p < 0.001$, **** $p < 0.0001$.

4. Discussion

SCD1 promotes tumorigenesis through a decreased ratio of saturated FAs to MUFAs [55–57]. Phospholipids containing MUFAs are less susceptible to lipid peroxidation than saturated FAs and PUFAs, therefore conferring resistance to ferroptosis [60,61]. Moreover, mass-spectrometry-based imaging showed that PCs containing MUFAs were more abundant in cancerous tissues compared to matched normal tissues [62]. Conversely, the accumulation of saturated FAs causes lipotoxicity, and in most cases cell death, by promoting endoplasmic reticulum stress [63]. These findings support a mechanism for how suppression of *SCD1* expression via p73α1 leads to decreased cancer cell viability in E12-KO cells. In the present study, we found that p73α1-knockdown decreased the ratio of stearic acid to oleic acid, while knockdown of both p73α1 and SCD1 reversed these effects. Interestingly, the reversal following concurrent knockdown was not observed in the ratio of palmitic acid to palmitoleic acid. One report noted that some cancer cells are able to utilize Δ6 desaturase (FADS2) to produce cis-6-C16:1 (FA 16:1; sapienate) [64], which differs from palmitoleic acid in the location of the double bond. By itself, FADS2 might be able to compensate for the loss of SCD1, which is why the ratio of FA 16:0 to FA 16:1 is not increased following SCD1 knockdown. However, we were unable to give detailed chemical analyses of the possible FA 16:1-containing isomers because current metabolomics methods cannot determine the location of double bonds in complex lipids. Such detailed analyses may be possible in the future by adding ultraviolet photodissociation mass spectrometry [65], chemical derivatization such as ozonolysis [66], or electron-activated dissociation mass spectrometry [67].

Cancer cells are able to increase uptake and/or biosynthesis of FAs, allowing for increased energy for various cellular processes, such as growth and proliferation [68]. In this study, we not only found that loss of *E12* altered the ration of saturated FAs to MUFAs, but we also showed that, overall, FA abundance was decreased upon E12-KO. We hypothesize that decreased FA abundance in E12-KO cells could also be contributing to the observed decrease in cell viability. Moreover, decreased abundance of FAs could lead to decreased mitochondrial FA oxidation, which has been shown to be increased in tumorigenic cells [68]. As such, it would be interesting to explore the relationship between cancer cell viability and FA abundance and oxidation in E12-KO cells in future work.

In addition to the actual biochemical differences that we observed, we are also able to interpret these changes with respect to the organelles that may be most likely involved. The peroxisome is a key organelle involved in lipid metabolism, immunometabolism, and cellular redox balance. It is the only organelle that catabolizes VLCFAs and branched-chain FAs, and converts FAs and alcohols to ether-linked lipids. Our data showed that the loss of *E12* resulted in increased catabolism of VLCFAs, indicating alterations to peroxisomal activity. Additional lines of evidence to support this notion are increased levels of ether-linked TG lipids in E12-KO cells compared to isogenic control cells. Interestingly, phosphoether lipids did not show differences in abundance, in contrast with ether-linked TG lipids. Such a phenomenon has not been reported before. Many studies have shown that peroxisomal alterations contribute to cancer and inflammation. A link of peroxisomal activity to cancer cell autophagy was previously shown by the impaired ability of CD8 + T-cells to kill malignant cells that were associated with an accumulation of LCFAs and VLCFAs within the tumor microenvironment [69]. Ether-linked lipids have also been shown to be elevated in various tumors compared to control tissues, and show a linear relationship with metastatic spread in breast, prostate, and lung cancers [68,70,71]. We previously reported that $E12^{+/-}$mice had increased immune cell infiltration and inflammation [37], which may be explained by peroxisomal-derived inflammatory cytokines and metabolites (prostaglandins, leukotrienes, thromboxanes) and immune cell activation through redox homeostasis. Future research will examine the role of the peroxisome in relationship to p73α1 to better understand tumor microenvironment and metabolism, and overall cancer cell phenotypes.

5. Conclusions

In this study, we identified a role for p73α1 in lipid metabolism through direct regulation of SCD1, which alters the ratio of saturated FAs to MUFAs and decreases cancer cell viability. Taken together, our data indicate that p73 has a critical role in regulating the metabolome and lipidome, which may contribute to oncogenesis, redox balance, and immunometabolic signaling. As such, it would be of great interest to further investigate how the various p73 isoforms alter biochemical pathways, thus influencing the tumor microenvironment and cancer metabolism.

Supplementary Materials: The following supporting information can be downloaded at: https://www.mdpi.com/article/10.3390/cells11162516/s1, Figure S1: Loss of *E12* alters the lipidome in H1299 cells; Figure S2: Metabolites involved in PC synthesis are altered upon loss of *E12*; Figure S3: *SCD1* transcript counts are increased in certain cancer types; Table S1: Primers used to generate expression vectors; Table S2: Primers used for qPCR and ChIP.

Author Contributions: Conceptualization, Z.R., K.L., T.S., S.M., J.Z., X.C. and O.F.; methodology, Z.R., K.L., T.S., S.M., J.Z., X.C. and O.F.; validation, Z.R., K.L., T.S. and S.M.; formal analysis, Z.R. and K.L.; investigation, Z.R., K.L. and X.K.; writing—original draft, Z.R. and K.L.; writing—review and editing, Z.R., K.L., O.F. and X.C.; visualization, Z.R. and K.L.; supervision, T.S., S.M., J.Z., O.F. and X.C.; funding acquisition, K.L., J.Z., O.F. and X.C. All authors have read and agreed to the published version of the manuscript.

Funding: This work was supported in part by NIH T32 HL007013 to K.L., NIH RO1 CA081237 to X.C., California TRDRP T31IP1727 to J.Z., P30 AG072972 and NIH U19 AG023122 to O.F.

Institutional Review Board Statement: Not applicable.

Informed Consent Statement: Not applicable.

Data Availability Statement: Available upon request.

Acknowledgments: The authors want to thank members of the Chen-Zhang and Fiehn Labs for their support.

Conflicts of Interest: The authors declare no conflict of interest.

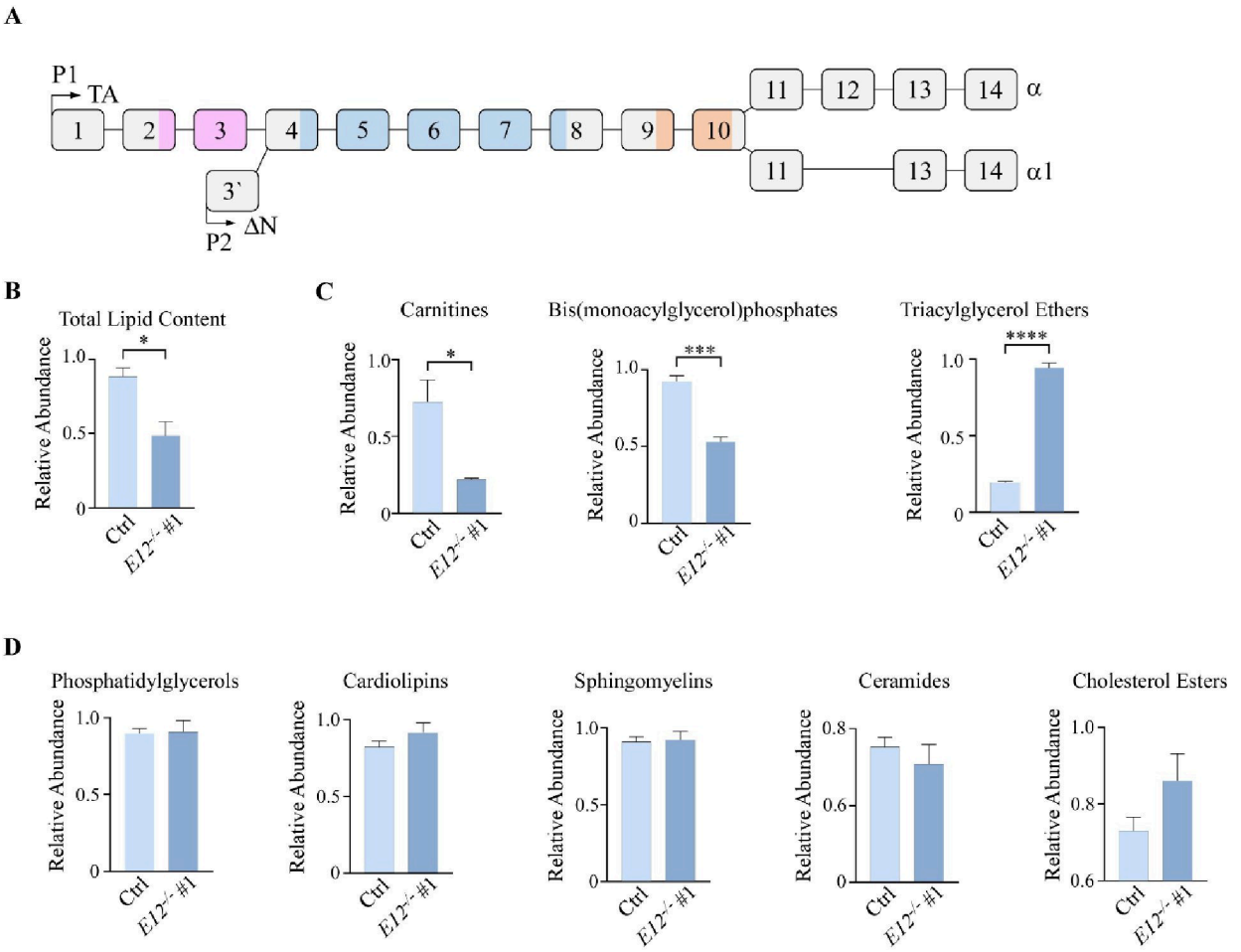

Fig. S1. Loss of *E12* alters the lipidome in H1299 cells.

A. *TP73* diagram showing that loss of exon 12 leads to isoform switch from p73α to p73α1. Pink region indicates transactivation domain, blue region indicates DNA binding domain, and orange region indicates oligomerization domain. P1: promoter 1; P2: promoter 2.

B. Relative abundance of total lipid content in isogenic control and *E12*$^{-/-}$ H1299 cells. Statistical significance was determined using Student's t-test.

C. Relative abundance of carnitines, bis(monoacylglycerol)phosphates, and triacylglycerol ethers in isogenic control and *E12*$^{-/-}$ H1299 cells. Statistical significance was determined using Student's t-test.

D. Relative abundance of phosphatidylglycerols, cardiolipins, sphingomyelins, ceramides, and cholesterol esters in isogenic control and *E12*$^{-/-}$ H1299 cells. Statistical significance was determined using Student's t-test.

For B-D. Data are presented as mean ± SEM. n = 3 independent experiments. * $p < 0.05$, *** $p < 0.001$, **** $p < 0.0001$.

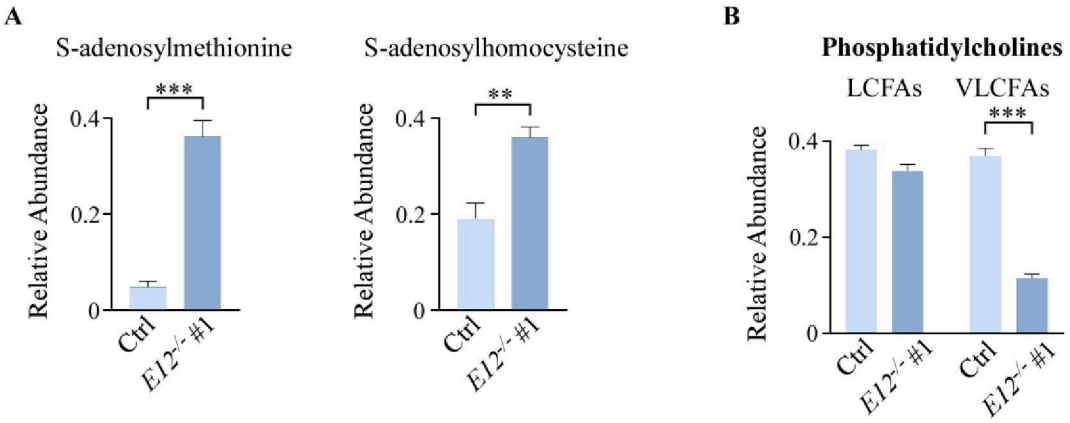

Fig. S2. Metabolites involved in PC synthesis are altered upon loss of *E12*.

A. Relative abundance of S-adenosylmethionine and S-adenosylhomocysteine in isogenic control and *E12*$^{-/-}$ H1299 cell lines. Statistical significance was determined using Student's t-test.

B. Relative abundance of PCs containing (left) long-chain fatty acids (LCFAs) and (right) very long-chain fatty acids (VLCFAs) in isogenic control and *E12*$^{-/-}$ H1299 cell lines. Statistical significance was determined using Student's t-test.

For A-B. Data presented as mean ± SEM. n = 3 independent experiments. ** $p < 0.01$, *** $p < 0.001$.

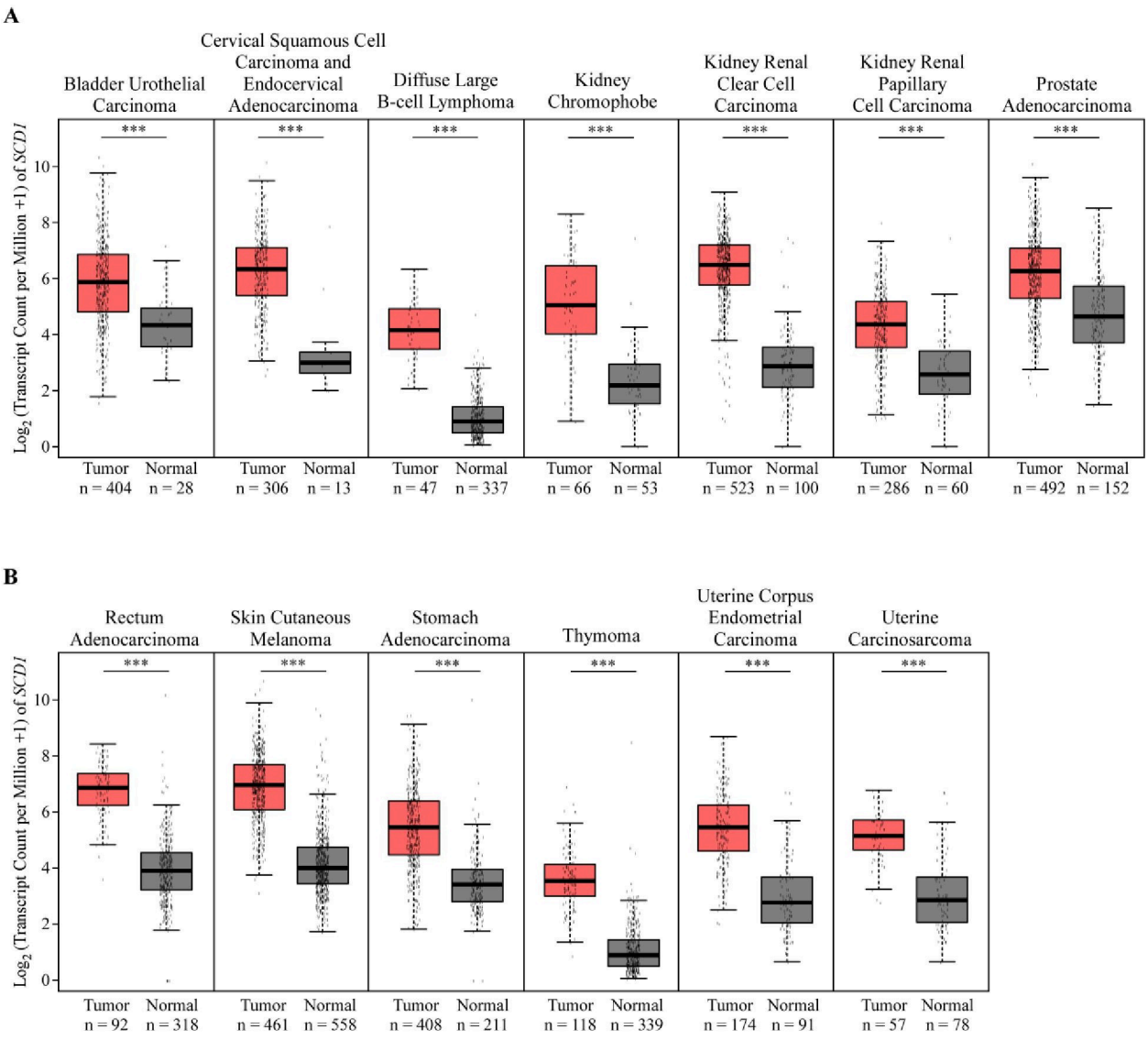

Fig. S3. *SCD1* transcript counts are increased in certain cancer types.

A-B. *SCD1* transcript counts in the indicated tumors (data from TCGA) and the matched normal tissues (data from TCGA and GTEx) were analyzed via Gene Expression Profiling Interactive Analysis (GEPIA, http://gepia.cancer-pku.cn/index.html). *** $p < 0.001$.

Table S1. Primers used to generate expression vectors.

Name	Oligonucleotide	Sequence
p73-E12-gRNA-1-pSpCas9(BB)-2A-Puro	Sense	5`-CACCGCGTCACATCGCCAGGCCTT-3`
	Antisense	5`-AAACAAGGCCTGGCGATGTGACGC-3`
p73-E12-gRNA-2-pSpCas9(BB)-2A-Puro	Sense	5`-CACCGCTGCTGCTCATCTCGCCGT-3`
	Antisense	5`-AAACACGGCGAGATGAGCAGCAGC-3`

Table S2. Primers used for qPCR and ChIP.

TP73α1	Sense	5`-CACCGTCAAACGTGGTGCCCCCATC-3`
	Antisense	5`-AAACGATGGGGGCACCACGTTTGAC-3`
SCD1	Sense	5`-CACTTGGGAGCCCTGTATGG-3`
	Antisense	5`-TGAGCTCCTGCTGTTATGCC-3`
PCYT1A	Sense	5`-GAGTTGCAGCATGTGCCGA-3`
	Antisense	5`-GCATTGACCTTGGCTGAACA-3`
CEPT1	Sense	5`-GGCAGTGATTGGAGGACCAC-3`
	Antisense	5`-TGCCAACACCACCTGTGAAG-3`
SMPD4	Sense	5`-GACTCCCAGCCCCGGTGT-3`
	Antisense	5`-CCACTCGGAACACCATGAG-3`
SLC44A1	Sense	5`-GCAGAGCTCCAAACGAGAA-3`
	Antisense	5`-AGCCACAAATAAATCCCATCCC-3`
HPRT1	Sense	5`-CACCGCGTCACATCGCCAGGCCTT-3`
	Antisense	5'-AAACAAGGCCTGGCGATGTGACGC-3`
SCD1-ChIP	Sense	5`-TGCAGGGGTTTTTCGGAGTTT-3`
	Antisense	5`-TGAACGCCCTATTCCAGCCTTA-3`
CDKN1A-ChIP	Sense	5`-GGTCTGCTACTGTGTCCTCC-3`
	Antisense	5`-CATCTGAACAGAAATCCCAC-3`
GAPDH-ChIP	Sense	5`-AAAAGCGGGGAGAAAGTAGG-3`
	Antisense	5`-AAGAAGATGCGGCTGACTGT-3`

References

1. Tocher, D.R. Chapter 6 Glycerophospholipid metabolism. In *Biochemistry and Molecular Biology of Fishes*; ScienceDirect: Amsterdam, The Netherlands, 1995; pp. 119–157. [CrossRef]
2. Kanno, K.; Wu, M.K.; Scapa, E.F.; Roderick, S.L.; Cohen, D.E. Structure and function of phosphatidylcholine transfer protein (PC-TP)/StarD2. *Biochim. Biophys. Acta-Mol. Cell Biol. Lipids* **2007**, *1771*, 654–662. [CrossRef]
3. Gibellini, F.; Smith, T.K. The Kennedy pathway-de novo synthesis of phosphatidylethanolamine and phosphatidylcholine. *IUBMB Life* **2010**, *62*, 414–428. [CrossRef] [PubMed]
4. Moessinger, C.; Klizaite, K.; Steinhagen, A.; Philippou-Massier, J.; Shevchenko, A.; Hoch, M.; Ejsing, C.S.; Thiele, C. Two different pathways of phosphatidylcholine synthesis, the Kennedy Pathway and the Lands Cycle, differentially regulate cellular triacylglycerol storage. *BMC Cell Biol.* **2014**, *15*, 43. [CrossRef] [PubMed]
5. Watkins, S.M.; Zhu, X.; Zeisel, S.H. Phosphatidylethanolamine-N-methyltransferase Activity and Dietary Choline Regulate Liver-Plasma Lipid Flux and Essential Fatty Acid Metabolism in Mice. *J. Nutr.* **2003**, *133*, 3386–3391. [CrossRef] [PubMed]
6. Michel, V.; Yuan, Z.; Ramsubir, S.; Bakovic, M. Choline transport for phospholipid synthesis. *Exp. Biol. Med.* **2006**, *231*, 490–504. [CrossRef]
7. Robichaud, P.P.; Surette, M.E. Polyunsaturated fatty acid-phospholipid remodeling and inflammation. *Curr. Opin. Endocrinol. Diabetes Obes.* **2015**, *22*, 112–118. [CrossRef]
8. Vance, D.E. Phospholipid methylation in mammals: From biochemistry to physiological function. *Biochim. Biophys. Acta-Biomembr.* **2014**, *1838*, 1477–1487. [CrossRef]
9. Harayama, T.; Eto, M.; Shindou, H.; Kita, Y.; Otsubo, E.; Hishikawa, D.; Ishii, S.; Sakimura, K.; Mishina, M.; Shimizu, T. Lysophospholipid acyltransferases mediate phosphatidylcholine diversification to achieve the physical properties required in vivo. *Cell Metab.* **2014**, *20*, 295–305. [CrossRef]
10. Cole, L.K.; Vance, J.E.; Vance, D.E. Phosphatidylcholine biosynthesis and lipoprotein metabolism. *Biochim. Biophys. Acta-Mol. Cell Biol. Lipids* **2012**, *1821*, 754–761. [CrossRef]
11. Hanahan, D.; Weinberg, R.A. Hallmarks of cancer: The next generation. *Cell* **2011**, *144*, 646–674. [CrossRef]
12. Snaebjornsson, M.T.; Janaki-Raman, S.; Schulze, A. Greasing the Wheels of the Cancer Machine: The Role of Lipid Metabolism in Cancer. *Cell Metab.* **2020**, *31*, 62–76. [CrossRef]
13. Saito, T.; Kuma, A.; Sugiura, Y.; Ichimura, Y.; Obata, M.; Kitamura, H.; Okuda, S.; Lee, H.C.; Ikeda, K.; Kanegae, Y.; et al. Autophagy regulates lipid metabolism through selective turnover of NCoR1. *Nat. Commun.* **2019**, *10*, 1567. [CrossRef] [PubMed]
14. Jain, M.; Nilsson, R.; Sharma, S.; Madhusudhan, N.; Kitami, T.; Souza, A.L.; Kafri, R.; Kirschner, M.W.; Clish, C.B.; Mootha, V.K. Metabolite profiling identifies a key role for glycine in rapid cancer cell proliferation. *Science* **2012**, *336*, 1040–1044. [CrossRef] [PubMed]
15. Daly, P.F.; Lyon, R.C.; Faustino, P.J.; Cohen, J.S. Phospholipid metabolism in cancer cells monitored by 31P NMR spectroscopy. *J. Biol. Chem.* **1987**, *262*, 14875–14878. [CrossRef]
16. Glunde, K.; Bhujwalla, Z.M.; Ronen, S.M. Choline metabolism in malignant transformation. *Nat. Rev. Cancer* **2011**, *11*, 835–848. [CrossRef]
17. Zheng, Y.; Rodrik, V.; Toschi, A.; Shi, M.; Hui, L.; Shen, Y.; Foster, D.A. Phospholipase D Couples Survival and Migration Signals in Stress Response of Human Cancer Cells. *J. Biol. Chem.* **2006**, *281*, 15862–15868. [CrossRef] [PubMed]
18. Gomez-Cambronero, J. Phosphatidic acid, phospholipase D and tumorigenesis. *Adv. Biol. Regul.* **2014**, *54*, 197–206. [CrossRef]
19. Han, H.; Qi, R.; Zhou, J.J.; Ta, A.P.; Yang, B.; Nakaoka, H.J.; Seo, G.; Guan, K.L.; Luo, R.; Wang, W. Regulation of the Hippo Pathway by Phosphatidic Acid-Mediated Lipid-Protein Interaction. *Mol. Cell* **2018**, *72*, 328–340. [CrossRef] [PubMed]
20. Foster, D.A. Phosphatidic acid signaling to mTOR: Signals for the survival of human cancer cells. *Biochim. Biophys. Acta-Mol. Cell Biol. Lipids* **2009**, *1791*, 949–955. [CrossRef]
21. Wang, B.; Wu, L.; Chen, J.; Dong, L.; Chen, C.; Wen, Z.; Hu, J.; Fleming, I.; Wang, D.W. Metabolism pathways of arachidonic acids: Mechanisms and potential therapeutic targets. *Signal Transduct. Target. Ther.* **2021**, *6*, 94. [CrossRef]
22. Kaghad, M.; Bonnet, H.; Yang, A.; Creancier, L.; Biscan, J.C.; Valent, A.; Minty, A.; Chalon, P.; Lelias, J.M.; Dumont, X.; et al. Monoallelically expressed gene related to p53 at 1p36, a region frequently deleted in neuroblastoma and other human cancers. *Cell* **1997**, *90*, 809–819. [CrossRef]
23. Jost, C.A.; Marin, M.C.; Kaelin, W.G., Jr. P73 is a human p53-related protein that can induce apoptosis. *Nature* **1997**, *389*, 191–194. [CrossRef] [PubMed]
24. Arrowsmith, C.H. Structure and function in the p53 family. *Cell Death Differ.* **1999**, *6*, 1169–1173. [CrossRef]
25. Tomasini, R.; Tsuchihara, K.; Wilhelm, M.; Fujitani, M.; Rufini, A.; Cheung, C.C.; Khan, F.; Itie-Youten, A.; Wakeham, A.; Tsao, M.S.; et al. TAp73 knockout shows genomic instability with infertility and tumor suppressor functions. *Genes Dev.* **2008**, *22*, 2677–2691. [CrossRef] [PubMed]
26. Zhu, J.; Jiang, J.; Zhou, W.; Chen, X. The Potential Tumor Suppressor p73 Differentially Regulates Cellular p53 Target Genes. *Cancer Res.* **1998**, *58*, 5061–5065.
27. Melino, G.; Bernassola, F.; Ranalli, M.; Yee, K.; Zong, W.X.; Corazzari, M.; Knight, R.A.; Green, D.R.; Thompson, C.; Vousden, K.H. P73 Induces Apoptosis via PUMA Transactivation and Bax Mitochondrial Translocation. *J. Biol. Chem.* **2004**, *279*, 8076–8083. [CrossRef]
28. Vernole, P.; Neale, M.H.; Barcaroli, D.; Munarriz, E.; Knight, R.A.; Tomasini, R.; Mak, T.W.; Melino, G.; de Laurenzi, V. TAp73α binds the kinetochore proteins Bub1 and Bub3 resulting in polyploidy. *Cell Cycle* **2009**, *8*, 421–429. [CrossRef]

29. Yang, A.; Walker, N.; Bronson, R.; Kaghad, M.; Oosterwegel, M.; Bonnin, J.; Vagner, C.; Bonnet, H.; Dikkes, P.; Sharpe, A.; et al. P73-deficient mice have neurological, pheromonal and inflammatory defects but lack spontaneous tumours. *Nature* **2000**, *404*, 99–103. [CrossRef]
30. Wilhelm, M.T.; Rufini, A.; Wetzel, M.K.; Tsuchihara, K.; Inoue, S.; Tomasini, R.; Itie-Youten, A.; Wakeham, A.; Arsenian-Henriksson, M.; Melino, G.; et al. Isoform-specific p73 knockout mice reveal a novel role for ΔNp73 in the DNA damage response pathway. *Genes Dev.* **2010**, *24*, 549–560. [CrossRef]
31. Zaika, A.I.; Slade, N.; Erster, S.H.; Sansome, C.; Joseph, T.W.; Pearl, M.; Chalas, E.; Moll, U.M. δNp73, a dominant-negative inhibitor of wild-type p53 and TAp73, is up-regulated in human tumors. *J. Exp. Med.* **2002**, *196*, 765–780. [CrossRef]
32. Steder, M.; Alla, V.; Meier, C.; Spitschak, A.; Pahnke, J.; Fürst, K.; Kowtharapu, B.S.; Engelmann, D.; Petigk, J.; Egberts, F.; et al. DNp73 Exerts Function in Metastasis Initiation by Disconnecting the Inhibitory Role of EPLIN on IGF1R-AKT/STAT3 Signaling. *Cancer Cell* **2013**, *24*, 512–527. [CrossRef] [PubMed]
33. De Laurenzi, V.; Costanzo, A.; Barcaroli, D.; Terrinoni, A.; Falco, M.; Annicchiarico-petruzzelli, M.; Levrero, M.; Melino, G. Two New p73 Splice Variants with Different Transcriptional Activity. *J. Exp. Med.* **1998**, *188*, 1763–1768. [CrossRef] [PubMed]
34. de Laurenzi, V.; Catani, M.V.; Terrinoni, A.; Corazzari, M.; Melino, G.; Constanzo, A.; Levrero, M.; Knight, R.A. Additional complexity in p73: Induction by mitogens in lymphoid cells and identification of two new splicing variants ε and ζ. *Cell Death Differ.* **1999**, *6*, 389–390. [CrossRef] [PubMed]
35. Rufini, A.; Agostini, M.; Grespi, F.; Tomasini, R.; Sayan, B.S.; Niklison-Chirou, M.V.; Conforti, F.; Velletri, T.; Mastino, A.; Mak, T.W.; et al. P73 in cancer. *Genes Cancer* **2011**, *2*, 491–502. [CrossRef] [PubMed]
36. Grespi, F.; Amelio, I.; Tucci, P.; Annicchiarico-Petruzzelli, M.; Melino, G. Tissue-specific expression of p73 C-terminal isoforms in mice. *Cell Cycle* **2012**, *11*, 4474–4483. [CrossRef]
37. Laubach, K.N.; Yan, W.; Kong, X.; Sun, W.; Chen, M.; Zhang, J.; Chen, X. p73α1, a p73 C-terminal isoform, regulates tumor suppression and the inflammatory response via Notch1. *Proc. Natl. Acad. Sci. USA* **2022**, *119*, e2123202119. [CrossRef]
38. Ran, F.A.; Hsu, P.D.; Wright, J.; Agarwala, V.; Scott, D.A.; Zhang, F. Genome engineering using the CRISPR-Cas9 system. *Nat. Protoc.* **2013**, *8*, 2281–2308. [CrossRef]
39. Chen, X.; Bargonetti, J.; Prives, C. p53, through p21 (WAF1/CIP1), Induces Cyclin D1 Synthesis. *Cancer Res.* **1995**, *55*, 4257–4263.
40. Liu, G.; Xia, T.; Chen, X. The Activation Domains, the Proline-rich Domain, and the C-terminal Basic Domain in p53 Are Necessary for Acetylation of Histones on the Proximal p21 Promoter and Interaction with p300/CREB-binding Protein. *J. Biol. Chem.* **2003**, *278*, 17557–17565. [CrossRef]
41. Matyash, V.; Liebisch, G.; Kurzchalia, T.V.; Shevchenko, A.; Schwudke, D. Lipid extraction by methyl-tert-butyl ether for high-throughput lipidomics. *J. Lipid Res.* **2008**, *49*, 1137–1146. [CrossRef]
42. Folz, J.; Oh, Y.T.; Blaženović, I.; Richey, J.; Fiehn, O.; Youn, J.H. Interaction of Gut Microbiota and High-Sodium, Low-Potassium Diet in Altering Plasma Triglyceride Profiles Revealed by Lipidomics Analysis. *Mol. Nutr. Food Res.* **2019**, *63*, 1900752. [CrossRef] [PubMed]
43. Showalter, M.R.; Nonnecke, E.B.; Linderholm, A.L.; Cajka, T.; Sa, M.R.; Lönnerdal, B.; Kenyon, N.J.; Fiehn, O. Obesogenic diets alter metabolism in mice. *PLoS ONE* **2018**, *13*, e0190632. [CrossRef] [PubMed]
44. Rabow, Z.; Morningstar, T.; Showalter, M.; Heil, H.; Thongphanh, K.; Fan, S.; Chan, J.; Martínez-Cerdeño, V.; Berman, R.; Zagzag, D.; et al. Exposure to DMSO during infancy alters neurochemistry, social interactions, and brain morphology in long-evans rats. *Brain Behav.* **2021**, *11*, e02146. [CrossRef] [PubMed]
45. Barupal, D.K.; Fiehn, O. Chemical Similarity Enrichment Analysis (ChemRICH) as alternative to biochemical pathway mapping for metabolomic datasets. *Sci. Rep.* **2017**, *7*, 14567. [CrossRef] [PubMed]
46. Eichmann, T.O.; Lass, A. DAG tales: The multiple faces of diacylglycerol—Stereochemistry, metabolism, and signaling. *Cell Mol. Life Sci.* **2015**, *72*, 3931–3952. [CrossRef]
47. Koundouros, N.; Poulogiannis, G. Reprogramming of fatty acid metabolism in cancer. *Br. J. Cancer* **2019**, *122*, 4–22. [CrossRef]
48. Chen, M.; Huang, J. The expanded role of fatty acid metabolism in cancer: New aspects and targets. *Precis. Clin. Med.* **2019**, *2*, 183–191. [CrossRef]
49. Nagarajan, S.R.; Butler, L.M.; Hoy, A.J. The diversity and breadth of cancer cell fatty acid metabolism. *Cancer Metab.* **2021**, *9*, 2. [CrossRef]
50. Paton, C.M.; Ntambi, J.M. Biochemical and physiological function of stearoyl-CoA desaturase. *Am. J. Physiol.-Endocrinol. Metab.* **2009**, *297*, 28–37. [CrossRef]
51. Nakamura, M.T.; Nara, T.Y. Structure, Function, and Dietary Regulation of Δ6, Δ5, and Δ9 Desaturases. *Annu. Rev. Nutr.* **2004**, *24*, 345–376. [CrossRef]
52. Ntambi, J.M. The regulation of stearoyl-CoA desaturase (SCD). *Prog. Lipid Res.* **1995**, *34*, 139–150. [CrossRef]
53. Enoch, H.G.; Catala, A.; Strittmatter, P. Mechanism of rat liver microsomal stearyl-CoA desaturase. Studies of the substrate specificity, enzyme-substrate interactions, and the function of lipid. *J. Biol. Chem.* **1976**, *251*, 5095–5103. [CrossRef]
54. Burlingame, B.; Nishida, C.; Uauy, R.; Weisell, R. Fats and Fatty Acids in Human Nutrition: Introduction. *Ann. Nutr. Metab.* **2009**, *55*, 5–7. [CrossRef] [PubMed]
55. Roongta, U.V.; Pabalan, J.G.; Wang, X.; Ryseck, R.P.; Fargnoli, J.; Henley, B.J.; Yang, W.P.; Zhu, J.; Madireddi, M.T.; Lawrence, R.M.; et al. Cancer cell dependence on unsaturated fatty acids implicates stearoyl-CoA desaturase as a target for cancer therapy. *Mol. Cancer Res.* **2011**, *9*, 1551–1561. [CrossRef]
56. Igal, R.A. Stearoyl-coa desaturase-1: A novel key player in the mechanisms of cell proliferation, programmed cell death and transformation to cancer. *Carcinogenesis* **2010**, *31*, 1509–1515. [CrossRef] [PubMed]

57. von Roemeling, C.A.; Marlow, L.A.; Radisky, D.C.; Rohl, A.; Larsen, H.E.; Wei, J.; Sasinowska, H.; Zhu, H.; Drake, R.; Sasinowski, M.; et al. Functional genomics identifies novel genes essential for clear cell renal cell carcinoma tumor cell proliferation and migration. *Oncotarget* **2014**, *5*, 5320–5334. [CrossRef]
58. Kirschner, K.; Samarajiwa, S.A.; Cairns, J.M.; Menon, S.; Pérez-Mancera, P.A.; Tomimatsu, K.; Bermejo-Rodriguez, C.; Ito, Y.; Chandra, T.; Narita, M.; et al. Phenotype Specific Analyses Reveal Distinct Regulatory Mechanism for Chronically Activated p53. *PLoS Genet.* **2015**, *11*, e1005053. [CrossRef]
59. Harms, K.; Nozell, S.; Chen, X. The common and distinct target genes of the p53 family transcription factors. *C. Cell. Mol. Life Sci.* **2004**, *61*, 822–842. [CrossRef]
60. Luis, G.; Godfroid, A.; Nishiumi, S.; Cimino, J.; Blacher, S.; Maquoi, E.; Wery, C.; Collignon, A.; Longuespée, R.; Montero-Ruiz, L.; et al. Tumor resistance to ferroptosis driven by Stearoyl-CoA Desaturase-1 (SCD1) in cancer cells and Fatty Acid Biding Protein-4 (FABP4) in tumor microenvironment promote tumor recurrence. *Redox Biol.* **2021**, *43*, 102006. [CrossRef]
61. Scott, J.S.; Nassar, Z.D.; Swinnen, J.V.; Butler, L.M. Monounsaturated Fatty Acids: Key Regulators of Cell Viability and Intracellular Signaling in Cancer. *Mol. Cancer Res.* **2022**, 1–11. [CrossRef]
62. Guo, S.; Wang, Y.; Zhou, D.; Li, Z. Significantly increased monounsaturated lipids relative to polyunsaturated lipids in six types of cancer microenvironment are observed by mass spectrometry imaging. *Sci. Rep.* **2014**, *4*, 5959. [CrossRef] [PubMed]
63. Ackerman, D.; Simon, M.C. Hypoxia, lipids, and cancer: Surviving the harsh tumor microenvironment. *Trends Cell Biol.* **2014**, *24*, 472–478. [CrossRef] [PubMed]
64. Vriens, K.; Christen, S.; Parik, S.; Broekaert, D.; Yoshinaga, K.; Talebi, A.; Dehairs, J.; Escalona-Noguero, C.; Schmieder, R.; Cornfield, T.; et al. Evidence for an alternative fatty acid desaturation pathway increasing cancer plasticity. *Nature* **2019**, *566*, 403–406. [CrossRef] [PubMed]
65. Williams, P.E.; Klein, D.R.; Greer, S.M.; Brodbelt, J.S. Pinpointing Double Bond and sn-Positions in Glycerophospholipids via Hybrid 193 nm Ultraviolet Photodissociation (UVPD) Mass Spectrometry. *J. Am. Chem. Soc.* **2017**, *139*, 15681–15690. [CrossRef]
66. Harris, R.A.; May, J.C.; Stinson, C.A.; Xia, Y.; McLean, J.A. Determining Double Bond Position in Lipids Using Online Ozonolysis Coupled to Liquid Chromatography and Ion Mobility-Mass Spectrometry. *Anal. Chem.* **2018**, *90*, 1915–1924. [CrossRef]
67. Baba, T.; Ryumin, P.; Duchoslav, E.; Chen, K.; Chelur, A.; Loyd, B.; Chernushevich, I. Dissociation of Biomolecules by an Intense Low-Energy Electron Beam in a High Sensitivity Time-of-Flight Mass Spectrometer. *J. Am. Soc. Mass Spectrom.* **2021**, *32*, 1964–1975. [CrossRef]
68. Carracedo, A.; Cantley, L.C.; Pandolfi, P.P. Cancer metabolism: Fatty acid oxidation in the limelight. *Nat. Rev. Cancer* **2013**, *13*, 227–232. [CrossRef]
69. Manzo, T.; Prentice, B.M.; Anderson, K.G.; Raman, A.; Schalck, A.; Codreanu, G.S.; Lauson, C.B.N.; Tiberti, S.; Raimondi, A.; Jones, M.A.; et al. Accumulation of long-chain fatty acids in the tumor microenvironment drives dysfunction in intrapancreatic cd8+ t cells. *J. Exp. Med.* **2020**, *217*, e20191920. [CrossRef]
70. Kim, J.A. Peroxisome Metabolism in Cancer. *Cells* **2020**, *9*, 1692. [CrossRef]
71. Smith, R.E.; Lespi, P.; di Luca, M.; Bustos, C.; Marra, F.A.; de Alaniz, M.J.T.; Marra, C.A. A reliable biomarker derived from plasmalogens to evaluate malignancy and metastatic capacity of human cancers. *Lipids* **2008**, *43*, 79–89. [CrossRef]